

**Tectono-sedimentary evolution of middle Miocene  
supra-detachment basins (western Crete, Greece)**

I n a u g u r a l - D i s s e r t a t i o n

zur Erlangung des Doktorgrades

der Mathematisch-Naturwissenschaftlichen Fakultät

der Universität zu Köln

vorgelegt von

Markus Seidel

aus Tegernsee

Köln 2003

Berichterstatter: Prof. Dr. Eberhard Seidel

Prof. Dr. Bernhard Stöckhert

Tag der mündlichen Prüfung: 17.02.2003

## Abstract

The island of Crete is a prominent horst structure in the fore arc of the Hellenic subduction zone, which is governed by roll back of the African slab. The evolution of the plate boundary between Eurasia and Africa during the last 35 Ma is recorded in the geology of Crete. The structure of Crete is characterized by a pile of nappes derived from different paleogeographic zones. The upper units (Uppermost Unit, Pindos Unit, Tripolitza Unit) are separated from the lower units (Phyllite-Quartzite Unit, Plattenkalk Unit) by a low-angle normal fault (detachment fault) of lower to middle Miocene age. The lower tectonic units were overprinted by high-pressure/low-temperature metamorphism in the late Oligocene/early Miocene and were back in the upper crust by ca. 19 Ma. By contrast, the higher tectonic units were not affected by Tertiary blueschist-facies metamorphism.

The detachment fault indicates exhumation of the HP-LT metamorphic units by extension. The exhumation of the high-pressure rocks was accompanied by structural disintegration of the hangingwall, leading to formation of sedimentary basins on top of the nappe pile in the lower to middle Miocene. The sedimentology of these supra-detachment basins reflects the tectonics of the Hellenic fore arc at that time. The basins are half-graben structures filled by huge masses of clastic sediments (breccio-conglomerates) exclusively derived from the upper units situated atop the detachment fault. This means that sedimentation took place before the high-pressure metamorphic units were exposed at the surface and accessible to erosion. Predominant clastic components are lagoonal limestones, dolomitic limestones and dolomites with microfacies and fossil assemblages corresponding to members of the Tripolitza Unit. Limestones with chert, radiolarites, sandstones and calcarenites can easily be derived from the Pindos Unit, whereas the provenance of some pebbles to slabs of marbles remains enigmatic.

Facies analysis shows that the fills of the half grabens vary from alluvial fan deposits in a terrestrial environment to turbiditic successions reflecting a marine environment. The Topolia alluvial fan complex in northwestern Crete is debris-flow-dominated, with poor sorting and clast-rich to matrix-supported deposits. SEM- and CL-studies reveal the high degree of compaction and cementation after deposition. The Lissos coastal alluvial fan complex in southwestern Crete, a thick fault scarp related wedge of sediments, includes subaerial waterlaid and debris-flow deposits as well as marine debris-flow and turbidite deposits.

Due to progressive extension, in places the western Cretan basin fills are now in tectonic contact with the HP-LT metamorphic Phyllite-Quartzite Unit along the brecciated detachment fault. The detachment zone is characterized by ferruginous alteration, with fracture- and vug-filling goethite.  $\delta^{18}\text{O}$  data of goethite give evidence for low-temperature precipitation. A comparison of the Cretan iron ores with products of ferruginous alteration and mineralization in detachment zones of Cordilleran metamorphic core complexes in North America indicates that the genesis of iron ores is a typical feature of detachment zones in general. The genesis of the two iron ore deposits in western Crete (Ravdoucha and Kakopetros) can also be related to the detachment zone.

Neogene deposits in the Lassithi region (eastern Crete) resemble the breccio-conglomerates of western Crete in their facies. Comparative studies show that sedimentation in each region was controlled by different tectonic processes. Contrary to the lower to middle Miocene basin fills in western Crete which were deposited during an extensional stage, the Neogene deposits in the Ierapetra region reflect blockfaulting during compressional tectonics.

The lower to middle Miocene fills of the half-graben structures in western Crete document the history of continuous extension in the fore arc of the roll back controlled Hellenic subduction zone and provide insight into the tectonic evolution of the island for the time span between 20 and 15 Ma otherwise not well recorded.

## Kurzfassung

Die Insel Kreta bildet einen Horst im Forearc der Hellenischen Subduktionszone, die durch das Zurückrollen (roll back) der abtauchenden Afrikanischen Platte charakterisiert ist. Die Entwicklung der Plattengrenze zwischen Eurasien und Afrika während der letzten 35 Ma ist in der Geologie Kretas dokumentiert. Der Baustil Kretas ist durch einen Stapel von Gesteinseinheiten, die aus unterschiedlichen paläogeographischen Zonen stammen, charakterisiert. Auf der Insel sind Krustenteile aufgeschlossen, die im späten Oligozän bis frühen Miozän eine Hochdruck-Niedrigtemperatur-Metamorphose durchlaufen haben und anschließend unter Dehnungseinfluss rasch exhumiert wurden. Um etwa 19 Ma befanden sie sich nur noch wenige Kilometer unter der Erdoberfläche. Diese hochdruck-niedrigtemperatur-metamorphen Einheiten (Plattenkalk-Einheit, Phyllit-Quarzit-Einheit) befinden sich heute unmittelbar unter Einheiten (Tripolitza-Einheit, Pindos-Einheit, Oberste Einheit), die nicht von der tertiären blauschieferfaziellen Metamorphose betroffen sind. Dazwischen liegt als tektonische Trennfläche eine flache Abschiebung (detachment fault), die die Exhumierung der hochdruck-niedrigtemperatur-metamorphen Einheiten durch Extensionstektonik erklärt.

In Westkreta geht die dehnungsgesteuerte Freilegung der hochdruckmetamorphen Einheiten mit der Entstehung von Halbgräben einher, die mit unter- bis mittelmiozänen klastischen Ablagerungen (Konglomerat- und Brekzienkalke) gefüllt wurden. Die Sedimentologie dieser "supra-detachment"-Becken reflektiert die tektonischen Vorgänge im Forearc der Hellenischen Subduktionszone in jener Zeit. Die Komponenten der Beckenfüllungen stammen dabei nur von den nicht metamorphen Deckeneinheiten im Hangenden der flachen Abschiebung. Das Geröllspektrum wird von Flachwasserkalken dominiert, die in ihrer Mikrofazies und ihrem Fossilinhalt den Kalken der Tripolitza-Einheit entsprechen. Komponenten, die dem Faziesbereich der Pindos-Einheit zugeordnet werden können, treten stark zurück. Die Herkunft von Marmorgeröllen bleibt rätselhaft (exotische Komponenten). Das Fehlen von Fragmenten aus dem Liegenden der Abschiebung weist darauf hin, dass die Beckensedimente geschüttet wurden, als die hochdruckmetamorphen Einheiten noch nicht an der Erdoberfläche anstanden.

Die terrestrischen Ablagerungen im Gebiet Topolia-Kakopetros sind auf alluviale Schuttströme zurückzuführen. Sie zeigen weitgehend schlechte Sortierung, sind klastenreich und matrixgestützt. Untersuchungen mit Rasterelektronenmikroskop und Kathodolumineszenz zeigen, dass die Sedimente nach der Ablagerung kompaktiert und zementiert wurden. Im Gebiet Lissos-Paleochora liegt ein mächtiger Sedimentkeil vor, der aus terrestrischen und marinen Schuttbildungen aufgebaut ist.

Durch anhaltende Dehnung treten diese westkretischen Beckenfüllungen heute stellenweise direkt mit der hochdruckmetamorphen Phyllit-Quarzit-Einheit entlang der Abschiebungsfläche in tektonischen Kontakt. Im Bereich der flachen Abschiebung sind die Gesteine stark brekziiert. Stellenweise bilden diese Brekzien eine mehrere zehn Meter mächtige Zone. Eine typische Erscheinung der Brekzien ist ihre Mineralisation mit Goethit.  $\delta^{18}\text{O}$ -Werte des Goethites zeigen eine niedrigtemperierte Entstehung der Erze an. Auch die Genese der Eisenerzlagerstätten von Ravdoucha und Kakopetros in Westkreta ist in diesen Zusammenhang zu stellen. Durch die Imprägnation mit Eisenhydroxid zeigt der brekziierte Bereich eine von weitem sichtbare gelb-orange-rote Farbgebung (ferruginous alteration), wie sie für flache Abschiebungsbahnen innerhalb von "metamorphic core complexes" in der nordamerikanischen Kordillere typisch ist.

Eine chaotische Sedimentassoziation an der Basis des Neogens in Ostkreta (Prina-Komplex) erinnert in ihrer Fazies an die Konglomerat- und Brekzienkalke in Westkreta. Vergleichende Betrachtungen zeigen jedoch, dass die Sedimentation in den beiden Regionen von unterschiedlichen tektonischen Prozessen gesteuert wurde. Die Sedimente in Westkreta wurden während einer Dehnungsphase abgelagert, die Sedimente in Ostkreta hingegen entstanden während einer Einengungsphase.

Die Sedimente der unter- bis mittelmiozänen Halbgräben in Westkreta zeichnen eine Phase kontinuierlicher Dehnung im Forearc der Hellenischen Subduktionszone auf und geben Einblick in die tektonische Entwicklung Kretas während der Zeit zwischen 20 und 15 Ma vor heute, die sonst kaum geologisch dokumentiert ist.

# Contents

ABSTRACT

GERMAN ABSTRACT / KURZFASSUNG

<b>1</b>	<b>OUTLINE OF THE GEOLOGY OF CRETE.....</b>	<b>1</b>
1.1	INTRODUCTION .....	1
1.2	SCOPE OF THE INVESTIGATIONS.....	2
1.3	GEOGRAPHICAL POSITION OF THE TARGET AREA.....	3
1.4	GEOLOGICAL SETTING .....	4
1.4.1	The Hellenic subduction zone and plate motions .....	4
1.4.2	The Cretan nappe pile.....	5
1.4.3	Synorogenic basin fills .....	7
1.5	PREVIOUS LITERATURE ON THE BASIN FILLS .....	7
<b>2</b>	<b>THE MIDDLE MIOCENE BASIN FILLS IN WESTERN CRETE.....</b>	<b>9</b>
2.1	SEDIMENTOLOGY OF THE BASIN FILLS.....	9
2.1.1	Introduction .....	9
2.1.2	Topolia alluvial fan complex .....	9
2.1.2.1	Sedimentary facies.....	9
2.1.2.2	Depositional model.....	14
2.1.3	Lissos coastal alluvial fan complex.....	16
2.1.3.1	Sedimentary facies.....	16
2.1.3.2	Depositional model.....	21
2.1.4	Fault scarp setting or range front setting?.....	23
2.1.5	Modelling the former catchment area .....	24
2.2	DIAGENETIC EVOLUTION OF THE BASIN FILLS .....	26
2.2.1	Introduction .....	26
2.2.2	SEM and EDX studies .....	27
2.2.2.1	Lissos coastal alluvial fan complex.....	27
2.2.2.2	Topolia alluvial fan complex.....	29
2.2.3	Cement stratigraphy.....	31
2.2.4	Diagenetic evolution of the Topolia alluvial fan complex .....	34
2.3	CLASTS WITHIN THE BASIN FILLS .....	36
2.3.1	Introduction .....	36
2.3.2	Topolia alluvial fan complex .....	36
2.3.3	Lissos coastal alluvial fan complex.....	41
2.3.4	Provenance and distribution of clasts.....	42
2.4	EXOTIC CARBONATE ROCKS WITHIN THE BASIN FILLS .....	43
2.4.1	Introduction .....	43

2.4.2	Exotic calcite marbles .....	43
2.4.2.1	Calcite twins as an easy-to-use geothermometer .....	43
2.4.2.2	Calcite textures and microstructures.....	45
2.4.2.3	Comparative studies of marbles from the Phyllite-Quartzite Unit.....	50
2.4.2.4	Discussion and interpretation .....	51
2.4.3	Exotic dolomite marbles.....	52
2.4.3.1	Coexisting calcite and dolomite as geothermometer.....	52
2.4.4	Further exotic carbonate rocks .....	53
2.4.5	Conclusions .....	54
<b>3</b>	<b>TECTONICS OF THE MID-MIOCENE BASINS IN WESTERN CRETE .....</b>	<b>55</b>
3.1	CONTACTS OF THE BRECCIO-CONGLOMERATES TO THE UNDERLYING UNITS.....	55
3.2	EXTENSION TECTONICS .....	56
3.2.1	Low- to moderate-angle normal faults.....	56
3.2.2	Tectono-sedimentary evolution.....	58
3.2.3	Brittle deformation within the detachment zone .....	58
<b>4</b>	<b>DATING OF THE BASIN FILLS.....</b>	<b>60</b>
<b>5</b>	<b>IRON ORE DEPOSITS IN THE DETACHMENT ZONE OF WESTERN CRETE.....</b>	<b>63</b>
5.1	INTRODUCTION .....	63
5.2	SETTING OF THE ORE DEPOSITS .....	63
5.3	MINERALOGY AND PETROGRAPHY.....	64
5.4	GEOCHEMISTRY .....	68
5.5	OXYGEN ISOTOPE GEOCHEMISTRY.....	69
5.6	FLUID FLOW PATTERNS.....	71
5.7	A COMPARISON WITH METAMORPHIC CORE COMPLEXES OF CORDILLERAN TYPE .....	73
<b>6</b>	<b>LINEAMENT ANALYSES ON SATELLITE IMAGES AND AERIAL PHOTOGRAPHS OF WESTERN CRETE .....</b>	<b>74</b>
<b>7</b>	<b>COMPARISON WITH BASIN FILLS IN EASTERN AND CENTRAL CRETE.....</b>	<b>76</b>
7.1	NEOGENE BASIN FILLS IN THE IERAPETRA REGION (EASTERN CRETE).....	76
7.1.1	Geology of the Ierapetra basin.....	76
7.1.2	Discussion .....	77
7.2	NEOGENE GRABEN FILLS IN THE IRAKLION AREA (CENTRAL CRETE) .....	78
7.2.1	Geological setting .....	78
7.2.2	Discussion .....	79
<b>8</b>	<b>SYNTHESIS .....</b>	<b>81</b>
<b>9</b>	<b>ANALYTICAL TECHNIQUES AND LABORATORY EQUIPMENT.....</b>	<b>85</b>
<b>10</b>	<b>REFERENCES .....</b>	<b>87</b>

<b>11</b>	<b>GEOLOGICAL MAPS.....</b>	<b>95</b>
	EXTENDED GERMAN ABSTRACT / AUSFÜHRLICHE ZUSAMMENFASSUNG.....	97
	LIST OF FIGURES .....	101
	LIST OF TABLES .....	103
	APPENDIX.....	104
	LIST OF SAMPLES CITED IN FIGURES AND TABLES.....	104
	ABBREVIATIONS.....	104
	ACKNOWLEDGEMENTS.....	105
	STATEMENT / ERKLÄRUNG.....	107
	CURRICULUM VITAE / LEBENSLAUF.....	108





# 1 Outline of the geology of Crete

## 1.1 Introduction

The mechanism of rapid tectonic uplift and exhumation of high-pressure/low-temperature (HP-LT) metamorphic rocks is still poorly understood. Especially extensional tectonic processes in the fore arc of convergent plate boundaries like the Hellenic subduction zone in the eastern Mediterranean stimulate new speculations. For the southern Aegean geological and geophysical data indicate that extensional processes in the upper plate are related to the roll back of the subducting African plate. There, extension resulted in the evolution of a low-angle normal fault (detachment fault) separating the HP-LT metamorphic units in the lower part from the nonmetamorphic units in the upper part of the Cretan nappe pile. Middle Miocene half-graben basins which developed simultaneously in this extensional regime were filled with huge masses of clastic sediments.

Information about the development of the detachment fault is provided by the middle Miocene basin fills (breccio-conglomerates) on top of the Cretan nappe pile in western Crete. These Neogene basin fills, with clastic components exclusively derived from the nonmetamorphic units, developed during the disintegration of the hangingwall of the detachment fault. Because of continuous extension, in some places, these clastic basin fills are now in tectonic contact with the HP-LT metamorphic units.

Investigations of these middle Miocene basin fills documenting long-lasting extension will contribute to a better understanding of the external part of the Aegean microplate, which was thinned by brittle deformation of the upper crust, and will provide insight into the tectonic evolution of the fore arc of the Hellenic subduction zone in a period of time otherwise not well recorded.

## 1.2 Scope of the investigations

The aim of the study was to get new information about the depositional and the tectonic setting, the sedimentology of the synorogenic basin fills in western Crete and the provenance of their clasts.

The following problems and questions are addressed:

- Facies analysis (marine, limnic, fluvial, terrestrial) in order to determine transport mechanisms and depositional processes. Investigations of the sedimentary structure of the breccio-conglomerates and analysis of their fabric.
- Analyses of matrix and cements in order to reconstruct the diagenetic and tectonic history of the breccio-conglomerates.
- Provenance of the clasts and their distribution in space and time. How did the paleomorphology look like during the sedimentation of the breccio-conglomerates? Were the clasts derived from an one-point source or from a multi-point source? Is sedimentation influenced by local effects?
- Dating of the basin fills in order to confine the time of sedimentation.
- To what extent is the tectonic evolution of the island of Crete recorded in the basin fills? Are the breccio-conglomerates bound to a special kind of fault scarps? Is their formation related to a period of compressional tectonics or to an extensional stage leading to the exhumation of the HP-LT metamorphic rocks?
- How far does the Cretan situation resemble the status of a metamorphic core complex as found in the Basin and Range Province in the North American Cordillera?

During the field studies detailed geological mapping and sampling was carried out. The results of the sedimentological and structural studies are pictured in block diagrams and geological maps of the working areas. In addition, comparative studies were carried out in eastern Crete in order to prove, whether Neogene deposits in the Lassithi region match the breccio-conglomerates of western Crete in tectonic setting, facies and spectrum of clasts.

### 1.3 Geographical position of the target area

The outcrops of the middle Miocene basin fills (breccio-conglomerates) are located in western Crete (Figure 1), west of the Levka Ori. The area is divided into two parts. One area is located in southwestern Crete between Paleochora and Sougia. The other area is located in northwestern Crete in the surroundings of the villages of Sirikari, Topolia and Kakopetros.

The southern part of the working area extends from ca.  $23^{\circ} 39' E$  to  $23^{\circ} 48' E$  (longitude) and from ca.  $35^{\circ} 13' N$  to  $35^{\circ} 17' N$  (latitude) and the northern working area has the geographical position from ca.  $23^{\circ} 39' E$  to  $23^{\circ} 46' E$  and from ca.  $35^{\circ} 24' N$  to  $35^{\circ} 29' N$ .

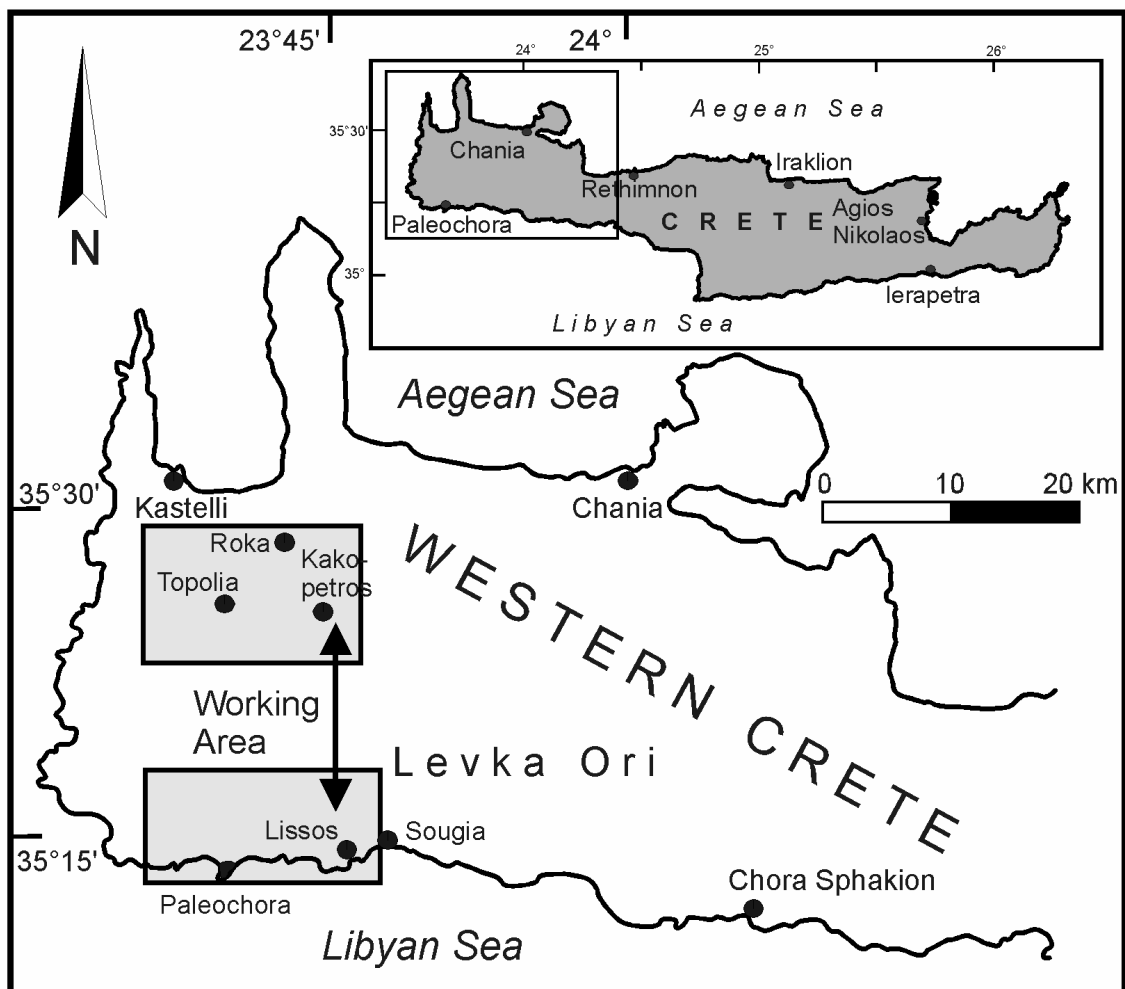


**Figure 1: Overview of the geographical distribution of the synorogenic sediments. The breccio-conglomerates occur at two locations in western Crete. In the southwest, outcrops are located in the vicinity of Paleochora, Lissos and Sougia. In the northwest, breccio-conglomerates occur in the area around Topolia, Roka and Kakopetros.**

## 1.4 Geological setting

The present state of the art in Aegean geology is described in Jacobshagen (1986). An overview of the active tectonics of the eastern Mediterranean region is given by Jackson (1994). In the following, the important facts are summarized (partly after Stöckhert 2001).

### 1.4.1 The Hellenic subduction zone and plate motions

The Hellenic subduction zone represents a world site for retreating convergent margins. In the central fore arc of the Hellenic subduction zone, which is governed by the roll back of the African slab, the island of Crete forms a significant horst structure developed within the last 5 million years. Crete provides excellent onshore access to the internal structure of the fore arc at various levels. The geologic chronicle of Crete documents the evolution of the plate boundary between Eurasia and Africa during the last 35 Ma, with an intermittent stage of microcontinent collision between about 30 and 20 Ma, and an incipient collision with the passive African continental margin today.

The geology-based NUVEL-1A model of relative plate motion predicts a convergence between Africa and stable Eurasia with a rate of 0.9 cm/year and a direction of  $353^\circ$  for the region of Crete (ca.  $25^\circ$  E /  $35^\circ$  N). The African plate moves towards north to northwest (Taymaz et al. 1990) and is being subducted underneath the Eurasian plate (Aegean microplate). Space geodesy reveals that Crete and the southern part of the Aegean is moving to the SSW with respect to stable Eurasia. The velocity of this motion is ca. 3 to 4 cm/year (Jackson 1994; Le Pichon et al. 1995; Cocard et al. 1999) and represents the rate of roll back of the subducting slab, resulting in a net convergence rate of 4 to 5 cm/year at the plate boundary (Figure 2). The Benioff zone seismicity reaches down to ca. 180 km (Makris & Röwer 1986), being situated at a depth of ca. 140 km underneath the magmatic arc, with volcanic activity on the islands of Aegina, Milos, Santorini and Nisyros. The slab has been traced to a depth of 600 km by seismic tomography (Wortel et al. 1990). The thickness of the crust beneath the Sea of Crete, i.e. between Crete and the magmatic arc to the north, is locally reduced to less than 16 km (Makris & Röwer 1986) correlated with a high heat flow. Active crustal stretching has not been detected by space geodesy, however. Deep topographic furrows to the south of Crete obviously represent fore-arc basins commonly related to strike-slip motion (e.g. Le Pichon et al. 1995). The 'backstop' to the active accretionary complex represented by the Mediterranean ridge (Masclé & Chaumillon 1997) is located further to the south. The thin continental crust of the upper plate extends for more than 100 km to the south and southwest of Crete (Truffert et al. 1993). This means that a thin lid of continental crust is sliding on top of the downgoing plate and that its southern edge acts as the backstop to active accretion.

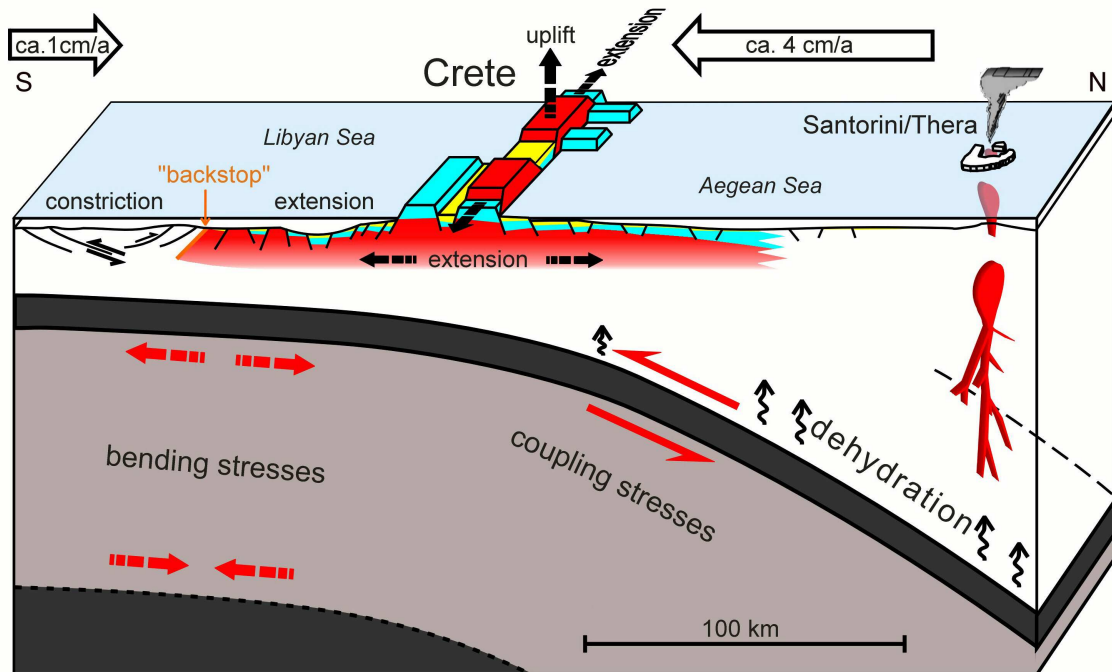


**Figure 2: Cartoon showing a schematic cross section of the Hellenic subduction zone and the geographic and tectonic setting of Crete in the central fore arc (modified after Papanikolaou & Stöckhert 1998).**

#### 1.4.2 The Cretan nappe pile

The structure of Crete is characterized by a pile of nappes (Figure 3) derived from different paleogeographic zones (Seidel & Wachendorf 1986). In the course of collision the lower tectonic units have been buried in a depth of more than 30 km and were overprinted by HP-LT metamorphism in late Oligocene/early Miocene (Seidel et al. 1982; Jolivet et al. 1996). By contrast, the higher tectonic units were not affected by Tertiary high-pressure metamorphism. The HP-LT units were exhumed within a very short time span after HP-LT metamorphism, forming the footwall of a fault zone interpreted as low-angle normal fault or detachment fault (Seidel & Theye 1993; Fassoulas et al. 1994; Jolivet et al. 1994 and 1996; Kiliyas et al. 1994; Ring et al. 2001) and were back in the upper crust by about 19 Ma (Thomson et al. 1998). The rates of burial and exhumation require a roll back of the subducting slab as demonstrated in the 'oblique buoyant escape'-model proposed by Thomson et al. (1998, 1999).

Immediately above the HP-LT metamorphic rocks (Plattenkalk Unit [Tripali Unit], Phyllite-Quartzite Unit), separated by the detachment fault of Miocene (pre-Serravallian) age, the nonmetamorphic higher nappes (Tripolitza Unit, Pindos Unit) follow in the upper part of the nappe pile. Locally in northwestern Crete the anchimetamorphic Ravdoucha beds (Sannemann & Seidel 1976) are sandwiched between the Phyllite-Quartzite Unit and the Tripolitza Unit. The top of the Cretan nappe pile is represented by the Uppermost Unit.

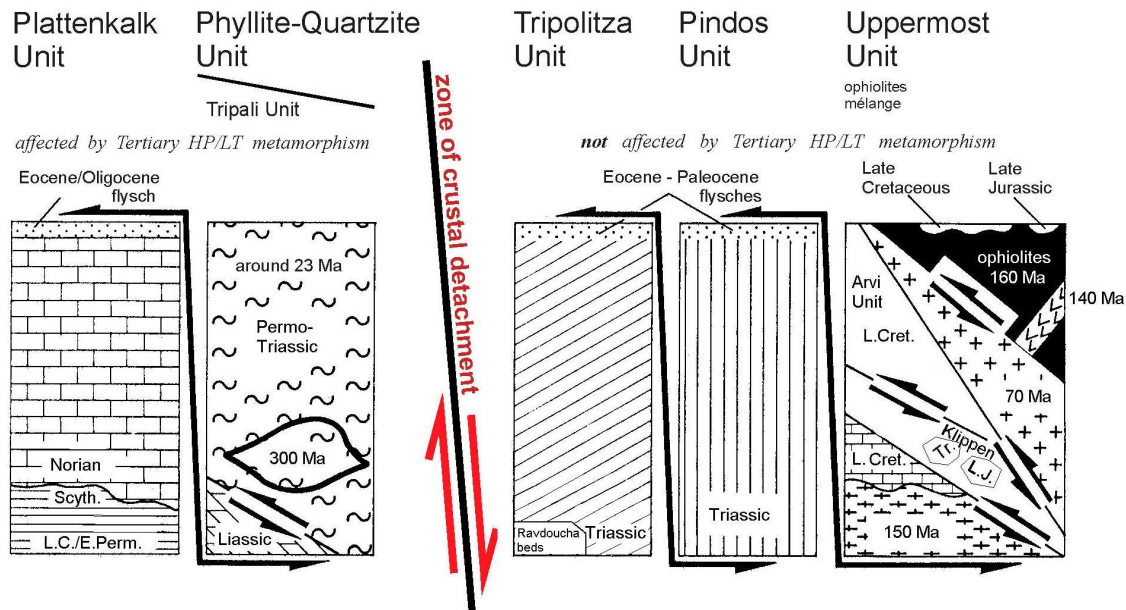


**Figure 3: Schematic illustration of the tectonostratigraphy of Crete (modified after Seidel et al. 1982 and unpublished).**

The Plattenkalk Unit forms the lowermost nappe. It consists of phyllites, dolomite and cherty calcite marbles and a calcareous metaflysch, and its age ranges from late Carboniferous/early Permian to Eocene (Fytrolakis 1972; Bonneau 1973; König & Kuss 1980) or even Oligocene (Bizon & Thiebault 1974). The Plattenkalk Unit shows high-pressure/low-temperature metamorphism as indicated by magnesiocarpholite in metabauxites (Seidel 1978; Seidel et al. 1982; Theye & Seidel 2001) and lawsonite in dolomite marbles (Theye 1988).

The Plattenkalk Unit is overlain by the Carboniferous to Triassic (Krahl et al. 1983) Phyllite-Quartzite Unit. In western Crete the Tripali Unit, a monotonous series of dolomite marbles, is wedged between the Plattenkalk Unit and the Phyllite-Quartzite Unit.

The Phyllite-Quartzite Unit consists of phyllites, quartzites, metaconglomerates, marbles, and metavolcanites. HP-LT metamorphism is indicated by Fe-Mg-carpholite and lawsonite as well as blue amphibole, sodium pyroxene and aragonite (e.g. Seidel 1978; Theye 1988). Locally, evaporites (anhydrite retrograded to gypsum, accompanied by rauhwackes) are intercalated in the succession. In eastern Crete slivers of the Variscan basement are incorporated. The Phyllite-Quartzite Unit entered the Hellenic subduction zone between ca. 36-29 Ma (Thomson et al. 1999). The rocks were metamorphosed at peak conditions of about 400°C and 10 kbar (Seidel & Theye 1993) around 23 Ma as shown by K-Ar and Ar-Ar ages from metamorphic white micas by Seidel et al. (1982) and Jolivet et al. (1996). The rocks cooled down to below 300°C before ca. 19 Ma and finally to less than 60°C at ca. 15 Ma (Thomson et al. 1998, 1999). Extensional deformation within the brittle field started at temperatures below ca. 300°C and at

pressures of less than 3-4 kbar corresponding to depths of less than ca. 10 km (Küster & Stöckhert 1997; Thomson et al. 1999).

The Phyllite-Quartzite Unit is overlain by the nonmetamorphic Tripolitza Unit which consists of upper Triassic to Eocene limestones and secondarily dolomites, deposited on a carbonate platform (Zager 1972; Leppig 1974). The top of the Tripolitza Unit is formed by the Eocene (Leppig 1974) to ?lower Oligocene (Wachendorf et al. 1980) Tripolitza flysch. Locally, in northwestern Crete the anchimetamorphic Ravdoucha beds (Sannemann & Seidel 1976) are sandwiched between the Phyllite-Quartzite Unit and the Tripolitza Unit, which are regarded as the sedimentary basis of the Tripolitza Unit.

The next nappe, the nonmetamorphic Pindos Unit is a sequence of deep-water sediments, ranging in age from Triassic to Paleogene. It is composed of pelagic limestones, radiolarites and shales, with interlayers of turbiditic limestones and a first flysch intermezzo in the Cenomanian/Turonian. The Pindos Unit ceases with the main (second) flysch of Paleocene to Eocene age (Seidel 1971; Wachendorf et al. 1980).

The top of the Cretan nappe pile is represented by the Uppermost Unit, which consists of an ophiolitic mélange in the lower part and Jurassic ophiolites in the upper part (e.g. Seidel et al. 1981). Outcrops of the Uppermost Unit are known from central and eastern Crete, but not from western Crete.

#### 1.4.3 Synorogenic basin fills

The breccio-conglomerates of western Crete were deposited in half-graben structures during disintegration of the nappe pile in Miocene times (Figure 4). Today, these clastic basin fills rest on rocks of the nonmetamorphic units as well as on HP-LT rocks (e.g. Aubouin & Dercourt 1965).

The Cretan nappe pile and the synorogenic basin fills are transgressively overlain by marine sediments of Tortonian age (e.g. Freudenthal 1969).

### 1.5 Previous literature on the basin fills

Aubouin & Dercourt (1965) were the first to describe the breccio-conglomerates ('les breches de la Crète occidentale'). Seidel (1968) calls them 'Konglomerat- und Brekzienkalke' and Kopp & Richter (1983) report on 'synorogenetische Schuttbildungen' (synorogenic sediments). Some authors have considered the breccio-conglomerates to be pre-Neogene deposits (geological maps of Freudenthal 1969; Kontopoulos et al. 1996). In the geological map of Crete 1 : 200,000 (Creutzburg et al. 1977) the age is given as mid-Miocene or older. Tataris & Christodoulou (1969) assign the sediments to the lower Miocene (upper Helvetian). Also Kopp & Richter (1983) provisionally attribute the synorogenic sediments to the lower (middle?) Miocene.

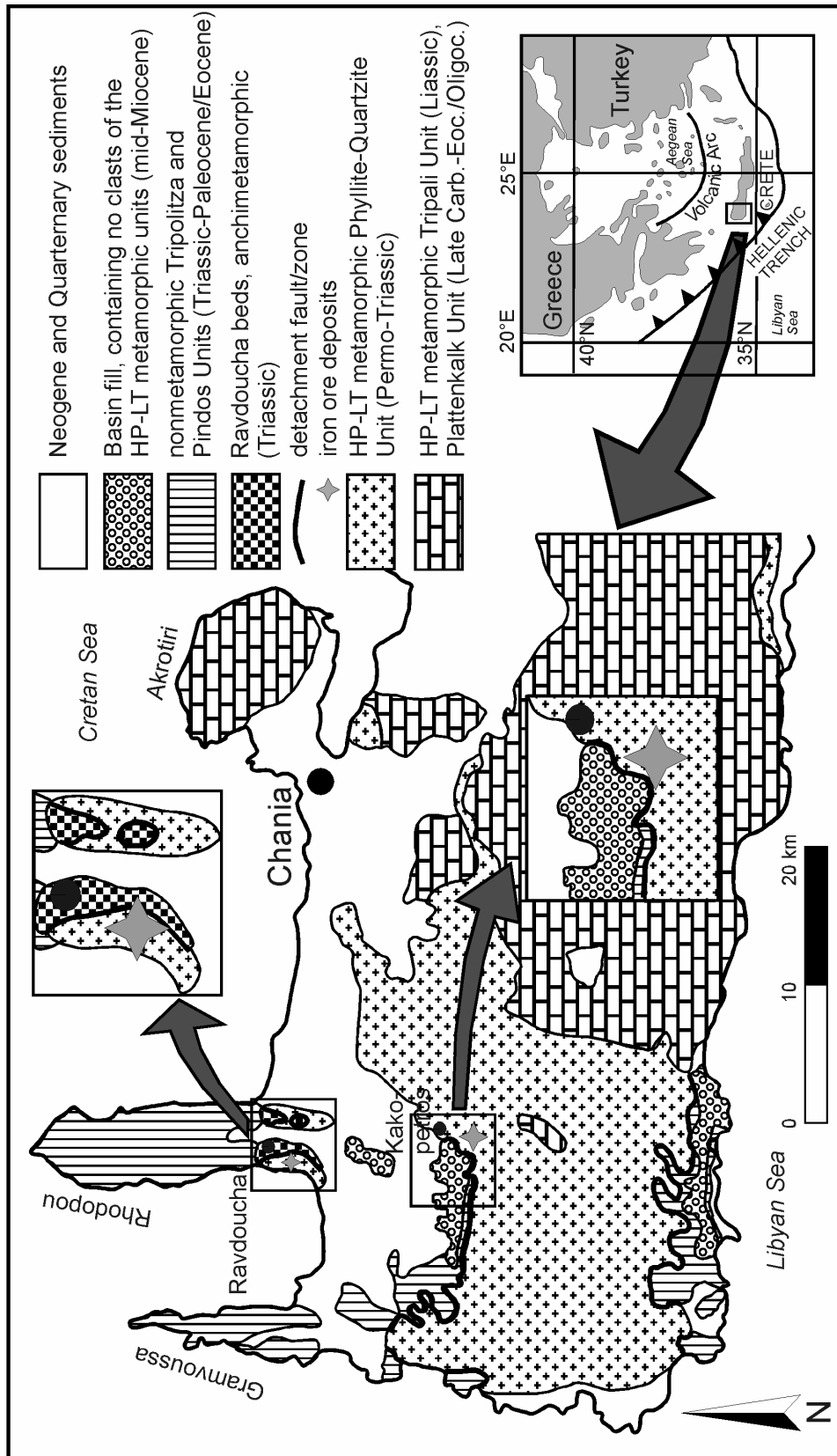


Figure 4: Generalized geological map of western Crete (modified from Creutzburg et al. 1977 and Kopp & Ott 1977) showing the tectonic units, the detachment fault and the major iron ore deposits located in the roof of the Phyllite-Quartzite Unit.



## 2 The middle Miocene basin fills in western Crete

### 2.1 Sedimentology of the basin fills

#### 2.1.1 Introduction

Facies analyses were carried out to obtain information about the sedimentary processes leading to the formation of the basin fills. The deposits were studied at several localities, especially in canyons cutting the breccio-conglomerates in the Topolia area and along the steep coast in the region of Lissos. The exposure height at these sites locally ranges to considerably more than 10 m. Thus, the cuts provide a reasonable representation of the long-term sedimentary processes forming the deposits. To cover all variants of stratigraphy in the clastic wedges it was necessary to study an adequate number of outcrops.

Two different types of clastic wedges can be distinguished due to their sedimentary setting. The results of facies analyses show that the fills of the half grabens vary from alluvial fan deposits in the northern working area to coastal fan deposits built up by terrestrial and marine sediments in the southern working area. The first basin fill is termed Topolia alluvial fan complex, the second is termed Lissos coastal alluvial fan complex. The term 'complex' is used to show that the fill of each basin is not formed by one fan only, but by a multitude of individual fans representing a multi-point source arranged along a fault scarp or range front.

#### 2.1.2 Topolia alluvial fan complex

The Topolia alluvial fan complex covers at present an outcrop area of about 15 km<sup>2</sup>. The facies descriptions of the Topolia alluvial fan complex together with sedimentological interpretations are presented in the following section.

##### 2.1.2.1 *Sedimentary facies*

#### ASSOCIATION 1: ROCKFALL DEPOSITS OF THE PROXIMAL FAN

**Facies A:** Coarse clasts ranging in grain size from boulder to block (or even slabs) can be observed in the canyons of Topolia and Sasalos. The oversized clasts are completely covered by younger alluvial fan deposits. Due to vegetation and weathering of the breccio-conglomerates it is even very difficult at some locations, to discern rockfall blocks from the surrounding coarse debris-flow deposits. Most of the large blocks consist of bluish-grey to grey limestones. Locally, blocks of marble were found.

The rockfall blocks were detached from a very steep slope (range front or fault scarp). After falling off, the fragments came to rest in the proximal fan and were embedded or

transported slightly down fan by later debris flows. The rockfalls may have been triggered by earthquakes, insolation or heavy rainfalls.

#### ASSOCIATION 2: DEBRIS-FLOW DEPOSITS OF THE PROXIMAL AND MEDIAL FAN

Debris-flow deposits dominate the proximal and medial part of the Topolia alluvial fan, accounting for about 70-80 % of the exposures. Three facies types (B1, B2, and C) are distinguished in this association 2. The deposits of all three facies types are commonly poorly sorted, contain matrix, and are either clast-supported, matrix-supported or both, depending on the position in the fan. The distal parts of the Topolia alluvial fan are dominated by water-flow deposits (association 3).

**Facies B1 (cohesive debris-flow deposits) and Facies B2 (noncohesive debris-flow deposits):** Facies B1 consists of matrix-supported mainly unsorted and disorganized, clast-rich gravel. The grain size ranges from granule (very fine pebble gravel) to coarse cobble gravel. Most clasts are coarse and very coarse pebbly gravel. Boulder-sized and block-sized clasts are volumetrically rare but can be observed at different locations and can be called outsized clasts (Figure 5).

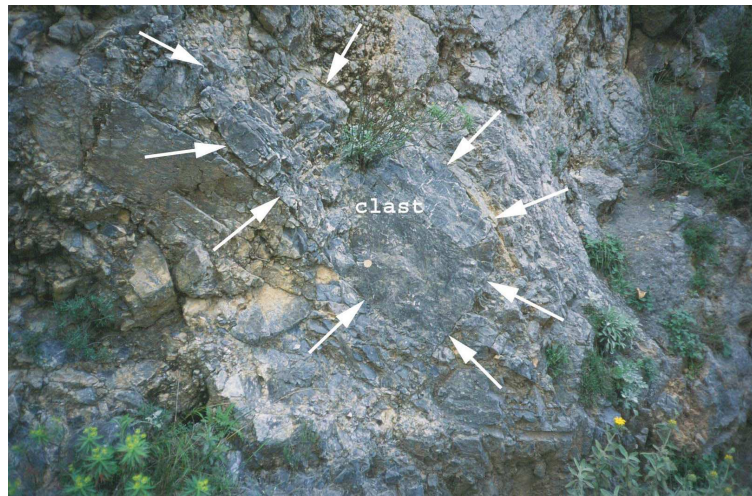


**Figure 5: Outsized clast (within the white arrows) in a matrix-rich debris-flow deposit. The dimensions of the clast are ca. 105 x 65 cm. Topolia gorge, roadside, ca. 50 m south of the traffic-lights south of the tunnel.**

In beds with higher gravel concentrations the clasts are partly in contact with each other and the overall fabric approaches one of clast support (transitional type to facies B2). Clasts are in most cases subangular to rounded. Only a small percentage of clasts is angular. This difference in roundness is a typical feature of such deposits. Smaller clasts are more rounded than larger ones. The shape of clasts varies from equant to bladed. The clasts consist mainly of grey or black limestones, dolomitic limestones or dolomites,

secondary of sandstones to greywackes. At some locations (e.g. Topolia and Sasalos canyon) oversized clasts with a diameter of more than 1 m can be observed.

The debris-flow deposits of facies B1 show no imbrication. No fossil was found in the fine-grained matrix. It is very difficult to discern individual beds. The sediments are highly amalgamated, boundaries between former individual beds are not visible. Changes in concentration of clasts, grain size distribution and changes from matrix-supported to matrix-rich parts or interbeds of other facies types give a hint for recognizing and estimating the thickness of the beds and the overall strike and dip. Only in some cases bedding is highlighted by grains which show alignment of their c-axes parallel to flow direction. In some individual beds inverse grading also helps to identify bedding.

Facies B2 is a derivative of facies B1 and is intercalated with the latter. In comparison with facies B1 the content of clay-size sediment is reduced. The fabric is clast-supported and matrix-rich. Locally even interclast pores are present. Bedding is visible at some locations. Clasts show orientation in most cases. The overall sedimentological features resemble those of facies B1.

The matrix-supported, unsorted and disorganized, muddy, sandy, slightly bouldery, granule (very fine pebble gravel) to coarse cobble gravel structure of facies B1 and B2 is diagnostic of debris-flow deposits (Selby 1994; Blair 1999b; Einsele 2000). The thickness, the extent, and the lateral termination of these beds, when discernible, all indicate that the debris flows were of high volume. After deposition, the debris-flow beds amalgamated with each other, both laterally and vertically, which makes the discrimination of individual deposits often very difficult or even impossible. The common inclusion of material whose grain size ranges from clay to gravel indicates that this was the typical sediment suite in the colluvial slopes fed by the catchment through weathering and tectonic dissection of the underlying carbonate bedrock. Sediment sorting was obviously poor. The debris flows were probably triggered by intense thunder-storms. After travelling through the catchment, the debris-flow masses were deposited predominantly on the proximal to medial alluvial fan as a result of thinning to critical levels under expansion (e.g. Blair 1999b).

**Facies C (clast-poor debris-flow deposits or mudflow deposits):** The dominant grain size classes of the mudflow deposits are clay, silt and sand. Gravel-sized clasts are sometimes embedded in the fine-grained matrix. Bed thickness reaches a maximum of 80 cm. These beds are interstratified with the debris-flow deposits of facies B-type rocks. Facies C beds are typically sharply bound and have a tabular to irregular geometry. These beds can easily be traced laterally in radial cuts (e.g. in Topolia canyon, Figure 6). At some localities microbialitic structures can be observed, giving evidence of sediment binding cyanobacteria or fungi. The microbialites consist of wavy, irregular laminations of microsparite alternating with thin mudstone laminae.

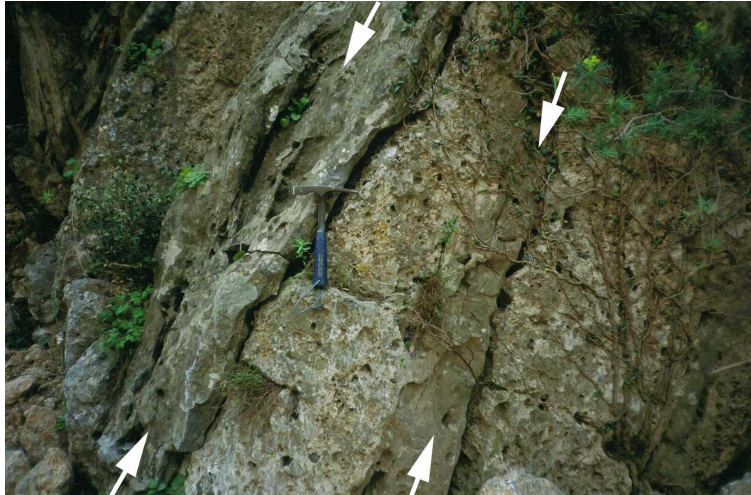


**Figure 6: Two intercalations (white arrows) of sand- to mudstone beds (lithified dolomite sands) in conglomerates of the Topolia alluvial fan complex, Topolia gorge. Hammer for scale. P01-03-020.**

The mudflows give evidence of the abundance of a high volume of fine-grained (clayey to sandy) sediments in the colluvium of the catchment area. This fine-grained material was washed downslope during rainfalls leading to the formation of mudflows. The mudflows came to rest on the active depositional lobe after their excess pore water had dissipated. The ‘freezing’ of such flows is accomplished either by cohesive freezing or, in case of a cohesionless sandy matrix, by frictional freezing, or by both processes (e.g. Einsele 2000).

The microbialites indicate, that there were small accumulations of water in depressions on the surface of the alluvial fan. Due to the underlying clayey sediments, the seepage of water was slow. In this water-filled pans microbialites developed very quickly before the water evaporated. Mud was washed episodically (e.g. during heavy rain falls) into this depression, covering the mats. Afterwards, new microbialitic structures developed.

### ASSOCIATION 3: WATERLAID DEPOSITS OF THE DISTAL (LOWER) FAN BODY

**Facies D:** Facies D is clast-supported and consists of fine to coarse pebble gravel. In many outcrops a weak imbrication is visible, because elongated pebbles show a preferred alignment of their long axes subparallel to direction of water flow. The water-flow deposits are sorted, clasts are rounded to well rounded, bedding is visible on account of changes in gravel mode, concentration and distribution (e.g. north of Kakopetros). The sediments show parallel bedding. Clast-supported fabric is most pronounced in beds consisting of granule to coarse pebble (Figure 7).

In general, grain size is decreasing with flow direction and increasing distance of transport to northern directions. Bed thickness reaches 20 to 25 cm in average. Different beds show different grades of cementation. At some localities stylolites are visible because of an intense pressure solution affecting the limestone clasts due to clast-supported structure.



**Figure 7: Clast-supported water-flow deposits northwest of Mesavlia. Due to tectonic displacement the sediments dip steeply to the north (to the right).**

Waterlaid deposits generally occur in the distal part of the alluvial fan. The partly imbricated and overall clast-supported structure is indicative of water flow in the surficial braided distributary channel (Koster & Steel 1984). Sometimes intercalations of waterlaid deposits can also be observed in the proximal to medial part. These deposits are interpreted to have developed during the recessional water-flood stage of one rainfall event (Blair & McPherson 1998), when the debris flows were no longer instigated by colluvial slope failure, but when the catchment continued to drain the rainfall (Blair & McPherson 1992, 1994, 1998). The deposition of waterlaid deposits took place in times when only a limited volume of sediment finer than medium sand was supplied by the catchment (cf. Blair 1999c), e.g. when the catchment was cleared from fine material due to preceding debris flows carrying away detritus of any grain size.

### 2.1.2.2 *Depositional model*

The case study of the Topolia alluvial fan complex provides a sedimentologic model for alluvial fans fed by huge masses of clastic material. The Topolia alluvial fan complex was formed by debris-flow deposits and waterlaid deposits derived from a catchment in the south, which was underlain predominantly by limestone and dolomite rocks, which formed a piedmonts flanking mountain range.

The debris-flow facies consists of very poorly sorted, matrix-supported, pebble, cobble, and boulder gravel, in general lacking discernible bedding due to amalgamation of the individual debrites and absence of internal fabric. Although Blair & McPherson (1994) stated that the weathering of pure limestone hinders the generation of sediment gravity flows, the Topolia alluvial fan complex demonstrates that the genesis of debrites in catchments mainly underlain by carbonate rocks is possible. The waterlaid deposits of the distal parts of the alluvial fan are attributed to sedimentation from a network of braided distributary channels as observed on active, modern fan surfaces (Koster & Steel 1984) or locally to recessional sheetflooding with non-catastrophic discharge resulting in 'braided-stream-like' coarse gravel lags as proposed by Blair (1999a). The occurrence of clast-supported interbeds in the proximal fan is related to a channel facies consisting of gravel lags concentrated by the local reworking of the debris-flow facies (Blair & McPherson 1992; Blair 1999c). In general, the change from debris flow to fluvial forms is obviously gradational (Johnson & Rodine 1984; Hooke 1987), which seems to be the case for the Topolia alluvial fans, too. In the models described above rapid drainage of a high volume of water is related to heavy rainfalls above the catchment area in an arid to semiarid climate. The same climatic conditions probably apply to the mid-Miocene Topolia alluvial fan complex.

The Topolia alluvial fan complex, characterized by a piedmont setting beneath a mountain range, is considered to be derived from a multi-point source draining a catchment area in the south (Figure 8). It displays a typical half-graben geometry maintained by continuous extension. The thickness of this clastic wedge decreases towards the north, with decreasing dip of strata and decreasing grain size, corresponding to the direction of transportation from south to north (Figure 9). The coarsest deposits, some with boulders and blocks, are close to the catchment. Farther from the mountains the deposits are finer. Roundness of clasts increases with increasing distance of transport. The thickness of the Topolia alluvial fan complex is estimated to be more than 500 m giving evidence of high sediment support by the catchment and of longlasting extension tectonics resulting in a high structural relief. On the basis of the outlined depositional model, the mid-Miocene basin fills (breccio-conglomerates) in the Sirikari-Topolia-Kakopetros region are classified as fanglomerates.

Field and laboratory studies, including SEM- and CL, revealed intense compaction and cementation after deposition.

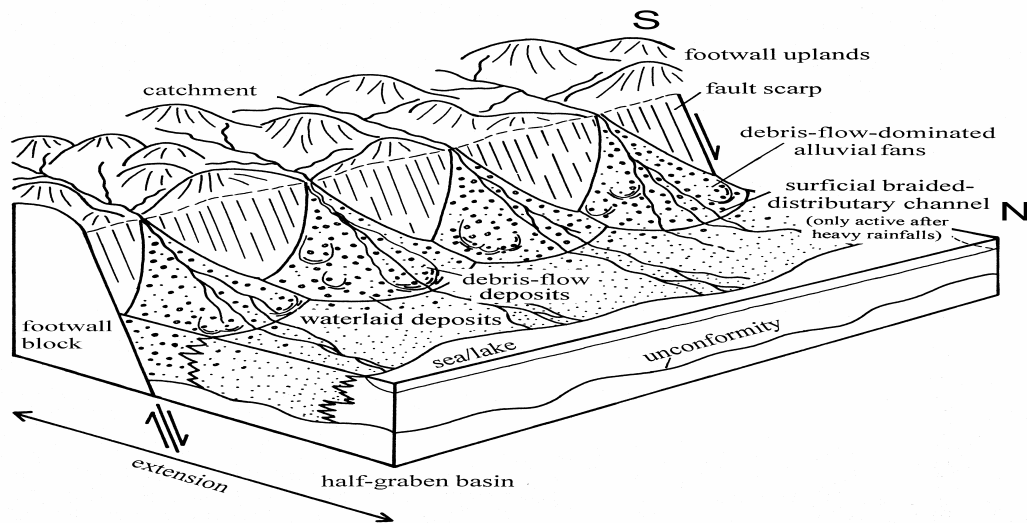
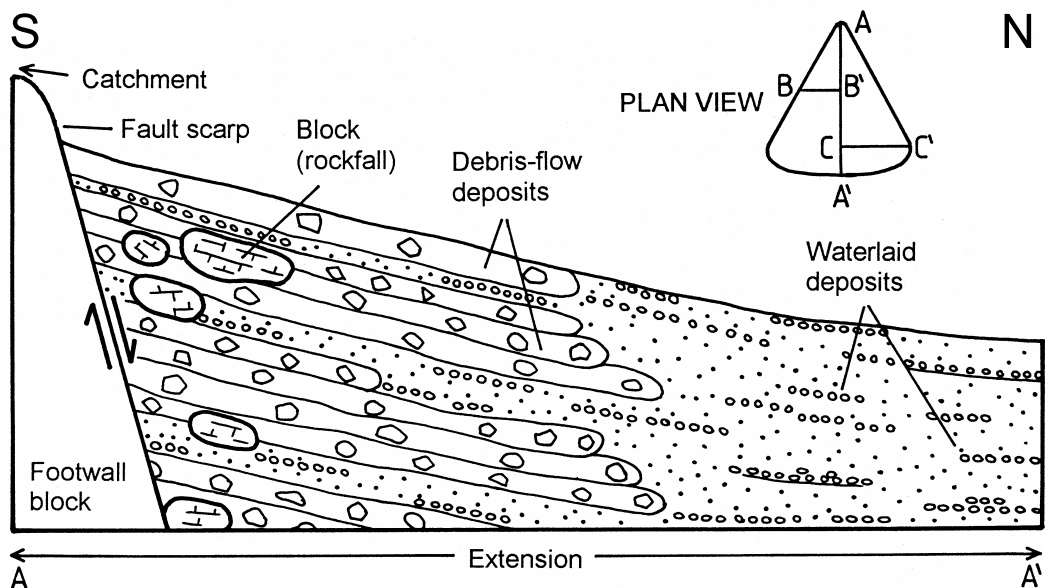
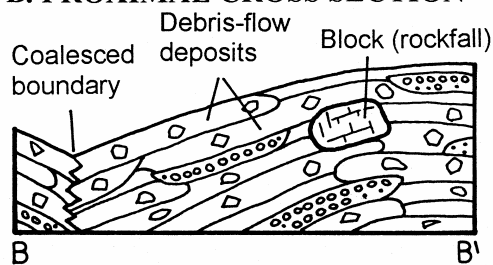


**Figure 8:** Schematic block diagram showing the catchment (drainage basin) and the depositional features of the Topolia alluvial fan complex. The sediments are derived from a multi-point source possibly arranged along a fault scarp. The individual fans are dominated by debris-flow processes.

#### A. RADIAL CROSS SECTION OF TOPOLIA ALLUVIAL FAN



#### B. PROXIMAL CROSS SECTION



#### C. DISTAL CROSS SECTION

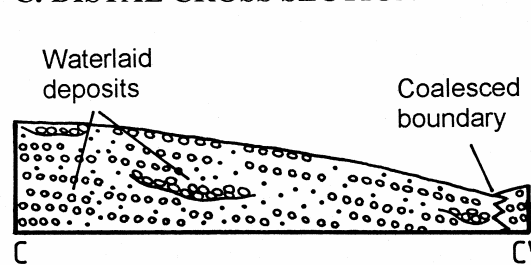


**Figure 9:** Vertical sections of the Topolia alluvial fan complex depicting facies and stratigraphy for: (A) a radial cut; (B) a proximal cross-fan cut; (C) a distal cross-fan cut.

### 2.1.3 Lissos coastal alluvial fan complex

A partly marine depositional environment is identified for the basin fills in the southern working area. There, a thick fault scarp or range-related wedge of sediments exists, including terrestrial and marine debris-flow and turbidite deposits.

The Lissos coastal alluvial fan sequence consists of olistoliths, breccias, conglomerates, sandstones and mudstones. Based on grain size and sedimentary features several facies types within the submarine deposits can be distinguished. The deposits are grouped into different facies and facies associations. Facies A is represented by subaerial alluvial fan deposits, facies B by submarine sediments of the steep-faced depositional lobe and facies C to H by deposits of the basin plain.

#### 2.1.3.1 *Sedimentary facies*

##### ALLUVIAL FAN

##### **Facies A (alluvial fan deposits)**

The sediments of the alluvial fan body in the area of Lissos and Paleochora are very similar to those observed in the region of Topolia. Therefore, we can dispense with the detailed description of the different facies types.

Typical waterlaid deposits occur in the region of Paleochora on the western flank of Wigles mountain. Debris-flow dominated alluvial fan deposits occur in the region between Paleochora and the area south of Prodromi. There, the deposits are matrix-supported, unsorted and characterized by amalgamation of the individual debris-flow beds.

##### SUBMARINE SLOPE

##### **Facies B (chaotic deposits)**

This facies is represented by unsorted, disorganized, matrix-supported to matrix-rich conglomerates. Bedding and preferred orientation of clasts is not visible in these rocks. These deposits can neither be related to pure debris-flow deposits because of the lack of bedding even in large-scale outcrops, nor to rockfall deposits because of the abundance of fine matrix material. It is assumed that former sedimentary structures were destroyed by slumping and sliding which commonly occurs in modern fan deltas (Prior & Bornhold 1990; Hwang & Chough 2000). Slumping and sliding may have started in the middle to the upper part of the steep-inclined clastic wedge and propagated upslope.

##### BASE OF SLOPE AND BASIN PLAIN

##### **Facies C (debris-flow deposits)**

This facies is represented by predominantly matrix-supported to matrix-rich, unsorted debris-flow deposits (Figure 10). The clasts are commonly angular to subangular and consist predominantly of greyish-white to dark grey and black dolomite rock and



limestone. Individual beds are amalgamated and therefore are rarely discernible. This facies type can be observed in the region between Paleochora and cape Elides, especially on the Monaprinos ridge. Because of subparallel interbeds of laminated mudstones it is assumed that the sediments of this facies C were deposited in the smooth dipping lower slope.



**Figure 10: Lithified debris-flow deposit near Lissos. The grain size of the clasts shows a great variety. Note lack of orientation of the clasts and lack of bedding. The debris flow is matrix-rich.**

#### **Facies D (olistostromes with olistoliths)**

The olistostromes are characterized by more or less chaotic mixtures of fine- to coarse-grained sediments and olistoliths of block to slab size. These deposits are variable in shape and thickness. Single isolated clasts are embedded in a fine-grained to even coarse-grained, mostly unstacked matrix. In some outcrops along the steep coast in the region of Lissos olistoliths occur which are embedded in a medium- to fine-grained sediment (Figure 11). The olistoliths consist of limestones or dolomites which according to their microfacies can be attributed to the Tripolitza Unit. Some of these limestones contain rudists. The diameters of oversized megaclasts range from several meters to hundred meters. For example, on the western slope of cape Elides limestones with rudists rest as large fragments probably on the Pindos Unit and are covered by conglomerates and sandstones of the synorogenic sediments.

The large oversized blocks are interpreted as olistoliths derived from the catchment underlain by rocks of the Tripolitza Unit. After travelling through the catchment the olistoliths reached the coastal fan and moved downslope. Due to the instability of the smoothly inclined, unconsolidated distal slope, the high-weight olistoliths were transported by gravity sliding within the plastic sediment to the base of the slope, where they finally came to rest. Due to the fact that many of the described facies types are transitional to each other, these large single clasts are sometimes embedded in fine-grained basin-plain deposits (e.g. homogenous dolomite rock sands of facies G).



**Figure 11: An olistolith (> 10 m x 3 m) of grey limestone with calcite veins (lower right) embedded in dark lithified dolomite sands of facies G (upper left). Steep coast east of cape Elides.**

### **Facies E (grain-flow deposits)**

Grain-flow deposits can be observed in the vicinity of Lissos beach. They consist of particles of sand to pebble gravel. The clasts are exclusively derived from dolomite rocks and limestones. These psephites form very thin interbeds (several centimeters) in mudstone or debris-flow deposits.

Grain flows require an environment with ready supply of sand (Einsele 2000). In the working area this sand comes from decomposed coarse (>250  $\mu\text{m}$ ) crystalline dolomite rocks presumably of the Tripolitza Unit. To overcome friction between the grains, a dispersive pressure must be developed which can only be achieved on steeply inclined slopes (Lowe 1976). This view corresponds very well with the fact that Lissos coastal alluvial fan is considered as a steep-sloped fan delta.

### **Facies F (turbidity-current deposits, turbidites)**

Centimeter to decimeter thick sheet-like sandy beds characterized by fining upward, crop out along the steep coast south and southwest of Lissos. At the western flank of cape Elides a succession of fine-grained sediments (Figure 12) of more than 6 m is intercalated in coarse-grained sediment-gravity-flow deposits. These turbidites reflect deposition from sandy turbidity currents. Each individual bed is graded with fining upward. Other internal sedimentary structures, such as Bouma cycles (Bouma 1962), have not been observed.

The fining upward sequences are related to sandy-silty turbidity currents, which originated from slope failure in the area of the (submarine) fan body. In times lacking turbidite deposition, sedimentation of limestones and mudstones took place in the area of the outer fan or the basin plain, indicating a distal setting of this log. This period of deposition of fine-grained material is superseded by debris-flow deposition.

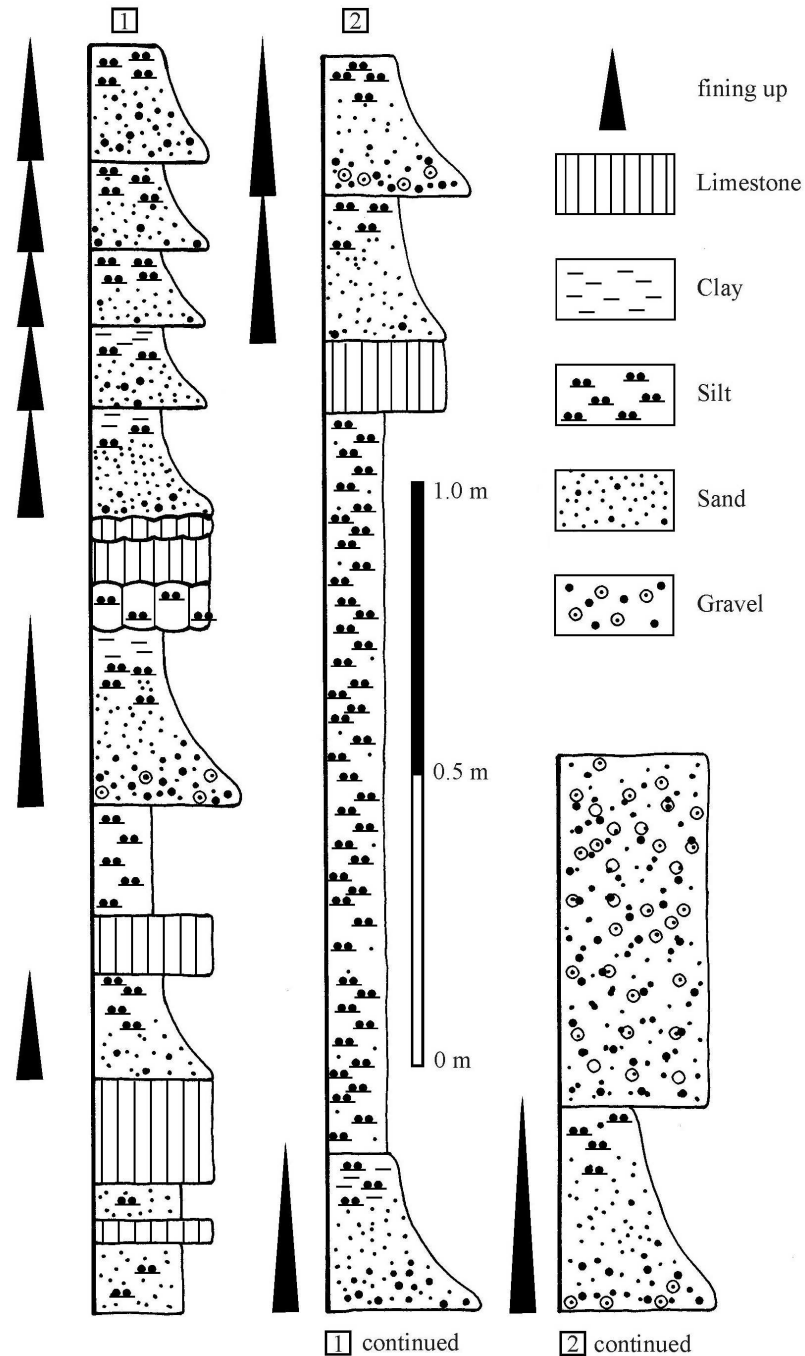


**Figure 12:** Detailed vertical log through a fine-grained sequence of the submarine part of the Lissos fan delta, at the western flank of cape Elides. The column shows a number of fining upward sequences, partly succeeded by limestones or mudstones.

### **Facies G (mudflows to muddy suspension current deposits)**

Mudflow deposits are the dominating facies type in some places, e.g. in the southern part of Lissos bay. The facies is represented by bedded, partly laminated sandstones to mudstones nearly exclusively composed of limestone and dolomite detritus. These rocks show locally extensive bioturbation. In facies G thin beds of coarse sandstones, disorganized conglomerates (debrites) and olistostrome deposits are intercalated.

The sediments of facies G are interpreted as basin-plain deposits. They were deposited by particle-by-particle settling of suspended fine material over a long period of time. Abundant trace fossils also suggest slow suspension fallout (hemipelagic setting). Intermittent sediment-gravity flows, such as fine-grained low-density turbidity currents and coarse debris flows (or even olistostromes), give evidence of a slope-near setting.

### **Facies H (marly limestones and limestones)**

Marly limestones to limestones (Figure 13) are also intercalated in the basin-plain deposits. The limestones display a thickness of several centimeters with colors ranging from white to light reddish. In thin sections the limestones are colorless. The individual limestone layers differ in their grade of lithification. At the top and at the bottom the limestone intercalations are terminated by a sharp boundary separating them from the other facies types.

The limestones of facies H are mainly composed of clear microcrystalline calcite crystals. It is assumed that they represent times of slow sedimentation due to the lack of detritus input by sediment-gravity flows.

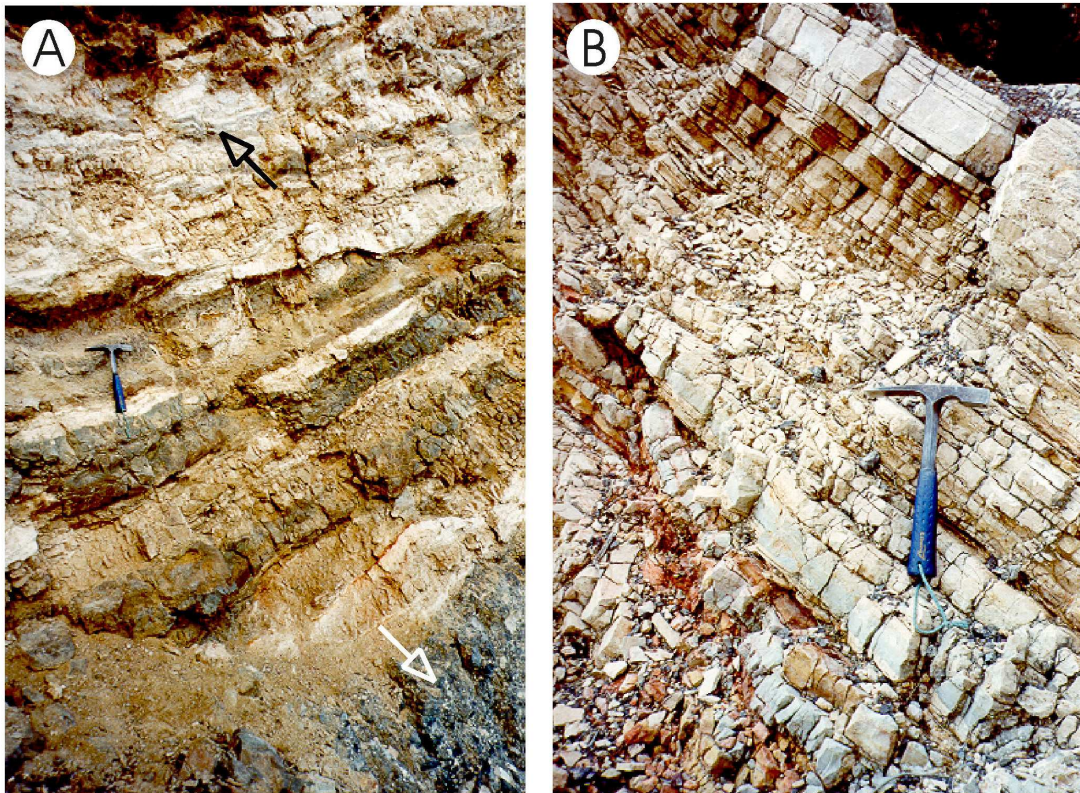


**Figure 13: (a) Succession of different facies types of the distal slope/basin plain. The white arrow points to a debris-flow deposit in the lower part of the section which is succeeded by turbidite deposits (in the middle part). The turbidites are unconformably overlain by porous white limestones (black arrow). (b) Succession of colored marly limestones and limestones.**

### 2.1.3.2 *Depositional model*

The schematic block diagram in Figure 14 summarizes the sedimentary processes and facies types during deposition of the sediments of the Lissos steep-sloped fan delta. It is suggested that the environment was characterized by clastic wedges built up by a multitude of mass flows. Different facies types show interfingering.

Sedimentary facies and the internal structure of the deposits (Figure 15) indicate that the system was formed in alluvial fan, submarine steep-faced slope and basin-plain environments, with typical features of a slope-type fan delta (Westcott & Ethridge 1980).

Ancient deposits displaying random distribution of the different facies classes resulting in irregular facies sequences can be regarded as debris-apron systems (Choe & Chough 1988). Using the classification of Nemec (1990), the terms scree-cone delta or scree-apron delta would also be appropriate for the Lissos deposits. Postma (1990) classifies the alluvial clastic basin influx according to the type of the feeder system. The Lissos slope-type fan delta, dominated by coarse-grained deposits, can thus be attributed to the type A feeder system, which is characterized by a very steep gradient (possibly as steep as 20-30° in extreme cases, Postma 1990, Fig. 2; cf. McPherson et al. 1987, Fig. 5) and can therefore be termed debris cone, representing a special kind of 'Gilbert-type' delta situated at the margin of a deep water basin.

The coastal alluvial fan in the vicinity of Lissos, with its deep water facies, shows a thickness of more than 250 m. It is assumed that the half-graben basin was bound to the north by a mountain range. The sediments were transported from a catchment in the north to the depositional area in the south and were largely derived from a multi-point source, which led to the formation of numerous coalescing fan-delta lobes. In the region of Lissos a large portion of the rocks is nearly exclusively formed by fragments of dolomite probably derived from the Tripolitza Unit.

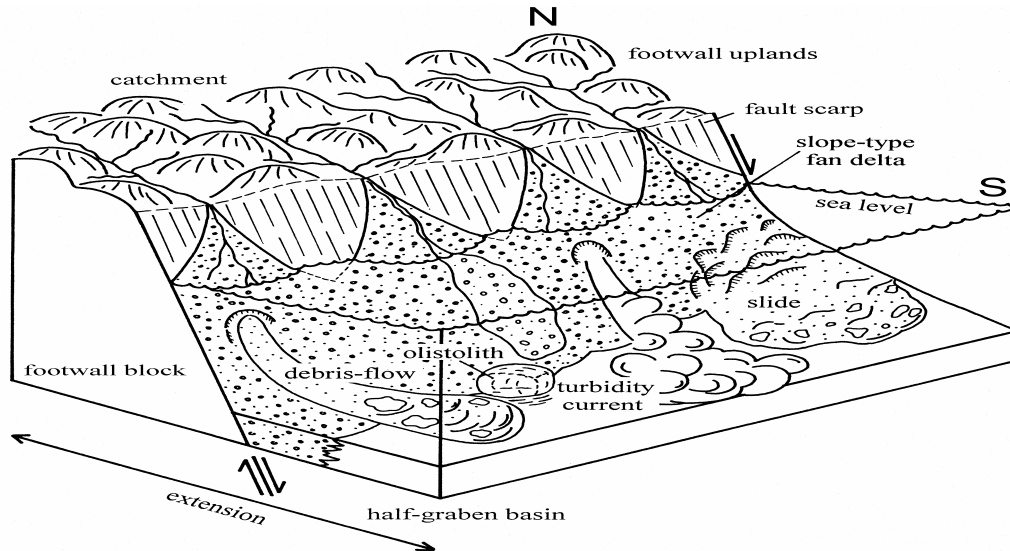


**Figure 14: Schematic diagram showing the mid-Miocene half graben, the catchment and the depositional features of the coastal alluvial fans in the surroundings of Lissos. The upper subaerial parts of the ancient alluvial fans are dominated by debris-flow processes. The lower submarine parts show a variety of slope processes like slides, debris flows and turbidity currents.**

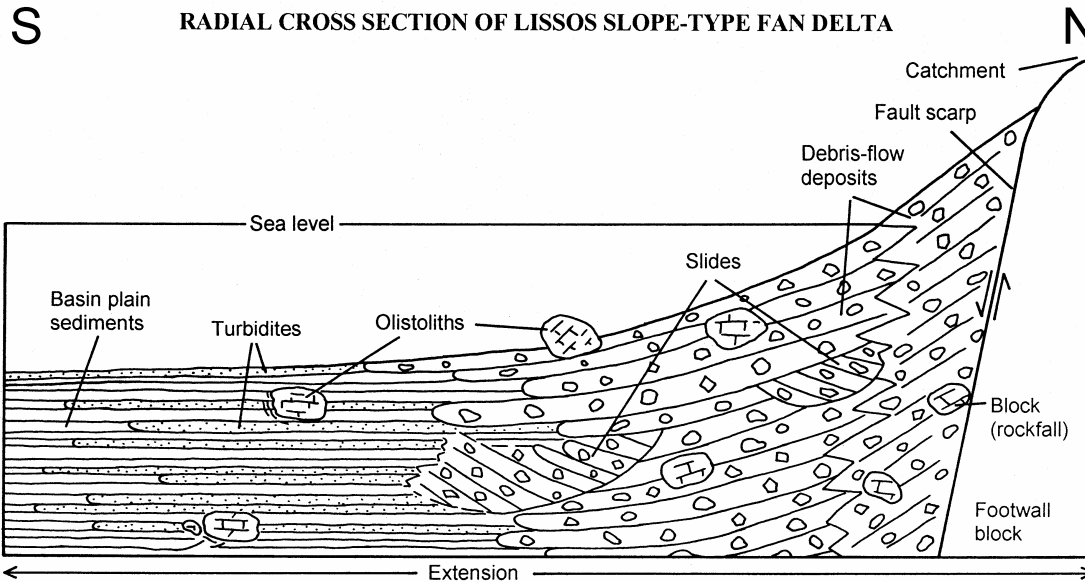


**Figure 15: Simplified radial cross section of Lissos slope-type fan delta illustrating different depositional settings and facies types. Coarse detritus (rockfall and debris-flow deposits) is deposited predominantly in proximal areas, near to the steep-faced slope formed by a fault scarp exposed at sea level. At some locations olistoliths - caused by longlasting sliding processes on the surface of the gentle inclined lower slope - are embedded in the fine-grained distal sediments dominated by a succession of turbidites.**

#### 2.1.4 Fault scarp setting or range front setting?

Two different models are applicable to the depositional setting (Leeder & Gawthorpe 1987; see also Miall 1996, Figs. 11.38 & 11.39) of the mid-Miocene basin fills. Both result in the genesis of half graben filling clastic wedges.

**Model 1: Fault scarp setting.** The clastic sediments were derived from an elevated source area, representing the footwall block and forming a mountain range with a high relief. The sediments were finally deposited on the surface of the sunken hangingwall block forming the half-graben basin. The alluvial fan is related to an active steep fault scarp separating the footwall and the hangingwall (Figure 16).

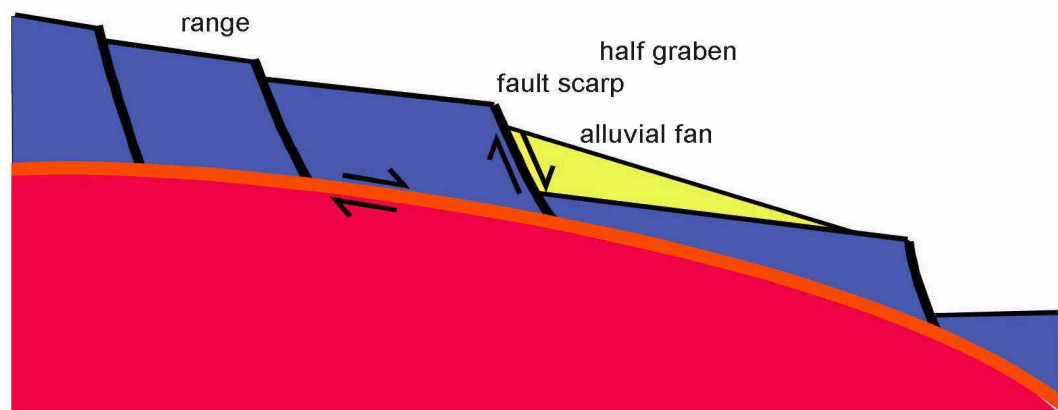


**Figure 16: Schematic cross section illustrating the depositional setting of the Topolia alluvial fan complex. The alluvial fan is situated beneath a fault scarp (model 1). Red: HP-LT units; orange: detachment fault; blue: nonmetamorphic units; yellow: middle Miocene basin fills.**

**Model 2: Range front setting.** The clastic sediments were derived from an elevated large source area, representing the tilted ‘uplifted’ part of the hangingwall block and forming a mountain range with a high structural relief. The sediments were finally deposited on the surface of the ‘subsided’ part of the hangingwall block forming the base of the asymmetric, wedge-shaped half graben. The fan is situated beneath the range front (Figure 17). This type of alluvial fan, displaying deposition on the hangingwall block, is termed hangingwall (alluvial) cone (Leeder & Gawthorpe 1987; see also Miall 1996, Figs. 11.38 & 11.39) forming a debris apron along the base of a mountain (piedmont setting). This model of depositional setting can be found for example on the western side of Death Valley, California, located in the Basin and Range Province of North America.

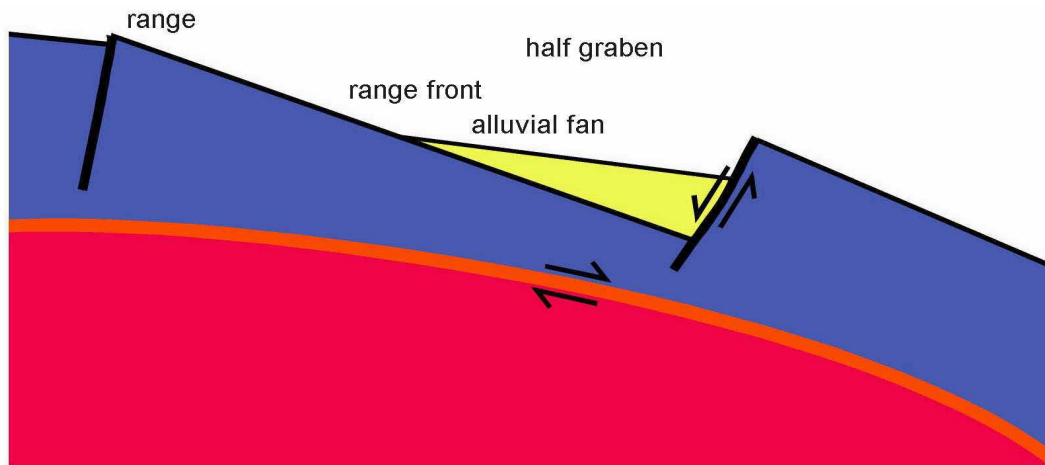


**Figure 17: Schematic cross section illustrating the depositional setting of the Topolia alluvial fan complex. The alluvial fan is situated beneath the range front (model 2). For color code see Figure 16.**

Low-gradient hangingwall dip slopes are the site for broad alluvial cones, while small, coarse alluvial fans prograde from the steeper slope of the footwall scarp (Miall 1996; Blair 1999a & b).

### 2.1.5 Modelling the former catchment area

At present, the air-line distance between the exposures of the Topolia alluvial fan complex in the northern part and the Lissos coastal alluvial fan complex in the southern part is ca. 18 km and the preserved W-E extension of the sediments in both areas is ca. 12 km. On Crete, the neotectonic stage is characterized by N-S and W-E extension. Thus, it can be assumed that the sediments of each half-graben basin were derived from a catchment that was at most ca. 9 km long (N-S direction). Assuming a multi-point source, we can conclude that there were at least three alluvial and coastal alluvial fans, respectively, arranged along a W-E-trending fault scarp referring to model 1 or a mountain range referring to model 2. The fans coalesced with each other and spread in the same direction, namely to the north and to the south, respectively (Figure 18). One can conclude that the catchment size of every individual catchment - according to the above data - is 36 km<sup>2</sup>, supposing a length of ca. 9 km and a width of ca. 4 km. Generally, the catchment areas of modern alluvial fans vary from less than 0.1 km<sup>2</sup> to more than 10000 km<sup>2</sup> (Hooke 1967; Kostaschuk et al. 1986; Damanti 1993).

Comparing the Cretan fanglomerates with recent alluvial fans known from Death Valley (e.g. Blair 1999a & b), one has to realize, that there the catchment is twice to fivefold larger than the catchment area assumed for the individual fans in western Crete. The Death Valley fans described by Blair (1999a & b) cover an area of 27 km<sup>2</sup> (Anvil fan) and 32.6 km<sup>2</sup> (Warm Spring fan). They have a radial length of 9.7 km and 8.1 km, respectively. These numbers are very similar to those assumed for the Cretan alluvial fan complexes. The radial length of the Topolia alluvial fan complex is at least 8 km,



whereas the radial length for the Lissos coastal alluvial fan complex is at least 3 km. The apex of the mass-flow dominated Topolia alluvial fans can be calculated to have been at least 550 m above the valley floor. This figure is based on an assumed slope gradient of about  $4^\circ$ , an average value for such fans (see McPherson et al. 1987), and a radial length of the fan of ca. 8 km. For both fan complexes, a catchment relief of about ca. 2000 m is assumed according to values known from Death Valley (see Blair 1999 a & b). This poses the problem, that in western Crete the Tripolitza Unit together with the Pindos Unit today reach a thickness of some hundred meters only. It is therefore unlikely that these units – judging from the current situation - were able to form such a structural relief. At least part of the thickness reduction can be explained by tectonic erosion (along the detachment fault) of the Tripolitza Unit from the base upwards. Another explanation is, that originally there were additional geological units on top of the Pindos Unit, which are now completely eroded. Components in the synorogenic sediments displaying an exotic lithology may represent remnants of those units.

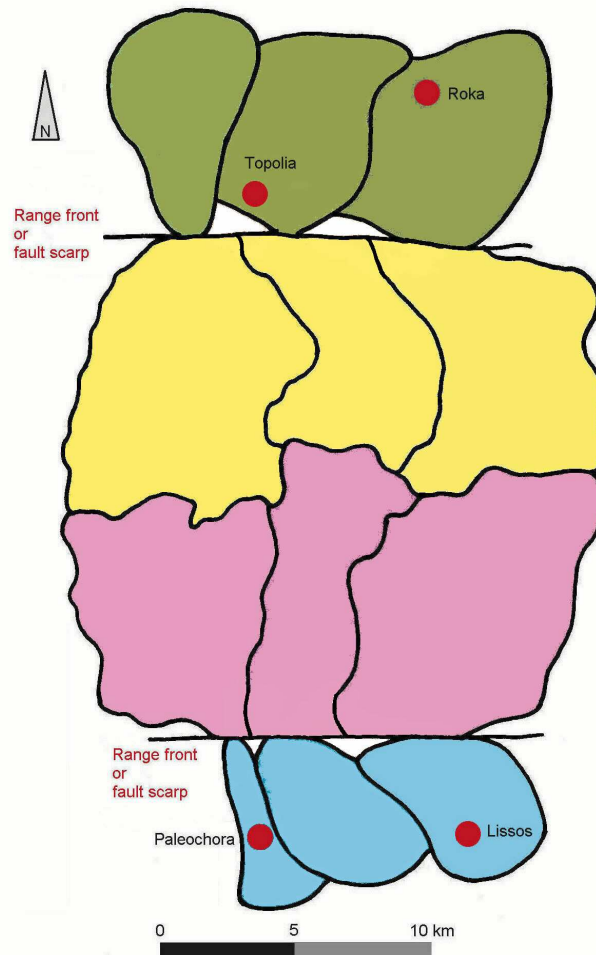


**Figure 18: Paleogeographic model at the time of deposition of the two clastic wedges. The sediments were derived from catchments draining the range to northern and southern directions and forming a multi-point source. Catchment of the Topolia alluvial fan complex in yellow, fan deposits in green; catchment of the Lissos coastal alluvial fan complex in red, fan deposits in blue. Exposed fault scarp or range front between the fans in white.**

## 2.2 Diagenetic evolution of the basin fills

### 2.2.1 Introduction

Optical microscopy, scanning electron microscopy (SEM) including an energy-dispersive X-ray analyzer (EDX), electron probe microanalyses (EPMA) and cathodoluminescence (CL) microscopy were used on diagenesis studies. This chapter deals with carbonate cement stratigraphy and gives examples of combining CL microscopy and electron probe microanalyses in order to interpret the cementation and burial history of the clastic basin fills.

Electron probe microanalysis was used for mineral identification and the investigation of the internal structure of calcite cements. It provides also information about the variation of the chemical composition of the calcite cements, which reflects changes in composition of the diagenetic fluids.

CL microscopy of natural cements provides data that can be used to identify diagenetic events of geologic materials in time and space. Carbonate minerals frequently exhibit luminescence. Natural calcite cements often show zonation. In general, it is accepted that the most important activator for the yellow, orange and red luminescence in calcite is  $Mn^{2+}$  and that  $Fe^{2+}$  acts as quencher (e.g. Marshall 1988; Machel & Burton 1991). Luminescence is visible even if the content of  $Mn^{2+}$  in calcite is below the detection limit of the electron microprobe (Miller 1988). Thus, CL is a powerful tool to detect very small amounts of manganese ions substituting  $Ca^{2+}$  in the calcite structure. Differences in the color of luminescence of the calcite cements are related to differences in the chemical composition (activator concentration and activator/quencher ratio).

Concentric zoning of Fe and Mn in calcite crystals is probably related to changes in the redox potential Eh. A decrease in Eh would yield first an increase in  $Mn^{2+}$  followed by a simultaneous increase in both  $Mn^{2+}$  and  $Fe^{2+}$  (Meyers 1991). Figure 19 shows the stability relations among the dissolved species  $Mn^{2+}$  and  $Fe^{2+}$  and the solids  $Mn^{4+}O_2$  and  $Fe^{3+}(OH)_3$  in Eh-pH diagrams.

For detailed information on the fundamentals and applications of cathodoluminescence the reader is referred to Marshall (1988) and Barker & Kopp (1991).

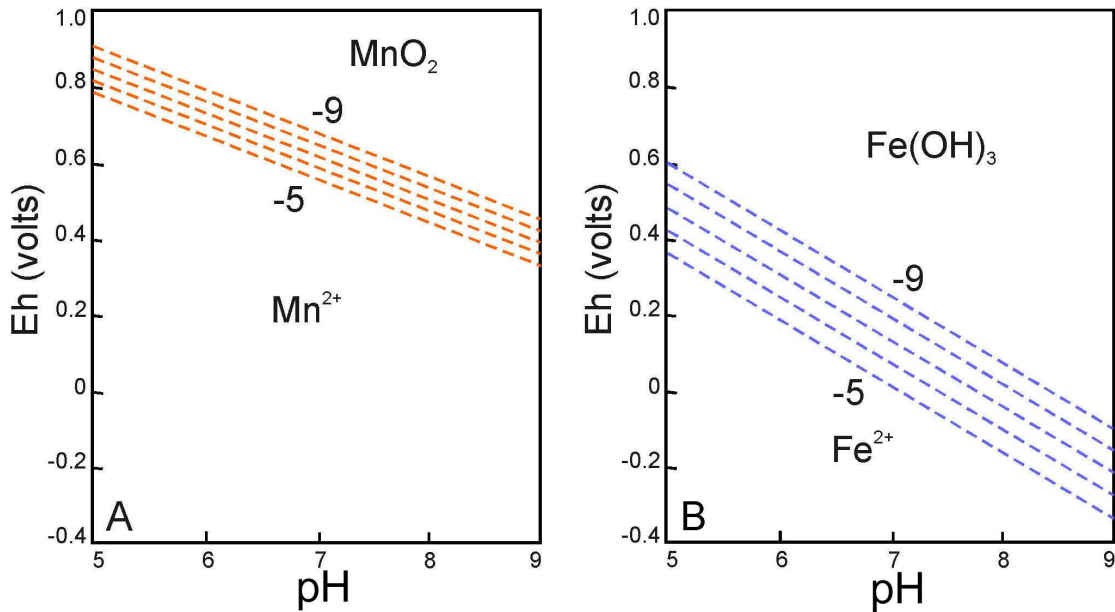


**Figure 19:** Part of Eh-pH diagrams for the systems Mn-O-H and Fe-O-H. (A) MnO<sub>2</sub> [c] and Mn<sup>2+</sup> [aq]. (B) Fe(OH)<sub>3</sub> [c] and Fe<sup>2+</sup> [aq]. Dashed lines, labelled -5 and -9, show field boundaries between solid phases and dissolved species for specified activities of Mn<sup>2+</sup> and Fe<sup>2+</sup> ions from  $a_{\text{Me}^{2+}} = 10^{-5}$  to  $10^{-9}$ . T = 25°C, P = 1 bar (from Machel & Burton 1991).

### 2.2.2 SEM and EDX studies

SEM studies were carried out on broken rock fragments of the Lissos coastal alluvial fan complex and the Topolia alluvial fan complex.

#### 2.2.2.1 Lissos coastal alluvial fan complex

Studies on mudstones of the submarine units yield that the marine depositional setting is also reflected by carbonate cements/crystals which grew in pores of the sediments (Figure 20). A substantial argument for early submarine cementation of the deposits is the ubiquity of dolomite as pore filling mineral.

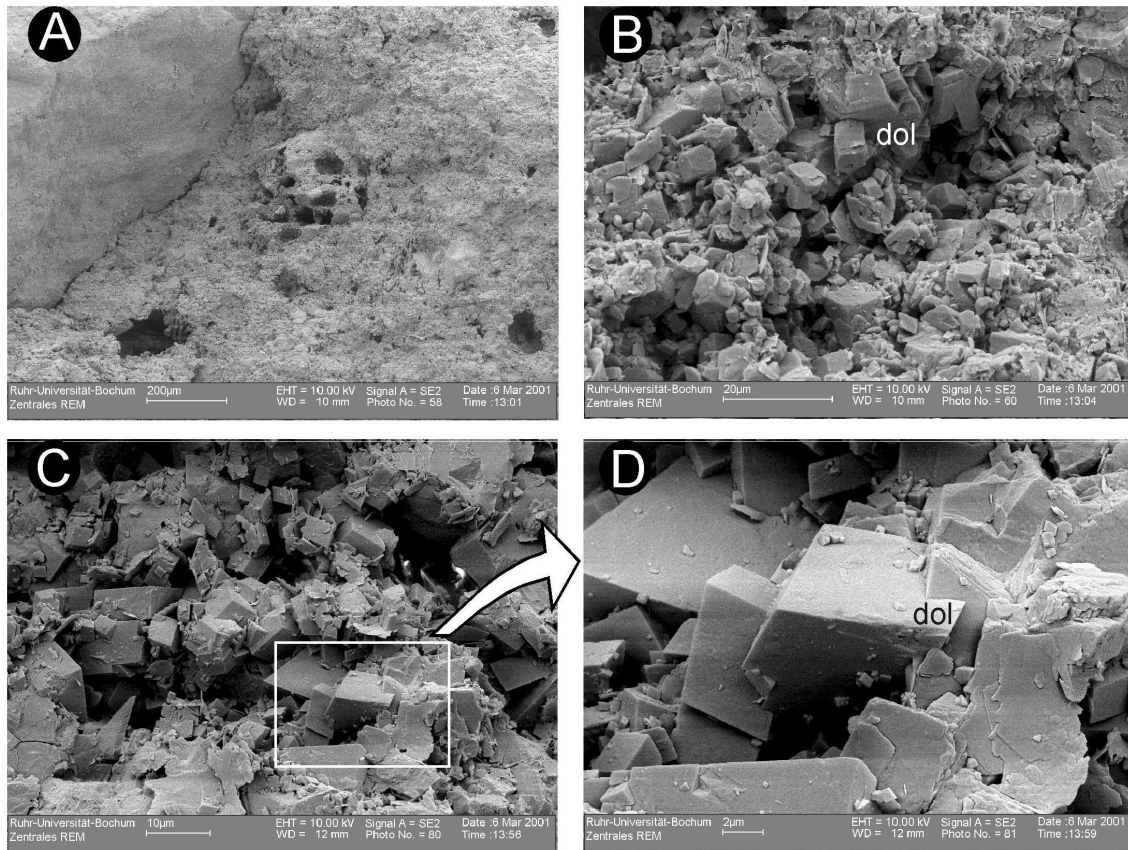


**Figure 20: SEM photomicrographs of marine sediments of the Lissos fan delta complex. (A) Rounded clast (upper left corner) embedded in fine-grained matrix. West of Lissos, M2-177-058. (B) Dolomite as cement in mudstones of the Lissos coastal alluvial fan complex. West of Lissos, M2-177-60. (C, D) Tiny euhedral dolomite crystals in mudstones of the Lissos coastal alluvial fan complex. Papura, M2-53-80, 81.**

SEM studies on sediments of the subaerial part show that the rocks underwent compaction and dissolution-precipitation processes. In the matrix these processes are leading to the loss of pore space accompanied by the formation of polyhedral grains and straight or only slightly curved grain-boundary contacts (mosaic structure) (Figure 21).

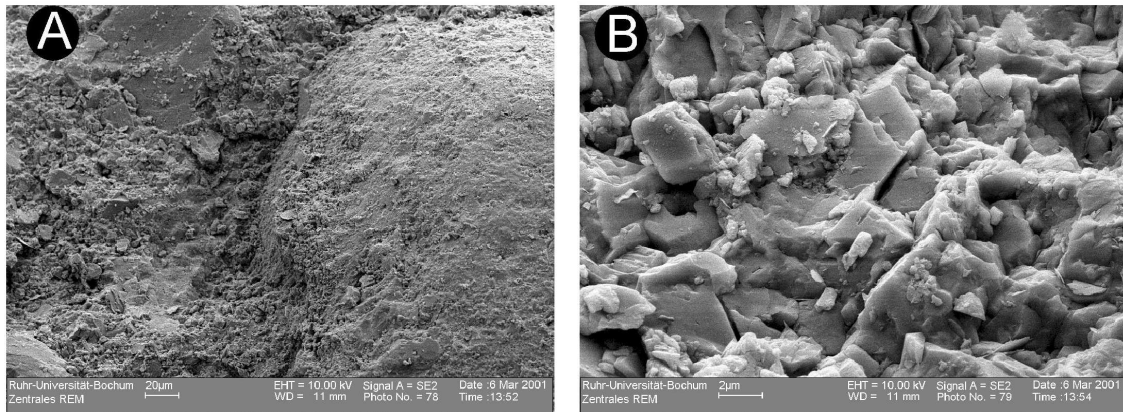


**Figure 21: SEM photomicrographs of subaerial sediments of the Lissos fan delta complex. (A) Rounded clast (right half) embedded in matrix predominantly consisting of calcite, dolomite and sheet silicates. Wiggles mountain, M2-311-78. (B) Calcite matrix of a fanglomerate showing mosaic structure. Wiggles mountain, M2-311-79.**

#### 2.2.2.2 Topolia alluvial fan complex

As described above, the proximal part of the Topolia alluvial fan complex is formed by coarse-grained and matrix-rich debris-flow deposits, which were poor in vugs, whereas the distal fan is formed by waterlaid deposits, which were rich in vugs at the time of deposition. Locally, the clast-supported fanglomerates show sutured contacts between the components (stylolites) resulting from pressure solution during compaction (Figure 22).



**Figure 22: Stylolites in clast-supported fanglomerates of the Topolia alluvial fan complex in the region north of Milia.**

Under the scanning electron microscope the grains of the matrix display a mosaic structure as a result of compaction and pressure solution (Figure 23a-c). Mosaic structure is also typical of the waterlaid deposits of the Topolia alluvial fan complex (Figure 23d-f).

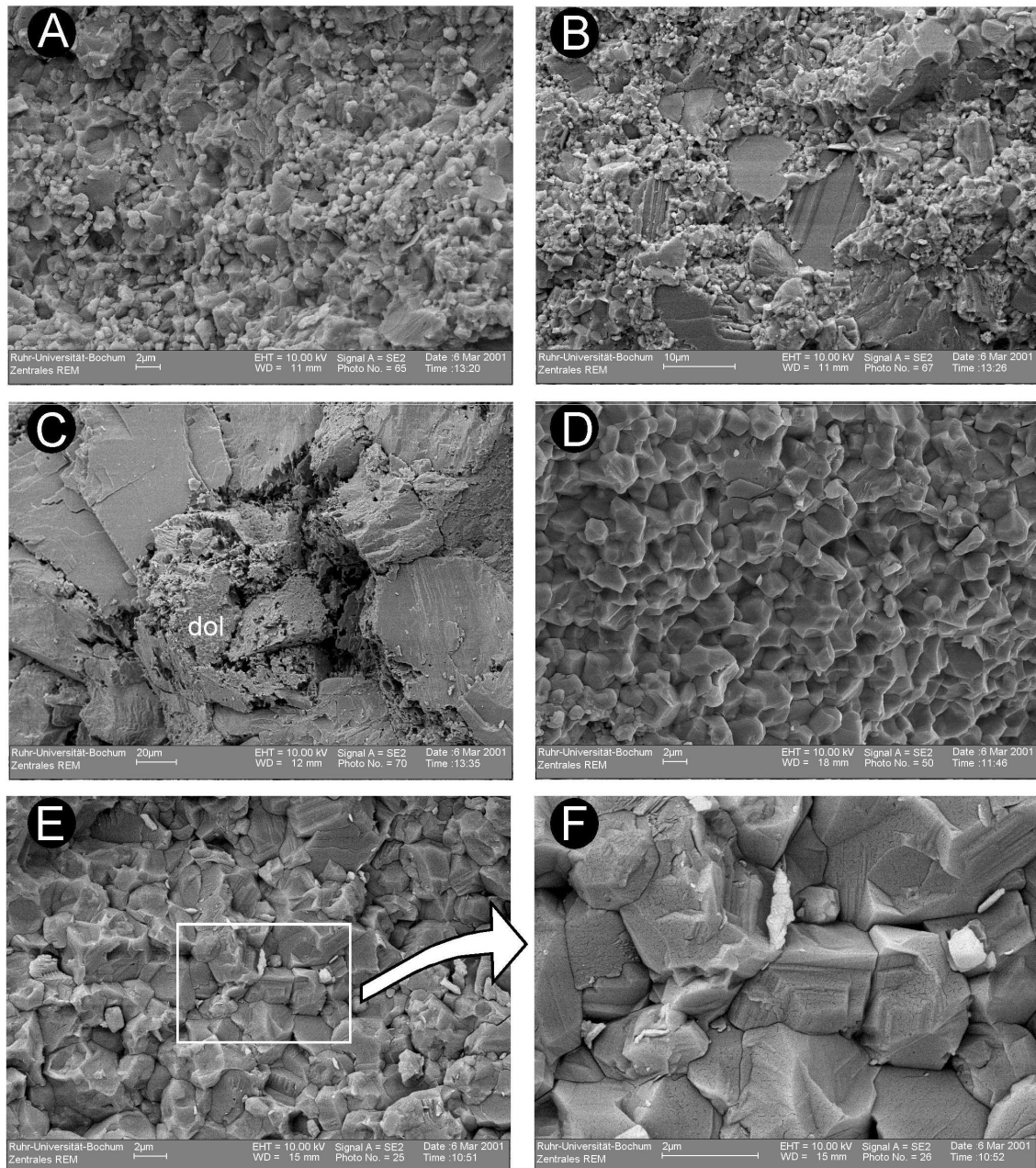


**Figure 23: SEM photomicrographs of the Topolia alluvial fan complex. (A) Fine-grained calcite matrix of a sample from a debris-flow deposit. NW Katsimatado, M2-198-65. (B) Matrix of a sample from a debris flow showing bimodal grain-size distribution. All particles consist of calcite single crystals (note perfect cleavage of larger crystals). NW Katsimatado, M2-198-67. (C) Matrix of a sample from a debris-flow deposit with weathered dolomite clast. Sasalos canyon, M2-38-70. (D) Sample from a waterlaid deposit showing mosaic structure of calcite. E Roka, M2-219-50. (E, F) Sample from a waterlaid deposit with mosaic structure. The calcite crystals show zonation as a result of dissolution/precipitation processes. Roka, M2-326-25, 26.**

### 2.2.3 Cement stratigraphy

In the following the results of the investigations on calcite cements of the fanglomerates of the Topolia alluvial fans are presented. Optical and CL-microscopy show that the individual grains are coated by several generations of calcite. Compositional zoning of calcite crystals, reflecting changes in the physico-chemical conditions, records the diagenetic history of the basin fill (Figure 24 - Figure 27).

In spite of generally low to very low contents of Mg, Fe and Mn derived from microprobe point analyses ( $\text{MgO} < 0.5 \text{ wt\%}$ ,  $\text{FeO} < 0.07 \text{ wt\%}$ ,  $\text{MnO} < 0.02 \text{ wt\%}$ ), microprobe mapping reveals chemical zonation of the calcite cements.

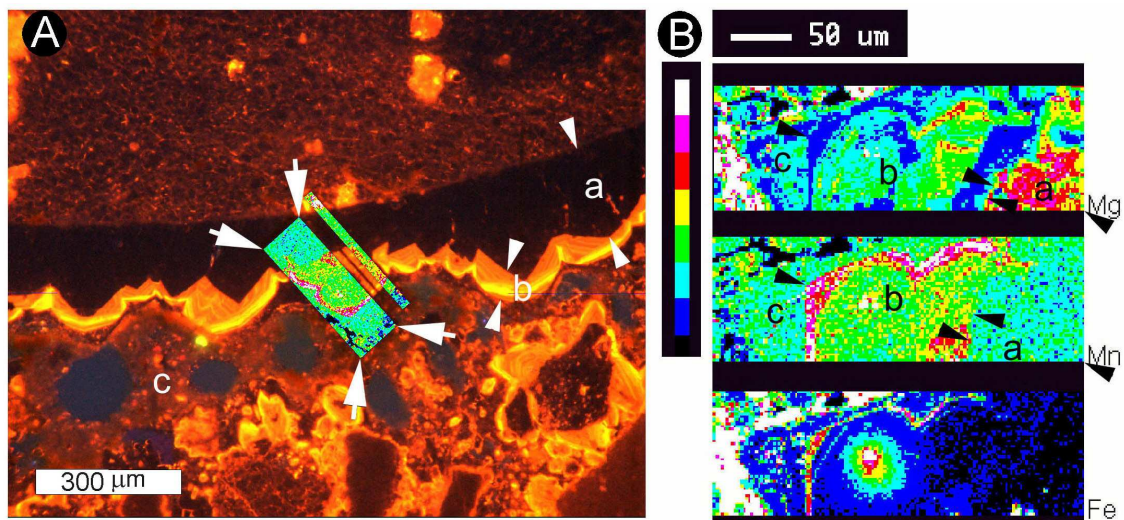


**Figure 24:** (A) Cathodoluminescence photomicrograph of calcite cement in a sample from the Topolia alluvial fan complex. A well-rounded limestone clast (upper part of the photomicrograph) is coated by two different generations of cement. A first nonluminescing generation a of meteoric vadose cement (microstalactitic cement) is followed by a second orange to yellow luminescing generation b which precipitated during deep burial diagenesis (meteoric phreatic). Concentric zoning corresponds to compositional variations and reflects successive changes in the chemistry of the diagenetic fluids. The younger calcite generation b is covered by vadose silt c (lower part of the photomicrograph) giving evidence of subaerial exposure of the rock afterwards. (B) Elemental maps of the area which is marked by white arrows in figure A. Pink to white colors correspond to the highest and blue to violet colors to the lowest elemental concentrations (high Mg and Fe concentrations on the left of the elemental maps are caused by the synthetic resin used for preparation of thin section). Cement generation a shows slightly higher Mg contents, Mn and Fe concentrations are higher in cement generation b. The yellow to red spot in the Fe map represents an iron-rich inclusion. NNW of Mesavlia, M2-241.

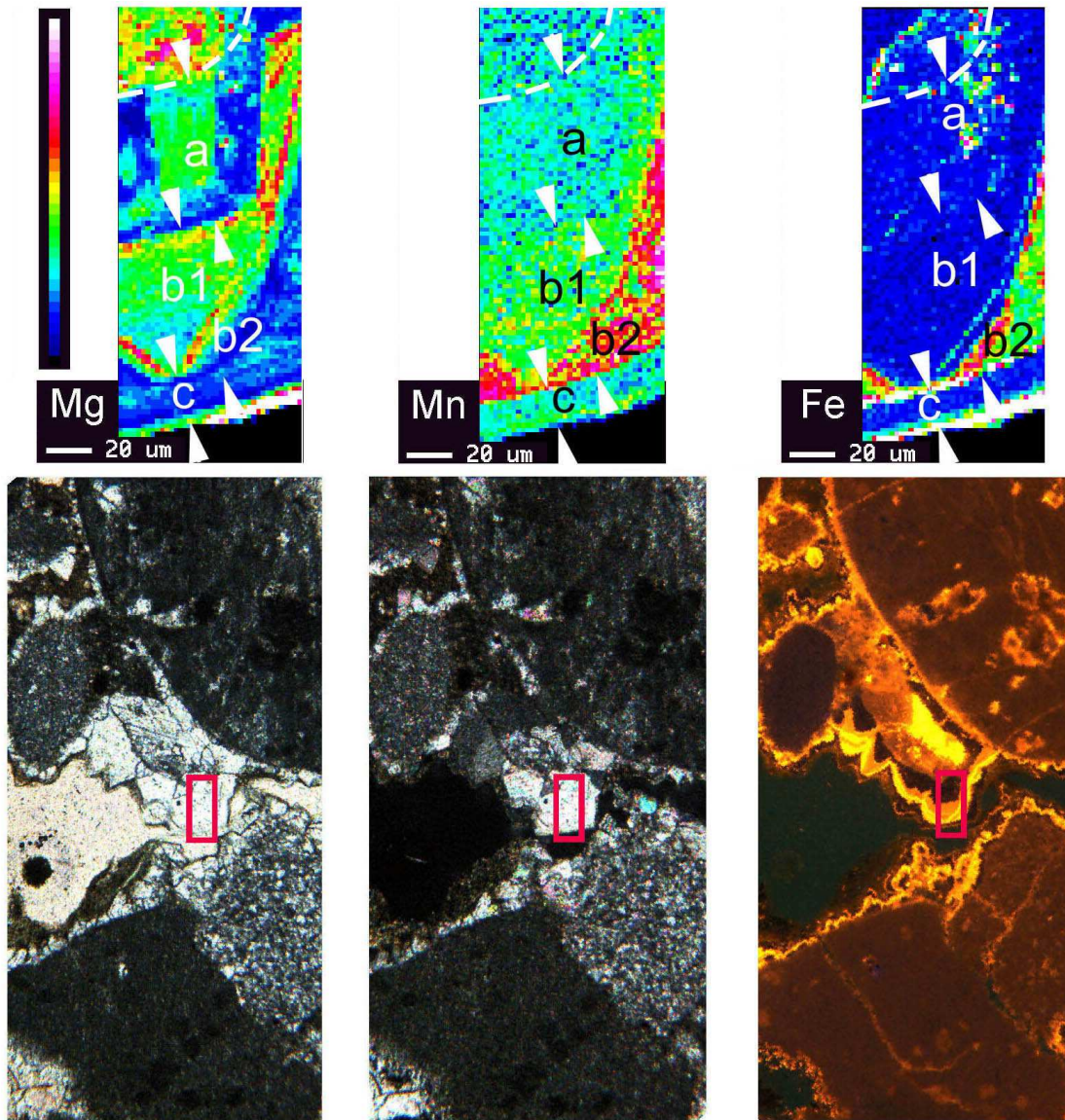


Figure 25: Elemental maps and photomicrographs of calcite cements in a fanglomerate sample from the Topolia alluvial fan complex (at the bottom: photomicrographs with PPL left, XPL middle and CL right; at the top: elemental maps of the area which is marked in the photomicrographs). Three generations of calcite cement can be distinguished. The first nonluminescing generation of meteoric vadose cement (a) shows local increase in Mg (color code as in Figure 24). This type of cement is only developed on the bottom side of the clasts and represents microstalactites (dripstone cement, gravitational cement). The second yellow luminescing generation of meteoric phreatic cement (b) can be subdivided into two concentric zones. The inner zone (b1) shows a slight increase in Mn. The outer zone (b2) is characterized by fairly high concentrations of Mn and Fe, reflecting continuous subsidence and deep burial diagenesis. The third generation of meteoric vadose cement (c) with dull luminescence consists of nearly pure calcite and is related to uplift. Local increase in Mg may be explained by the mixing of meteoric and marine waters during transgression in upper Tortonian. NNW of Mesavlia, M2-241.



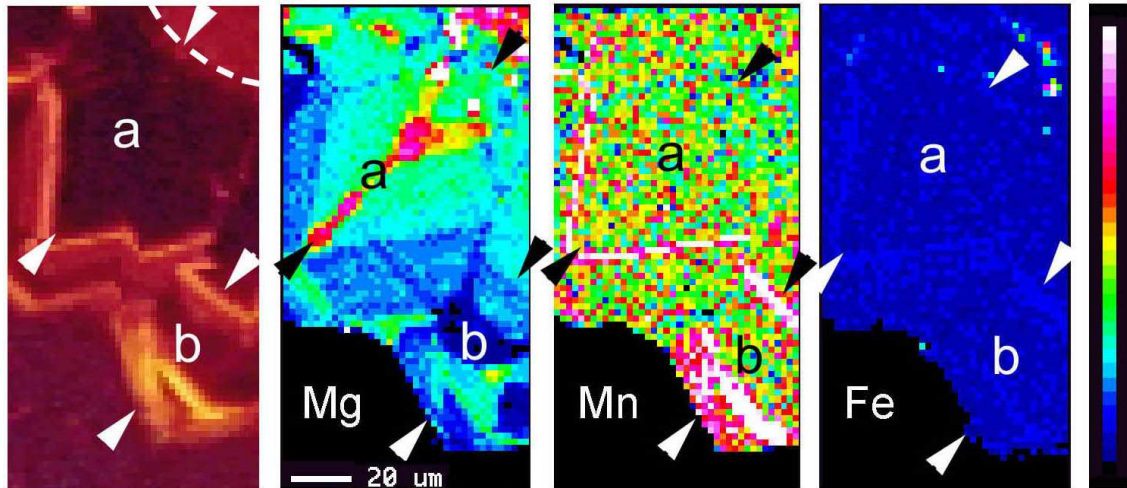


Figure 26: Cathodoluminescence photomicrograph and elemental maps of calcite cement in a sample from the Topolia alluvial fan complex. A rounded clast (upper right corner) is coated by a first nonluminescing generation a of meteoric vadose cement (microstalactitic cement), followed by a second orange to yellow luminescing generation b (meteoric phreatic). The areas of cement b with bright luminescence show increased concentrations of manganese (color code as in Figure 24). Roka, M2-326.

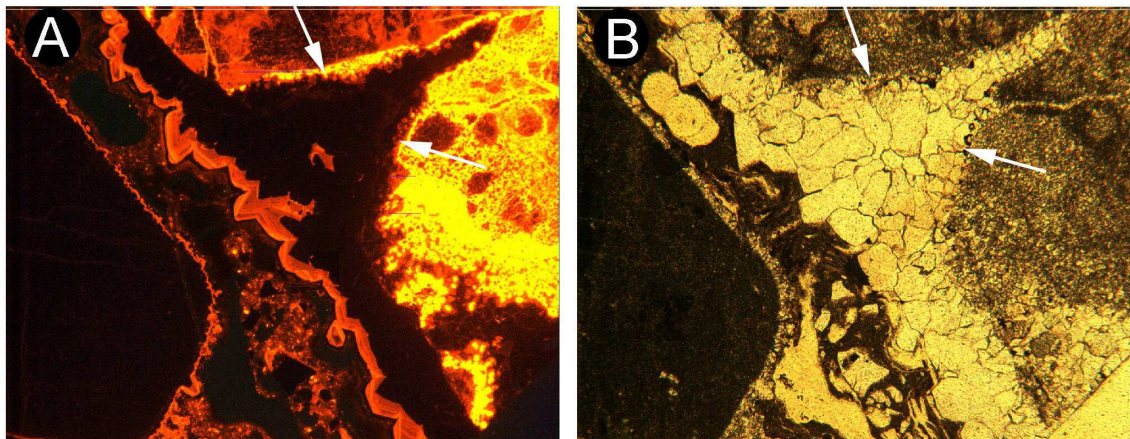
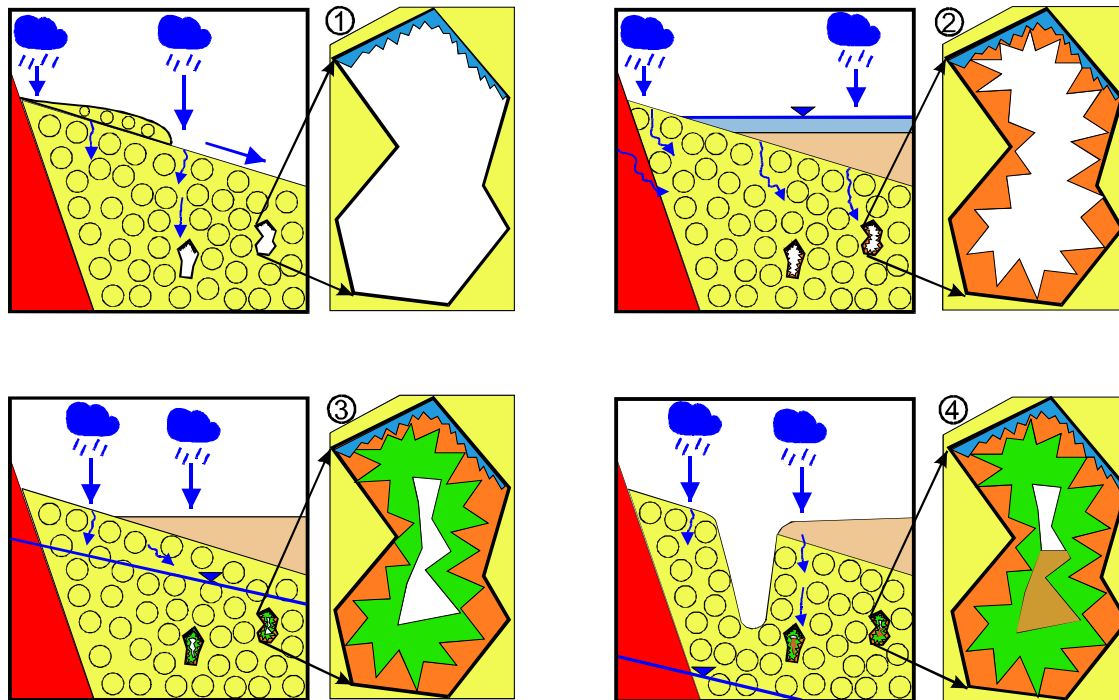


Figure 27: Photomicrographs of meniscus calcite cement in a fanglomerate sample from the Topolia alluvial fan complex (with CL left and PPL right). Meniscus cement (white arrows) fills the space between clasts giving evidence of meteoric vadose setting. The brown band between the calcite cement and the clast at the left consists of vadose silt. NNW Mesavlia, M2-241.

## 2.2.4 Diagenetic evolution of the Topolia alluvial fan complex

Microprobe maps and CL patterns illustrate the diagenetic history of the fan conglomerates. The cement stratigraphy is consistent with the general geological evolution of western Crete in middle to upper Miocene times. The main phases of the diagenetic evolution of the Topolia alluvial fan complex are schematically depicted in Figure 28 and Figure 29.



**Figure 28: Sketch of the diagenetic evolution showing a cross section of the Topolia alluvial fan complex and a magnified vug. The diagenetic history is deduced from combined electron probe microanalyses and CL studies. The different cement generations reflect changes in diagenetic conditions (further explanations see text). Red: basement; yellow: debris flows; blue: first cement generation; orange: second cement generation; green: third cement generation; brown: vadose silt.**

Phase 1, meteoric vadose stage during sedimentation: Debris flows are triggered by heavy rain falls. Meteoric water migrates into the sediments of the subaerial alluvial fan. First generation of calcite cement is precipitated: (Micro-)stalactitic cement on the underside of the clasts and meniscus cement between the clasts precipitates. The ground water level is below the basis of the Topolia alluvial fan complex. Compaction of the sediment starts.

Phase 2, meteoric phreatic stage during burial: Transgression of the sea in upper Tortonian. Ground waters, which may be partly contaminated by marine water, migrates into the sediment. The second generation of calcite cement precipitates. It is enriched in Mn and Fe (reducing conditions).

Phase 3, meteoric vadose stage at the beginning of uplift: Oxygenated meteoric vadose water gains increasing influence over ground and pore waters. Precipitation of the third generation of calcite cement begins. This cement is only partly developed.

Phase 4, meteoric vadose stage (continued uplift) with erosion and carstification: The lithified sediment is accessible to erosion. Rivers cut deep valleys into the conglomerates. Vadose silt is washed into the vugs and covers the last cement generation.

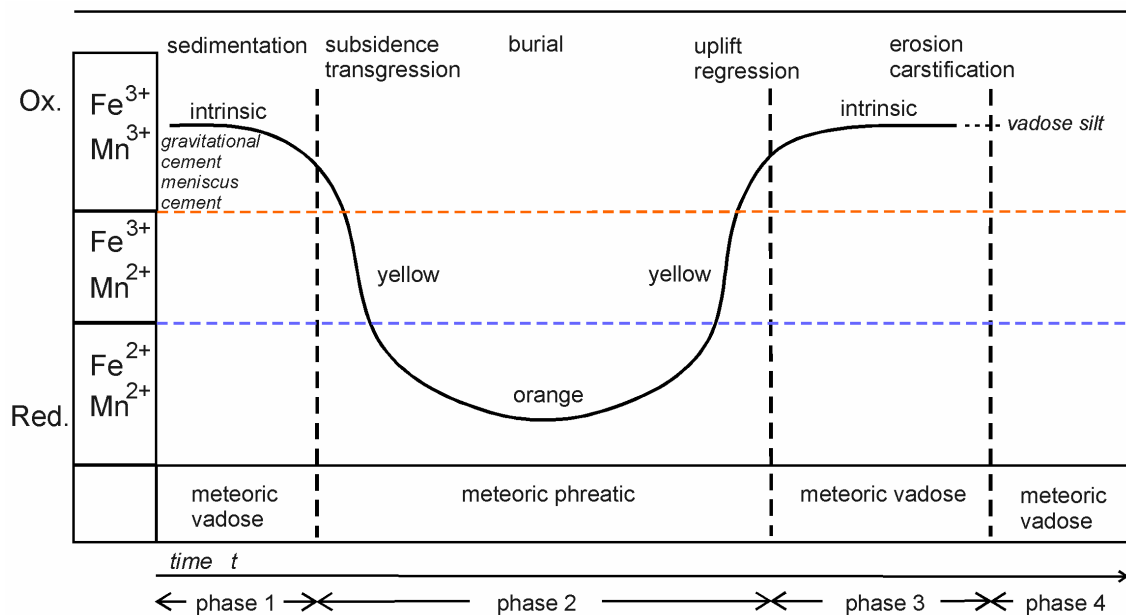


**Figure 29: Schematic succession of cement generations and pathway of tectonically controlled subsidence and uplift of the Topolia alluvial fan complex with hypothetical evolution of pore water Eh during diagenesis (for the dashed red and blue lines see Figure 19).**

## 2.3 Clasts within the basin fills

### 2.3.1 Introduction

The lithologic and petrographic characterization of the clasts in the basin fills is one of the aims of this work. The investigations will give information about the provenance of the clasts and possible variations of the spectrum of clasts in space and time.

There are many localities in the working area suitable for clast studies. At first an overview of the clasts at the different localities is given and then the results of the lithologic and petrographic investigations are presented.

### 2.3.2 Topolia alluvial fan complex

#### *Region Topolia – Katsimatado (Topolia gorge)*

The tough and hard fanglomerates wall the narrow gorge of Topolia between the villages of Katsimatado and Topolia (Figure 30). Topolia gorge (type locality) is an excellent area for studying and sampling clasts embedded in the lithified basin fills.

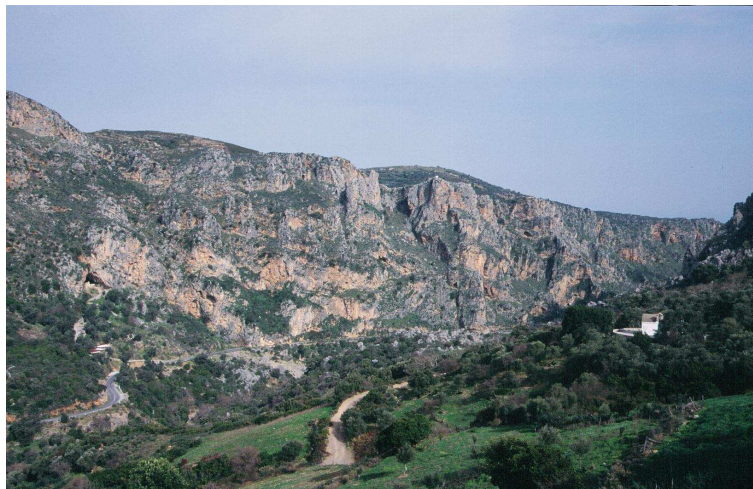


**Figure 30:** View from east of Katsimatado to the northwest in the Topolia gorge. The alluvial fan deposits in the background reach a thickness of more than 500 m. The strata dip with about 50 to 60° to the north.

The following clasts were studied in the section of the Topolia gorge:

Recrystallized limestones: The recrystallized limestones are light beige, beige grey, beige brown or brownish-grey colored, sometimes with a light yellow to pink hue, and partly contain white calcite veins.

Microscopic studies show that the recrystallized limestones are composed of finely to medium crystalline (50 to 150  $\mu\text{m}$ ), inequigranular calcite crystals displaying a polygonal fabric. Enfacial junctions were not observed. Grain boundaries of insular quartz are sutured due to pressure solution. Larger calcite crystals partly show thin twin lamellae. No fossils were found in these limestones. In some clasts different generations of calcite veins and en echelon arranged extension fissures were observed.

Clasts of limestones with fossils: The clasts of fossiliferous limestones are colored in different shades of grey. Their microfacies varies from mudstones (biomicrites) to grainstones and rudstones (biosparites). Some of the clasts contain euhedral dolomite rhombs and stylolites.

Fossils: *Discocyclus* sp., *Nummulites* sp., benthic foraminifers, Corallinaceae (*Pseudolithothamnion* sp., *Lithophyllum* sp.), encrusting foraminifers (*Gypsina linearis*, *Acervulina* sp.), *Operculina* sp., serpulids, fragments of ostracods or decapods, fragments of oysters, fragments of echinoderms, shell fragments.

Partially dolomitized limestones, dolomites and dedolomites: Several clasts of limestones embedded in the breccio-conglomerates show different grades of dolomitization. Some of the clasts of the carbonate rocks are partially dolomitized, others are completely composed of dolomite and others are characterized by dedolomitization.

The color of the partially dolomitized limestones is characterized by different shades of grey. They show idiomorphic to hypidiomorphic dolomite crystals with grain sizes ranging from 250 to 400  $\mu\text{m}$  (Figure 31). In some laminated samples lamination is due to different intensity of dolomitization. In general, the dolomite rhombs are embedded in a very finely to finely crystalline matrix of calcite.

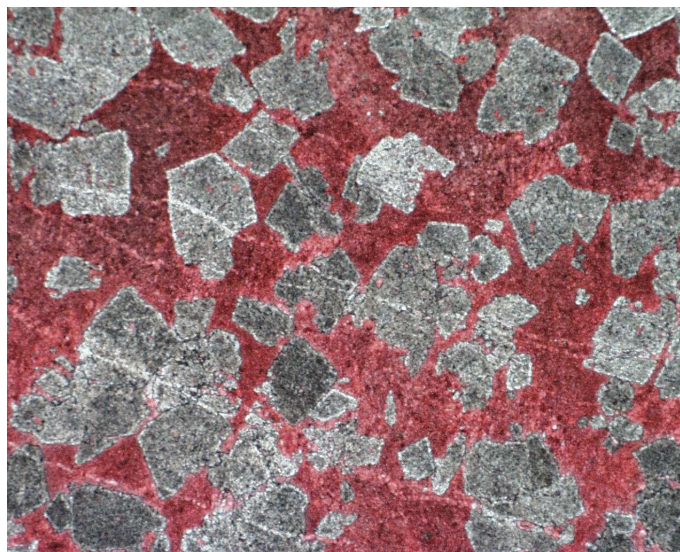


**Figure 31: Photomicrograph of a stained thin section of a partially dolomitized limestone clast with idiomorphic to hypidiomorphic dolomite crystals. 2.6 mm, PPL, M2-23.**

The dolomites are greyish-white and sometimes laminated. The finely grained dolomite crystals form an inequigranular anhedral structure with disseminated ironhydroxides. Lamination is due to variation of grain size and portion of calcite crystals in the various layers.

Two types of dedolomites were observed: The first is a greyish-white, coarse crystalline limestone (dedolomitized dolomite). Former dolomite rhombs are replaced by a mosaic of fine calcite crystals. Only some anhedral dolomite crystals are preserved within the calcite matrix. In one sample the former dolomite rhombs reach a size of up to 1.5 mm. In this case, the rhombs are replaced by single large calcite crystals showing partly concentric zonation. The second dedolomite type is a light brownish-beige to light grey mottled limestone with an inequigranular mosaic structure. Dolomite is replaced by calcite with retention of relic or 'ghost' structure. The initial rock was a partially dolomitized limestone with dolomite crystals up to 250  $\mu\text{m}$  in size. In thin section some quartz was identified as accessory.

Micritic limestones with radiolarians: The sparse to packed biomicrites (wackestones) are light olive-colored to light brownish-beige. The original opaline silica of radiolarians (circular sections up to max. 100  $\mu\text{m}$ , type of Spumellaria) has been replaced by a mosaic of calcite spar. Additionally, sponge-spicules have been identified. Detrital white mica and quartz are present as accessories.

Calcarenites: The calcarenites can be interpreted as turbiditic limestones. They contain ooids (partly surrounded by authigenic quartz), oncoids, fragments of benthic foraminifers and red algae and clasts of chlorite and quartz as well as fragments of sandstones and recrystallized limestones in a sparitic matrix.

Exotic lithologies: At several locations along Topolia gorge pebbles to slabs of carbonate rocks were found which display an exotic lithology. They show strong recrystallization and slight foliation. On the basis of their macroscopic appearance these rocks have to be classified as marbles. They are described in more detail in chapter 2.4.

### ***East of Katsimatado (Lewenties mountain)***

Among components already described above further types of gravel-sized clasts occur in the breccio-conglomerates at this location:

These are biomicrites with rudists (Figure 32), biomicrites with small foraminifers and bryozoans, darkgrey micrites without fossils, biosparites and oosparites (grainstones), limestones with intercalations of chert and skeletons of radiolarians, marly limestones, recrystallized limestones, dolomites and sandstones. In the fine-grained matrix of the breccio-conglomerates small fragments of quartz and phyllites were found.

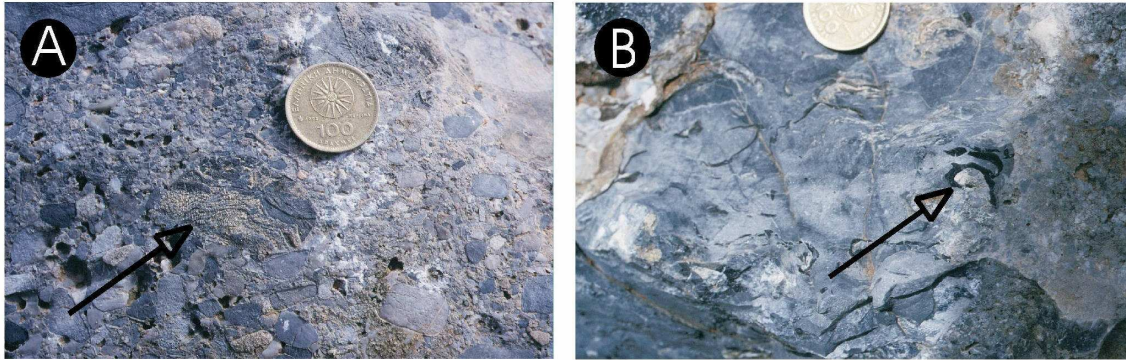


**Figure 32: (a) and (b) Clasts of biomicrites with rudists (arrows) in the sediments of the Topolia alluvial fan complex. East of peak of Lewenties.**

#### *Northwest of Milia (Kria Vrisi mountain)*

In this area beds of clay- to sand-sized carbonate grains are intercalated in the coarse-grained debris-flow deposits of the Topolia alluvial fan complex. They consist predominantly of dolomite clasts. Clasts of quartz, white mica, chlorite and epidote are subordinate. These beds correspond to those observed in Topolia gorge (cf. facies C).

#### *Mountain ridge NNW of Mesavlia*

In the southern part of the mountain ridge NNW of Mesavlia the Topolia alluvial fan complex is composed nearly exclusively of black, grey and white clasts of dolomite rock. In the northern part the conglomerates consist of cobbles and boulders of dolomites, white, beige and light pink limestones, marly limestones, calcarenites, limestones with chert, sandstones, grey cherts and reddish radiolarites.

Some clasts of limestones contain large foraminifers of the middle Eocene and other fossils (Figure 33):

- Biomicrites (pack-/rudstones) with *Discocyclina* sp., *Lepidocyclina* sp., *Asterocyclina* sp., *Nummulites* sp., encrusting foraminifers (*Gypsina* sp. [syn: *Acervulina*], *Sphaerogypsina globulus*), fragments of Corallinaceae (e.g. Peyssonelliaceae), fragments of echinoderms, bryozoans, fragments of oysters, agglutinating foraminifers, shell fragments, peloids (M2-137 a, c d, e, g, h)
- Biosparite (rudstone) with *Discocyclina* sp., *Nummulites* sp., encrusting foraminifers (*Gypsina* cf. *ogormani*), Corallinaceae (*Archaeolithothamnion* sp., *Pseudolithothamnion album*), bryozoans, fragments of echinoderms (M2-137b)

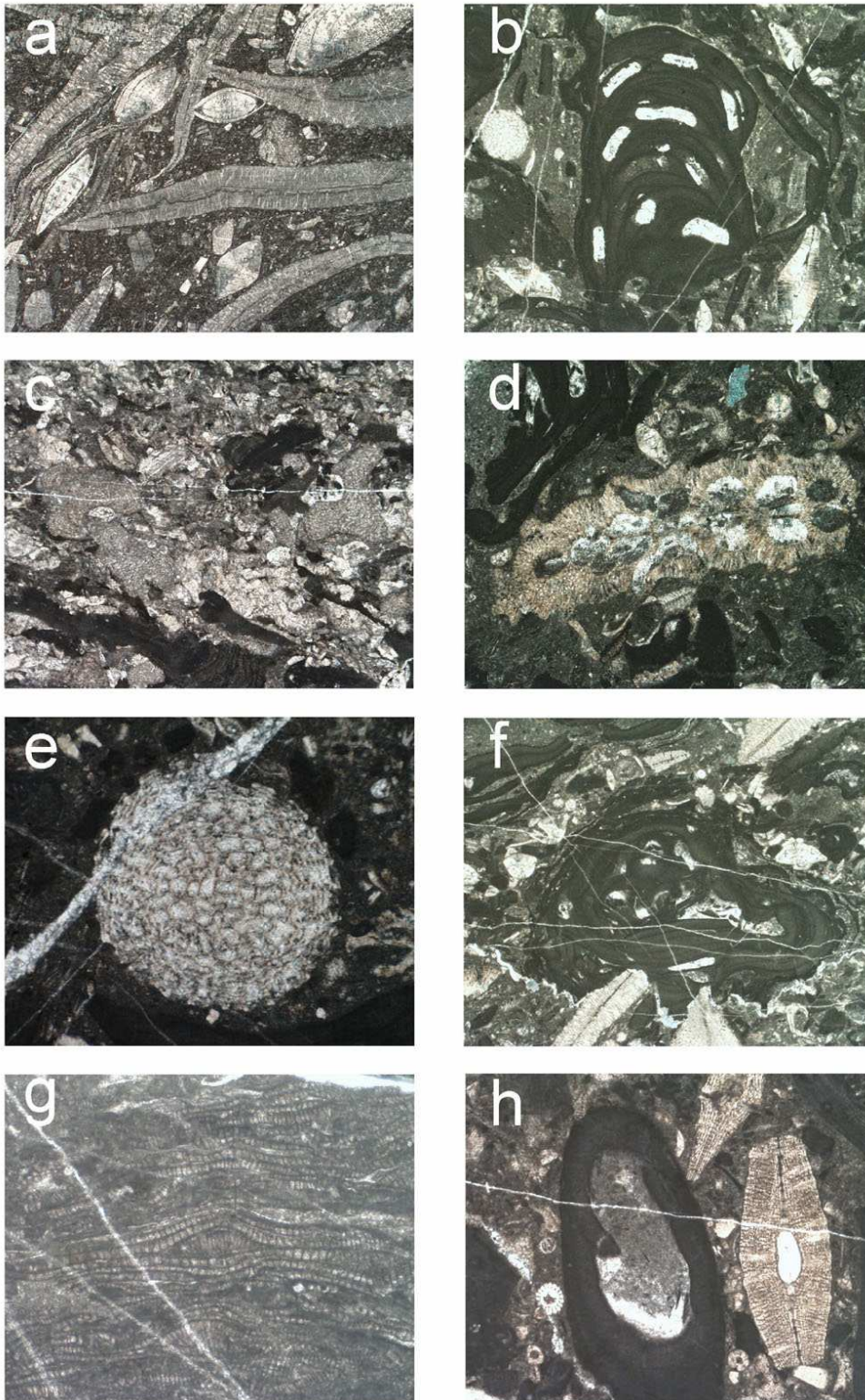


**Figure 33: Photomicrographs of clasts embedded in the Topolia alluvial fan complex, north of the mountain top NNW of Mesavlia. (a) *Nummulites* sp. and *Lepidocyclina* sp.. 11.0 mm, XPL, M2-137. (b) *Archaeolithothamnion* sp.. 5.8 mm, PPL, M2-137. (c) Rudstone with *Gypsina linearis*. 4.5 mm, PPL, M2-137. (d) Bryozoan fragment. 4.4 mm, PPL, M2-137. (e) *Sphaerogypsina globulus*. 2.0 mm, PPL, M2-137. (f) Rhodolith of *Lithothamnion* sp.. 7.4 mm, XPL, M2-137. (g) *Peyssonellia* sp.. 1.9 mm, PPL, M2-137. (h) Spicule of sea urchin, *Lithothamnion* sp. and *Discocyclina* sp.. 3.0 mm, PPL, M2-137.**



### ***Sasalos gorge***

Sasalos gorge is walled by fanglomerates with a grain size ranging from granule to boulder. Circa 20 m south of the bend of the road from Malathiros to Sasalos a block larger than 10 m is embedded in the conglomerates, which consists of a dark brownish-grey limestone (biomicrite). The limestone shows internal brecciation and contains small foraminifers and algae. A paleontologic age determination of the limestone failed.

### ***Southwest of Kakopetros (Fterolakkos mountain)***

In this area the middle Miocene basin fill is composed of clasts of limestones, recrystallized limestones, partly dolomitized limestones, dolomites, dedolomites and micritic limestones with microfossils (e.g. small foraminifers). Fragments of sandstones, radiolarites and cherts were not observed.

In the valley west of Fterolakkos mountain and along the mainroad Floria-Kakopetros (south of the pass) the breccio-conglomerates are underlain by huge fragments of light grey, partly light yellow or light pink colored limestones. These limestones are considered to be outsized clasts within the basin fill.

## **2.3.3 Lissos coastal alluvial fan complex**

### ***Lissos***

In the region of Lissos within the synorogenic sediments those composed of dolomite debris dominate. Huge fragments of limestones with rudists and light pink to yellow limestones occur as outsized clasts. Clasts of chert, sandstones, calcarenites and grains of clastic quartz were not observed in the basin fills of Lissos.

### ***Southwest of Prodromi***

At this locality the clasts of the basin fills predominantly consist of limestones and dolomites. Some of the limestone clasts contain *Nummulites* sp. and *Discocyclina* sp.. Other clasts are limestones with chert, cherts and sandstones. Clastic grains of quartz and white mica and some sand-sized fragments of metamorphic rocks were observed in the matrix.

### ***West of Asfendiles (Patella mountain)***

In this area the clasts of the breccio-conglomerates consist of dolomites, limestones, limestones with small nodules of chert, cherts and sandstones. In the matrix small fragments of metamorphic rocks (quartzites, phyllites) and some clastic grains of quartz, epidote and phyllosilicates were observed.

### ***Northeast of Paleochora***

In the area northeast of Paleochora (between the river Azogirianos and Kakodikianos) the basin fills are built up by conglomerates for which boulders of limestones with *Discocyclus* sp. and *Lepidocyclus* sp. are typical.

### ***Wigles***

Locally, conglomerates occur at Wigles mountain (see geological map). These conglomerates are characterized by high amounts of pebbles of sandstones and exotic rocks (see chapter 2.4).

## **2.3.4 Provenance and distribution of clasts**

All components of the basin fills are derived from the tectonic units on top of the detachment fault. Predominant clasts are lagoonal limestones, biomicrites, biosparites, slightly recrystallized limestones, dolomitic limestones, dolomites and dedolomites with microfacies and fossil assemblages corresponding to members of the Tripolitza Unit (Seidel 1968; Zager 1972; Leppig 1974).

Radiolarites, micritic limestones with radiolarians (pelagic limestones), calcarenites (turbiditic limestones), sandstones, and limestones with chert are restricted. They can easily be derived from the Pindos Unit (cf. Seidel 1971). The same holds good for sand-sized clasts of quartz, phyllosilicates and epidote and fragments of metamorphic rocks (Cretaceous and Tertiary flysch).

Clasts derived from the high-pressure/low-temperature metamorphic units below the detachment fault never have been found in the breccio-conglomerates of western Crete (Aubouin & Dercourt 1965 and Kopp & Richter 1983). The provenance of the exotic carbonate rocks is discussed in chapter 2.4.

No variation of the spectrum of clasts in space and time was recognized in the mid-Miocene breccio-conglomerates of western Crete. The bulk of the clasts of the basin fills is derived from the Tripolitza Unit. Components derived from the Pindos Unit are only locally concentrated, but they are not enriched at the base of the synorogenic sediments as would be expected.

## 2.4 Exotic carbonate rocks within the basin fills

### 2.4.1 Introduction

Pebbles to slabs of carbonate rocks of unknown place of origin and age were detected during field work within the breccio-conglomerates and in their neighbourhood. Some of these carbonate rocks show recrystallization and foliation in macroscopic scale already, which leads to the conclusion that the rocks have undergone metamorphism. Due to the lack of metamorphic index minerals an attempt was made to classify the carbonate rocks on the basis of their calcite microstructure. As summarized by Burkhard (1993) the appearance of calcite twins (calcite microstructure) is proposed as an approximate but rapid and easy-to-use geothermometer in low temperature environments. Textural data resulting from electron backscattered diffraction (EBSD) technique complement the dataset. In one case coexisting calcite and dolomite in a dolomite marble were used as geothermometer.

### 2.4.2 Exotic calcite marbles

The rocks described in this section mainly consist of calcite. Slabs of carbonate rocks which partly exhibit slight foliation even in macroscopic scale occur at the mountain crest west of the top of Wigles mountain and on its eastern slope. Furthermore gravel-sized clasts of carbonate rocks which macroscopically look like marbles occur in the conglomerates on the western flank of Wigles mountain and in the southern part of Wigles mountain along the road Paleochora to Koudoura. At two other locations in the northern part of the working area carbonate rocks were detected which resemble the rocks of Wigles. North of the small village Milia outcrops of grey and white, slightly foliated carbonate rocks were found. They rest on rocks of the Pindos Unit and are covered by the breccio-conglomerates. The extend of the occurrence is approximately 25 x 20 x 12 m. In the southern part of Topolia gorge at least 3 large blocks of carbonate rocks crop out partially consisting of fibrous calcite. On the basis of their macroscopic appearance these rocks have to be classified as marbles.

#### 2.4.2.1 *Calcite twins as an easy-to-use geothermometer*

In the following, a brief summary of the geometry, appearance and significance of calcite twins is given. This introduction to calcite microstructure extracts parts from the review article of Burkhard (1993). For a review of EBSD technique the reader is referred to Lloyd (1987, 1994) and Prior et al. (1999).

Twin lamellae are a widely distributed feature in calcites of any type and origin. An individual e-twin can be considered as a zone of perfect simple shear with known shear direction, shear sense and angular shear ( $34.7^\circ$ ). Partial dislocations associated with

e-twinning have the shortest Burger's vector ( $1.27\text{\AA}$ ) and the smallest Peierl's potential of known glide systems in calcite explaining the ease of twin gliding (very low critical resolved shear stress, weak temperature dependence) in terms of dislocation theory (Burkhard 1993). Different types of e-lamellae can be classified according to various criteria. One of these is the thickness of twins, another is the geometry of the twin boundary.

Most authors consider the thickness of twins as function of deformation temperature (Groshong et al. 1984; Rowe & Rutter 1990; Ferrill 1991). The same amount of strain in a calcite grain can be achieved by many thin twins or alternatively by a few thick twins. Possible reasons for the formation of thick twins at elevated temperatures could be the stress dependence of twinning (Burkhard 1993). Sauvagne & Authier (1965) and Barber (1985) suggest, that enlargement of an existing twin - depending on various factors as for instance temperature, shear stress, confining pressure - is easier than the initiation of a new one. The development of larger twins could also be related to minimization of surface energy of the (twin-)grain boundary (Burkhard 1993).

The other important feature is the geometry of the twin boundary. The appearance of curved twin boundaries above ca.  $200^{\circ}\text{C}$  (Burkhard 1993) can be related to intracrystalline deformation (Turner & Orozco 1976) such as r- and f-glide which is strongly temperature dependent (Wenk 1985; De Bresser 1991 in Burkhard 1993). Irregularly shaped, sutured and bulged twin boundaries are a product of twin boundary migration recrystallization (e.g. Vernon 1981) which is also a temperature dependent process frequently observed at temperatures above ca.  $250^{\circ}\text{C}$  (cf. Burkhard 1993).

type	I	II	III	IV
temperature	< $200^{\circ}\text{C}$	150 - $300^{\circ}\text{C}$	> $200^{\circ}\text{C}$	> $250^{\circ}\text{C}$
geometry	- thin twins	- thick ( $>> 1\ \mu\text{m}$ )	- curved thick twins	- thick, patchy
description	- straight	- straight	- twins in twins	- sutured twin boundaries
	- rational	- slightly lense shaped	- completely twinned	- trails of tiny grains
	- 1,2 or 3 sets per grain	- rational	- irrational	- irrational
interpretation	- little deformation	- considerable deformation	- large deformation	- large deformation
	- little cover	- completely twinned grains are possible	- intracrystalline deformation mechanismus (r- & f-glide)	- dynamic recrystallization, grain boundary migration (post deformational)
	- very low temperature	- syn- or post-metamorphic deformation	- syn-metamorphic deformation	- pre- or syn-metamorphic deformation
	- (post-metamorphic)			
	- (late tectonic)			

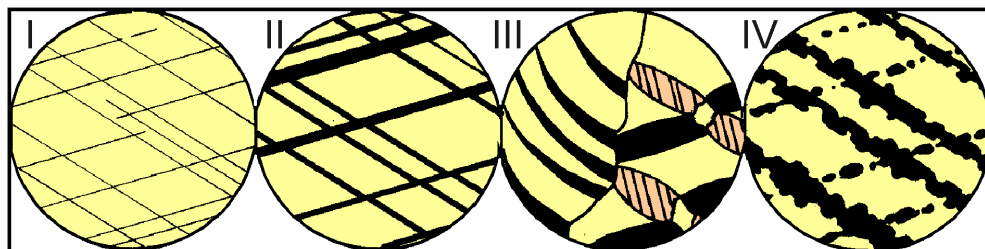


**Figure 34: Classification of twins into 4 categories (type I: thin twins; type II: thick twins; type III: curved twins and twins in twins; type IV: recrystallized twins) according to their appearance in thin section. The 4 different types of twins are distinguished and interpreted in terms of deformation temperature and mechanisms (modified after Burkhard 1993; cf. Weiss 1954; Ferrill 1991 and Passchier & Trouw 1996).**

Due to the fact, that the calcite twin type is thought to be mainly a function of deformation temperature, and only to a minor degree depends on differential stress and/or strain rate, the appearance of calcite e-lamellae (twin type) is thus proposed as a textural thermometer within representative moderately deformed country rocks, excluding major thrust zones and normal fault zones (Burkhard 1993).

Straight narrow lamellae and micro-twins ( $<1 \mu\text{m}$ ) (Figure 34) are typical of very low temperatures where no other slip system competes and where the absence of effective recovery mechanisms prohibits large strains by twinning (type I). Fewer but thicker twins ( $>1\text{-}5 \mu\text{m}$ , type II) appear above ca.  $150^\circ\text{C}$ . From ca.  $200^\circ\text{C}$  to ca.  $300^\circ\text{C}$  curved (bent) twins, twinned twins and completely twinned grains (type III) are developed indicating the progressive importance of other slip systems. Above ca.  $250^\circ\text{C}$  straight twin lamellae are modified into irregular geometries by dynamic recrystallization (type IV).

#### 2.4.2.2 *Calcite textures and microstructures*

Microscopic investigations concerning the geometry of calcite grains and calcite twins were carried out on thin sections and ultra thin sections ( $< 3$  up to  $10 \mu\text{m}$ ) where calcite appears under crossed polars in first to third order colors. The electron backscattered diffraction technique has been used to study the crystallographic orientation of the calcite crystals. These textural observations complement microstructural data and allow a reconstruction of the deformational and the thermal history of these rocks. According to their microfabric two rock types can be distinguished:

Type A: The rock samples partly show a slight foliation which is caused by dark, smooth to wiggly, discrete, anastomosing or parallel stylolites alternating with layers of equigranular calcite crystals with shape-preferred orientation. The angle between the long axis of the elongated crystals and the foliation is ca.  $70^\circ$  (Figure 35a) (cf. Brady et al., *subm.*). The grains are inequigranular with interlobate grain boundaries, which means that they show strong saturation caused by pressure solution and reprecipitation processes (Figure 35b-d). The elongated calcite crystals have no lattice-preferred orientation (Figure 38).

In some cases, the calcite crystals show straight, thick twins, and partly twins in twins. In other grains, twin boundaries are slightly or strongly sutured due to grain boundary migration recrystallization (bulging). The observations show that the microstructure of the individual crystals varies in a broad range from type II to type IV (according to Burkhard 1993). The large crystals show undulatory extinction due to deformation of the lattice leading to the formation of subgrain boundaries (Figure 35e). Locally, domains of fine-grained crystals of inequigranular size occur which show no twinning and which have more regular, smoother grain boundaries. A slight shape-preferred orientation in these domains is related to dynamic recrystallization. Tiny white mica may occur as accessory.

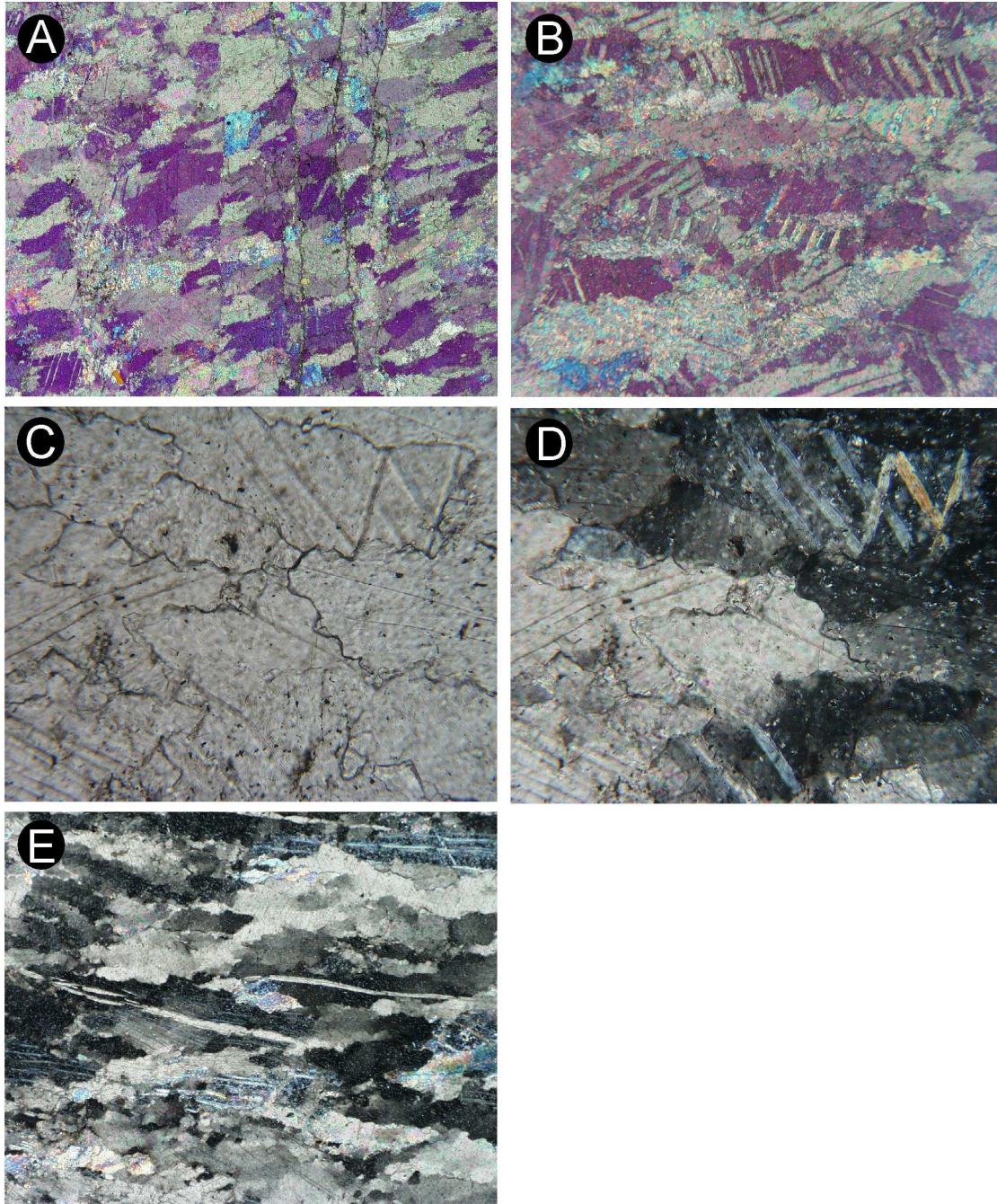


**Figure 35: Photomicrographs of carbonate rocks with type A microstructure in thin section. (A) Carbonate rock with foliation (steep). The calcite crystals show shape-preferred orientation. Angle between long axis of elongated crystals and foliation is ca.  $70^\circ$ . 4.1 mm, XPL with gypsum plate, M1N-189-1. (B) Elongated, intensely twinned calcite crystals with shape-preferred orientation. 1.3 mm, XPL with gypsum plate, M2N-286-1. (C) Twinned calcite crystals with strongly sutured grain boundaries. 0.5 mm, PPL, M2-35-009. (D) Same area as in C, with crossed polars. 0.5 mm, XPL, M2-35-010. (E) Large, strongly sutured calcite crystals with undulatory extinction and shape-preferred orientation. 3.2 mm, XPL, M2-35-005.**

**Type B:** The rock samples exhibit microfolds and only a partly developed, loose cleavage. The samples show a bimodal grain-size distribution with an inequigranular to seriate fabric. Coarse calcite crystals are characterized by  $120^\circ$  triple point contacts with other crystals, interlobate to even amoeboid grain boundaries and undulatory extinction. The larger crystals show also shape-preferred orientation. Lattice-preferred orientation was not observed. The microstructure on the grain scale within type B rocks is characterized by curved thick twins (Figure 36a), twins in twins, and sutured twin boundaries (type III and type IV according to Burkhard 1993). Grain boundary migration recrystallization is observed clearly on thick twins locally leading to destruction of twin lamellae and recovery of the host crystal (see Figure 37d).

In contrast to the strongly sutured grain boundaries of coarse and intermediate grains, smaller grains show polygonal to lobate grain boundaries. These recrystallized ‘matrix’ grains nucleate along subgrain boundaries and grain boundaries (including twin boundaries which can be viewed as grain boundaries with a special geometry). Undulatory extinction in the recrystallized tiny crystals and the smooth transition from these ‘matrix’ grains to subgrains of strongly strained larger crystals give evidence for progressive replacement of the coarse grains by the small ‘matrix’ grains (subgrain rotation recrystallization) (see Figure 37). Bulging of the grains documents grain boundary migration. Both processes are mechanisms of dynamic recrystallization (e.g. Passchier & Trouw 1996). The small grains show no twinning, but a slight shape-preferred orientation, which is characteristic of dynamic recrystallization (Figure 36b). In some rock samples very small plates of white mica were observed.

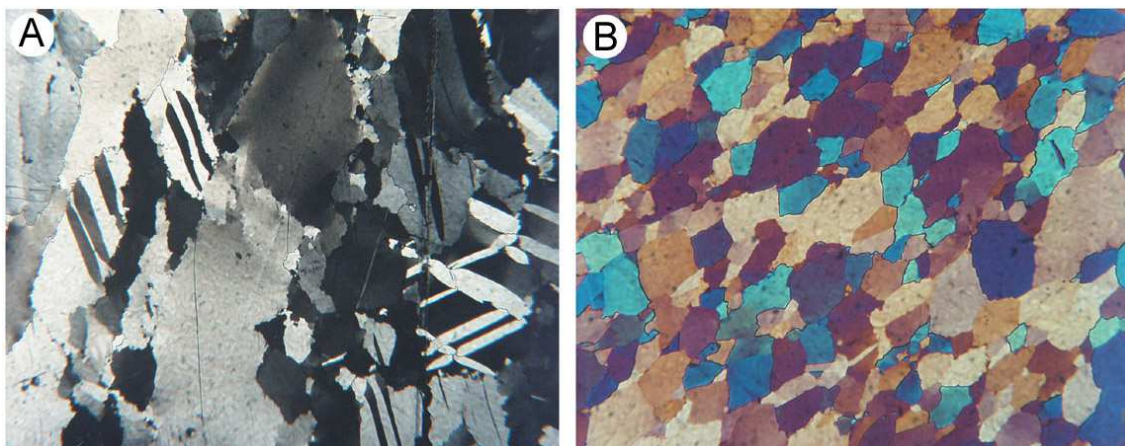


**Figure 36: Microstructure of a sample of a marble in ultra thin (<3  $\mu\text{m}$ ) section. (A) Domain of large twinned calcite crystals with sutured grain boundaries and undulatory extinction. 0.5 mm, XPL, M1-118. (B) Fine-grained matrix of the same sample showing shape-preferred orientation. 0.32 mm, XPL with gypsum plate, M1-118.**

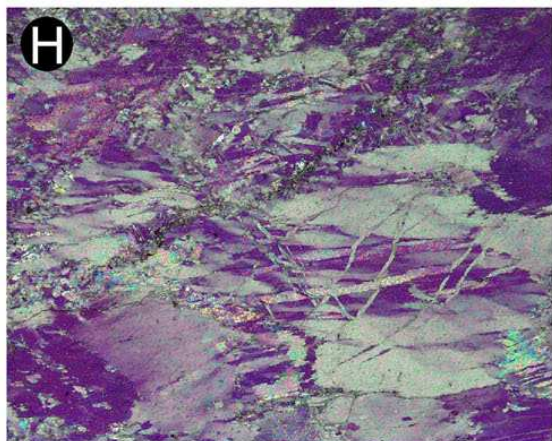
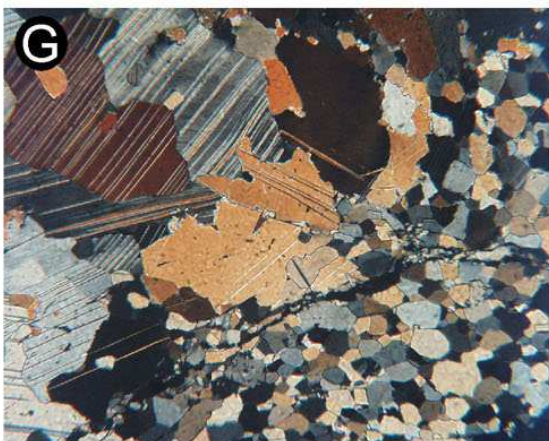
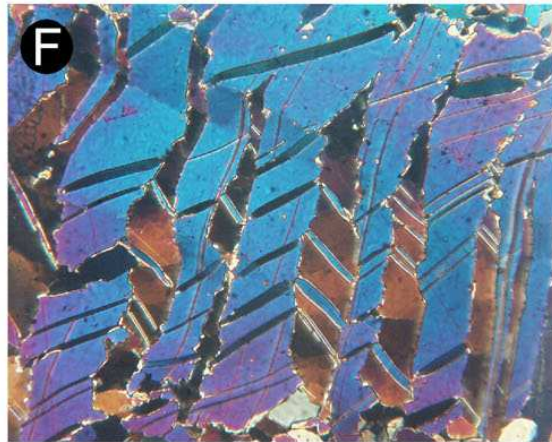
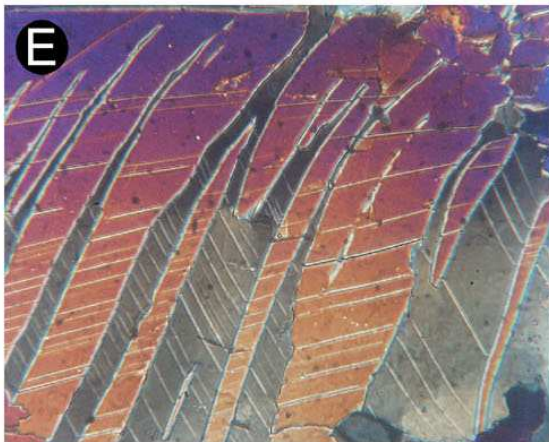
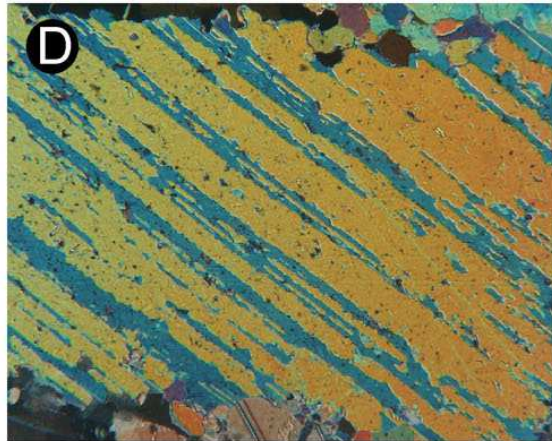
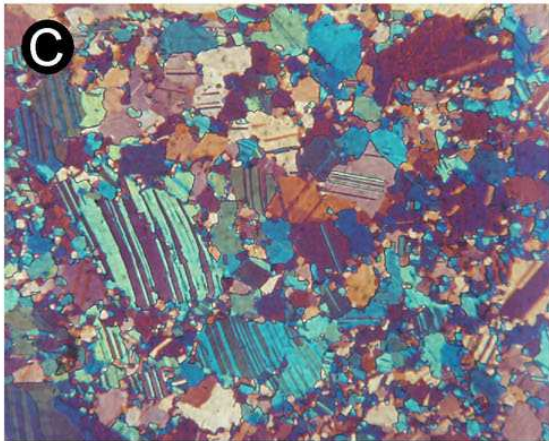
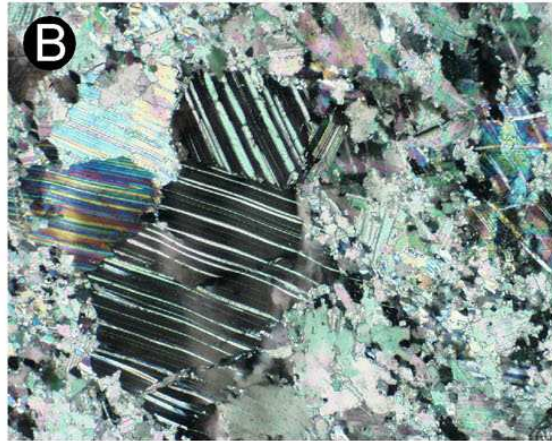
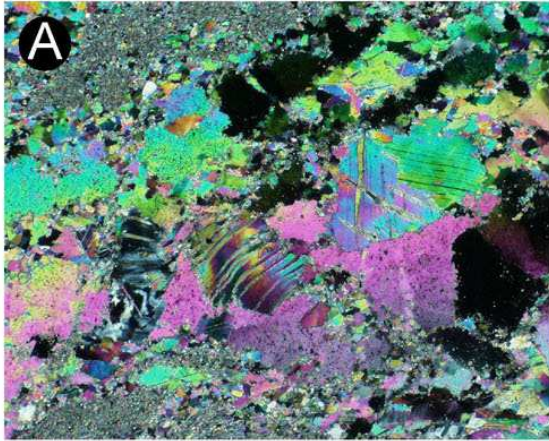




**Figure 37: Microstructures of calcite marbles. (A) Large calcite crystals with sutured grain boundaries and bent twin lamellae embedded in a partly recrystallized matrix of finer crystals. 2.0 mm, XPL, M1N-147-2. (B) Closeup view of deformed large calcite crystals with undulatory extinction and bent twin lamellae. 2.0 mm, XPL, M1N-147-1. (C) Large calcite crystals with sutured twin boundaries surrounded by a partly recrystallized fine ‘matrix’. 0.32 mm, XPL with gypsum plate, M1U-169-1. (D) Strongly sutured twin lamellae. Recrystallization is post-dating twinning. 0.5 mm, XPL, M1U-169-2. (E) Bent twinned twins. 0.2 mm, XPL, M1U-114-1. (F) Twins in twins with sutured twin boundaries. 0.32 mm, XPL, M1U-114-4. (G) Large twinned calcite crystals with lobate grain boundaries and undulatory extinction (upper left) surrounded by a fine, recrystallized ‘matrix’ of undeformed grains (lower right). 0.5 mm, XPL, M1U-185-1. (H) Large deformed calcite grains with undulatory extinction. 4.1 mm, XPL with gypsum plate, M1N-119-1.**

EBSD studies reveal that the calcite grains of both rock types have no lattice-preferred orientation (Figure 38) which was also verified by orientation imaging microscopy (OIM).

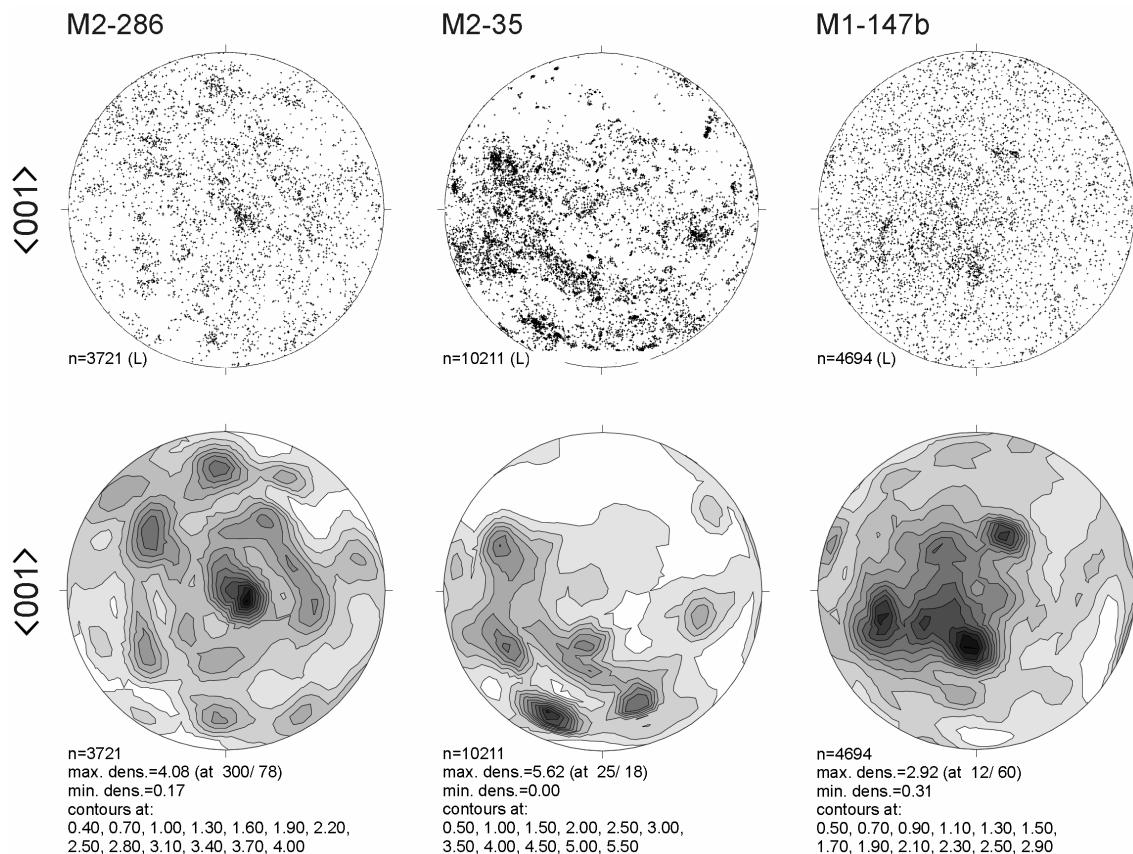


**Figure 38: Orientation of c-axis of calcite of three rock samples (type A: M2-286, Wigles mountain; M2-35, Topolia gorge; type B: M1-147b, north of Milia) as determined by EBSD. Areas of high pole density reflect multiple measurements of c-axis orientation within large individual grains due to the fact that the diagram is based on an EBSD scan. However, the distribution of the poles gives evidence that there is no lattice-preferred orientation. n = number of directions plotted; contour levels are multiples of random distribution; Schmidt net; upper hemisphere. Upper row: Stereogram; Lower row: Density stereogram.**

### 2.4.2.3 Comparative studies of marbles from the Phyllite-Quartzite Unit

During field work also rock samples of marbles from the HP-LT metamorphic Phyllite-Quartzite Unit were collected at three different localities.

(i) Marble with fibrous calcite, north of Kontokinigi, southwestern Crete. In ultra thin section this marble shows elongated calcite crystals with  $120^\circ$  triple point contacts and irregular grain boundaries. The elongated calcite crystals have shape-preferred orientation and thick and straight twin lamellae (type II according to Burkhard 1993) (Figure 39a+b). They show undulatory extinction and subgrain boundaries. Post-deformational recrystallization was not observed. Locally, aggregates of white mica occur.

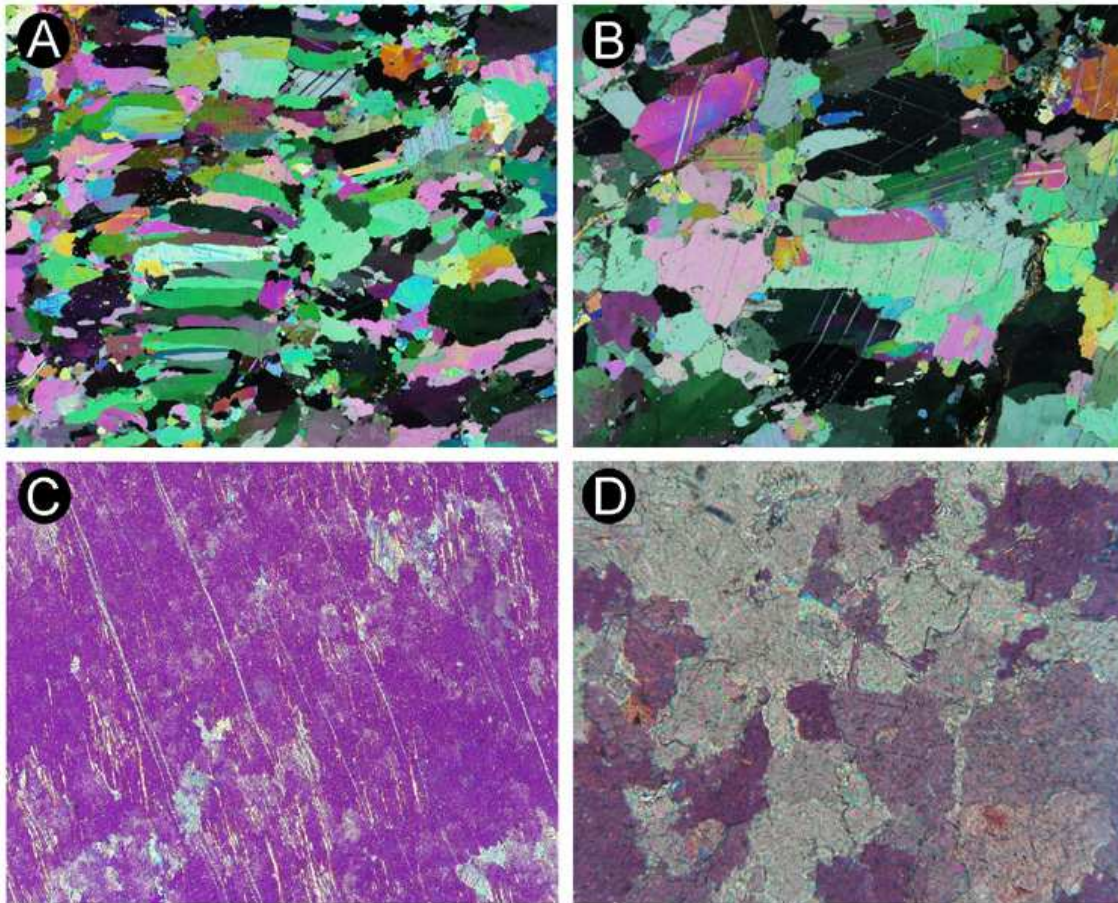


**Figure 39: Microstructures of marbles from the HP-LT metamorphic Phyllite-Quartzite Unit. (A) Fibrous calcite crystals with shape-preferred orientation. Roadside N of Kontokinigi. Ultra thin section, 6.5 mm, XPL, M1-184-2. (B) Calcite crystals with thick, straight twins of type II. Roadside N of Kontokinigi. Ultra thin section, 4.1 mm, XPL, M1-184-3. (C) Calcite 'mega'-crystals with lattice-preferred orientation and some straight twins. Note internal deformation due to the development of subgrains. Bay of Vai. Thin section, 4.1 mm, XPL with gypsum plate, K01-9A. (D) Dolomite marble with sutured grain boundaries. Roadside E of Mesavlia. Thin section, 0.5 mm, XPL with gypsum plate, M2-242-1.**

(ii) Calcite marbles assemblaged with ankerite marbles, bay of Vai, eastern Crete. In thin section, the calcite marbles show very coarse ( $> 1$  cm) calcite crystals with lattice-preferred orientation and strongly sutured grain boundaries. The microstructure is characterized by a lot of subgrain boundaries and thick, slightly curved and sutured twin lamellae. (Figure 39c).

(iii) Dolomite marble, east of Mesavlia, western Crete. This rock is characterized by an inequigranular and interlobate fabric of untwinned dolomite crystals (Figure 39d) and the occurrence of white mica.

HP-LT metamorphism of the Phyllite-Quartzite Unit in western Crete took place within the stability field of aragonite (Theye & Seidel 1993; Wachmann 1997; Stöckhert et al. 1999). This is in accordance with the occurrence of aragonite marbles in this area. During exhumation aragonite was partially or completely transformed to calcite (Theye & Seidel 1993). It is reasonable to assume that the marble north of Kontokinigi (see above) was an aragonite marble which transformed to calcite marble during exhumation. Recently, shape-preferred orientation of fibrous calcite needles (as in the sample from Kontokinigi) was also reported for reverted aragonite marbles from Syros (e.g. Brady et al., *subm.*). How far the calcite marbles have taken over the fabric of their precursor is open to discussion. In any case, the microstructure of the calcite crystals can only record the deformational history after the aragonite-calcite transformation, which means the younger section of the retrograde P-T-t path.

#### 2.4.2.4 Discussion and interpretation

Type A rocks: Twinning (twin type II to IV) predates grain boundary migration recrystallization (including bulging of twin boundaries) and gives evidence of pre- to syn-metamorphic deformation. The lack of lattice-preferred orientation shows that no clear relation exists between calcite crystallography and shape of the grains. Most deformation is caused by pressure solution leading to shape-preferred orientation. Using microfabric criteria (Burkhard 1993), we can conclude, that the minimum temperature during metamorphism was 250°C. Whether the shape-preferred orientation of the calcite needles is related to aragonite-calcite transformation can not be decided.

The fibrous calcite marbles of the Phyllite-Quartzite Unit in western Crete, which most probably represent reverted aragonite marbles, display different microfabrics. They show weak to considerable deformation of the individual calcite grains (twin type II according to Burkhard 1993). Twinning took place during exhumation and therefore postdates metamorphism, which means after aragonite-calcite transformation.

Type B rocks: The high amount of curved twins is related to the onset of intracrystalline deformation mechanisms other than e-twinning, particularly r- and f-glide, which are both temperature dependent (De Bresser 1991 in Burkhard 1993). This criterion

indicates that the temperatures during metamorphism were at least 200°C. The bulging of twin boundaries and the partial formation of an irregular foam structure in the fine-grained domains show that deformation was accompanied by dynamic recrystallization during metamorphism and suggest a temperature above 250°C. According to their microstructure an attribution of type B rocks to the Phyllite-Quartzite unit can be excluded.

Besides differences in microstructure, the lack of quartzite or phyllite clasts in the mid-Miocene basin fills is a strong argument against the provenance of the exotic carbonate rocks from the Phyllite-Quartzite Unit. Phyllites and quartzites are ubiquitous and dominant in the Phyllite-Quartzite Unit, whereas marbles are subordinate.

### 2.4.3 Exotic dolomite marbles

One sample of dolomite marble was collected some hundred meters north of the top of Wigles mountain.

#### 2.4.3.1 *Coexisting calcite and dolomite as geothermometer*

The use of coexisting calcite and dolomite as geothermometer involves determining the mol per cent  $\text{MgCO}_3$  once dissolved in calcite equilibrated with dolomite (Powell et al. 1984; see also Deer et al. 1992). It is not suitable for temperatures above ca. 650°C and is not well constrained below 400°C. Experimental studies in order to calibrate the iron correction were undertaken by Anovitz & Essene (1987).

In one sample from a dolomite marble of the exotic rocks coexisting calcite and dolomite in a vein filling were observed. The calcite twins in this vein filling belong to type III of Burkhard (1993). Microprobe data yield  $X_{\text{Mg}} = 0.015$  for the calcite (Table 1). The iron content was below the detection limit of the microprobe. The temperature determined by carbonate geothermometry (according to Powell et al. 1984; see also Deer et al. 1992, Fig. 228) is ca. 320°C. Albeit the number is in the temperature range which is not well constrained, it is in fairly good agreement with the results of microstructure analyses.

**Table 1: Electron probe microanalyses (wt%) and cation proportions per formula unit of dolomite and calcite from sample M1-22.**

	Dolomite	Calcite
MgO (wt%)	21.2	0.62
CaO	31.0	56.9
Total	52.2	57.5

Cation proportions		
Mg	0.975	0.015
Ca	1.025	0.985
Total	2.000	1.000
n	7	7

Iron and manganese were also measured, but the values were below the detection limit. n = number of point analyses.

#### 2.4.4 Further exotic carbonate rocks

Dolomitic stromatolites and brecciated dolomite rocks: The mountain top of Wigles, north of Paleochora, is built up by dolomitic stromatolites and dolomite breccias which were thought to be parts of the ‘Lissos-Schichten’ (Kopp & Richter 1983). But in reality there is no evidence to support this assumption. Outcrops of these dolomite rocks occur also on the little mountain ridge NE of Paleochora, east of Kakodikianos river, and along the road from Paleochora to Anidri, at the southern part of the small gorge.

The stromatolites and wavy-laminated peloidal grainstones to boundstones are dolomitized and intensely brecciated and dip with a high angle to the south (175-180/80) or even overturned steep to the northeast (045/80). The succession is at most 250 m thick and is in parts covered by the breccio-conglomerates with an unconformity in between. Field investigations show that the stromatolites rest on rocks of the Pindos Unit.

Microscopic studies (including staining of thin sections) reveal complete dolomitization of this shallow-water rocks, too. Fossils for confining the age of these rocks have not been found. Only some foraminifers (indicating a marine environment), gastropods and ostracods were indentified. The laminated dolomites display characteristic birds-eye structure in thin sections. The overall geologic features of this shallow-water stromatolites give reason to classify them as rocks deposited on a carbonate platform. Wether the stromatolitic dolomites have undergone a metamorphic overprint could not be clarified. At any case, these rocks clearly differ from the dolomite marbles in the Phyllite-Quartzite Unit (e.g. dolomite marble from Mesavlia, see 2.4.2.3).

Dolomitic stromatolites and laminated and brecciated, dark dolomites up to 250 m thick occur in the Tripolitza Unit in central Crete (Zager 1972). They are of lower Cretaceous age (Leppig 1974). A comparative study shows that the attribution of the dolomitic stromatolites and breccias exposed at Wigles mountain to rocks of the Tripolitza Unit is very unlikely due to differences in lithology and microfacies.

Carbonate rocks with chlorophyta: Grey to dark grey dolomitic limestones crop out at the southwestern top of Wigles (above the road Paleochora-Kontokinigi) which occasionally contain rock-forming Chlorophyta (Dasycladaceae). Due to complete recrystallization a more precise identification of these algae in thin sections was not possible. Analyses of etched rock samples allowed to classify them as *Griphoporella* sp. mainly known from Triassic. These rocks may be derived from the Tripolitza Unit.

Limestones: Blocks to slabs of limestone fragments occur at the base of the synorogenic sediments at some localities in the region of Kakopetros - Mesavlia (e.g. at the eastern roadside south of the pass). At the western flank of Deliana canyon, north of Mesavlia, a layer of unbedded limestones, tens of meters thick, separates Pindos Unit and breccio-conglomerates. The color of the limestones varies from grey to yellowish-grey or reddish-grey. The limestones are slightly recrystallized. Fossils have not been found, neither in the field nor in thin section. An attribution of these rocks to the Pindos Unit is very unlikely due to differences in lithology and microfacies.

#### 2.4.5 Conclusions

The place of origin of all the rocks described above remains enigmatic due to the fact that their attribution to one of the tectonostratigraphic units known from the Hellenides is problematic. The study shows that a part of the exotic carbonate rocks can be classified as marbles probably generated during low-grade metamorphism.

The exotic rocks may be regarded as...

- (i) ... olistolith-like blocks within the Tertiary Pindos flysch. However, there is no clear evidence in the field that these blocks definitely belong to the flysch of the Pindos Unit.
- (ii) ... remnants of the Uppermost Unit which represents a composite nappe. The assignment of the exotic carbonate rocks to the Uppermost Unit of the Cretan nappe pile (on top of the Pindos Unit) is also questionable, because the carbonate rocks within the Uppermost Unit are always associated with other sedimentary and metamorphic rocks (e.g. Seidel & Wachendorf 1986) and with ophiolites not found as pebbles and slabs within the mid-Miocene basin fills and in their neighbourhood.

In conclusion, the exotic carbonate rocks are regarded as remnants of a lost terrane within the Hellenides.

### 3 Tectonics of the mid-Miocene basins in western Crete

#### 3.1 Contacts of the breccio-conglomerates to the underlying units

The breccio-conglomerates rest with a tectonic contact on the Phyllite-Quartzite Unit (Figure 40) and with an unconformity on the Pindos Unit. No clear evidence for a sedimentary or tectonic contact with the Tripolitza Unit has been found.

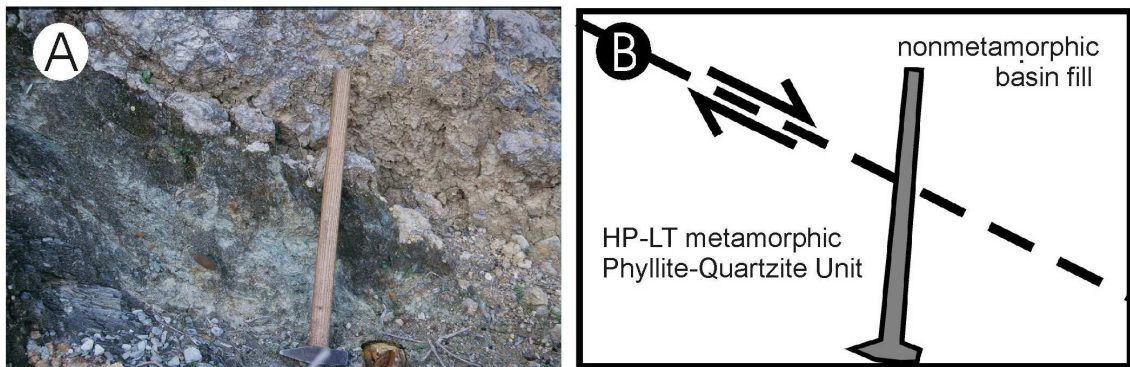


**Figure 40: (A) Tectonic contact of the nonmetamorphic basin fill (upper right corner) with the HP-LT metamorphic Phyllite-Quartzite Unit (lower left part of the picture). At the contact zone the rock is microbrecciated and shows intensive mylonitization. Hammer for scale. (B) The sketch on the right side illustrates the photo.**

Aubouin & Dercourt (1965) not only emphasize that they never observed a sedimentary contact between the basin fills and the Phyllite-Quartzite Unit, but also describe the contact as a fault zone. After Kopp & Richter (1983), the breccio-conglomerates together with the Tripolitza Unit and the Pindos Unit were thrust onto the Phyllite-Quartzite Unit. In the scope of actual tectonic models, the fault zone between Phyllite-Quartzite Unit and the upper units including the mid-Miocene basin fills is interpreted as a low-angle normal fault (detachment fault) (see 1.4.2).

The contact between the basin fills and the Pindos Unit is blurred by debris masses or is tectonically obscured. Evidence for a sedimentary contact is provided by the distribution of both units (geological map). At the west flank of cape Elides, west of Lissos, the conglomerates cover Cretaceous dolomites and limestones with rudists which may be attributed to the Tripolitza Unit. To the north, the conglomerates are underlain by the Pindos Unit. Possibly the Cretaceous rocks represent huge fragments within the breccio-conglomerates.

In the field, the contact between the breccio-conglomerates and the Phyllite-Quartzite Unit was observed at different locations (e.g. NNW Mesavlia). The boundary is always

of tectonic origin. Two kinds of tectonic contacts were observed: The first is formed by a low-angle detachment fault, with down-sliding of the nonmetamorphic units onto the Phyllite-Quartzite Unit, the second is formed by younger (high-angle) normal faults, which in places cut the detachment zone (Figure 41). Both contacts reflect extensional tectonics.

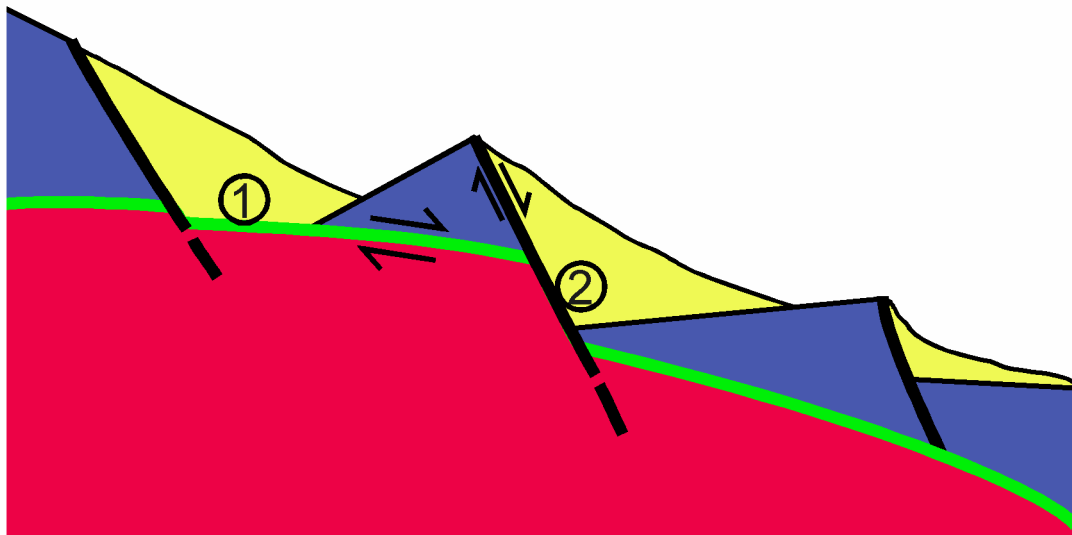


**Figure 41:** Schematic cross section showing the tectonic contact of the breccio-conglomerates (yellow) and the Tripolitza/Pindos Unit (blue) with the high-pressure metamorphic rocks of the Phyllite-Quartzite Unit. At '1' the basin fills are in immediate tectonic contact with the crushed rocks of the Phyllite-Quartzite Unit (red) along the detachment fault (green). At '2' the sediments are in tectonic contact with the Phyllite-Quartzite Unit along a high-angle normal fault. In these zones of nearly vertical movement the rocks are often microbrecciated or even pulverized.

## 3.2 Extension tectonics

### 3.2.1 Low- to moderate-angle normal faults

During the extensional phase a system of low- to moderate-angle normal faults developed within the Phyllite-Quartzite Unit by brittle deformation and stretching (cf. Thomson et al. 1999). The strike of the faults is preferentially E–W, indicating N–S extension. The stereographic projection illustrates these tectonic features (Figure 42). All over Crete this low-angle normal fault pattern of extension can be observed in the Phyllite-Quartzite Unit (Figure 43).



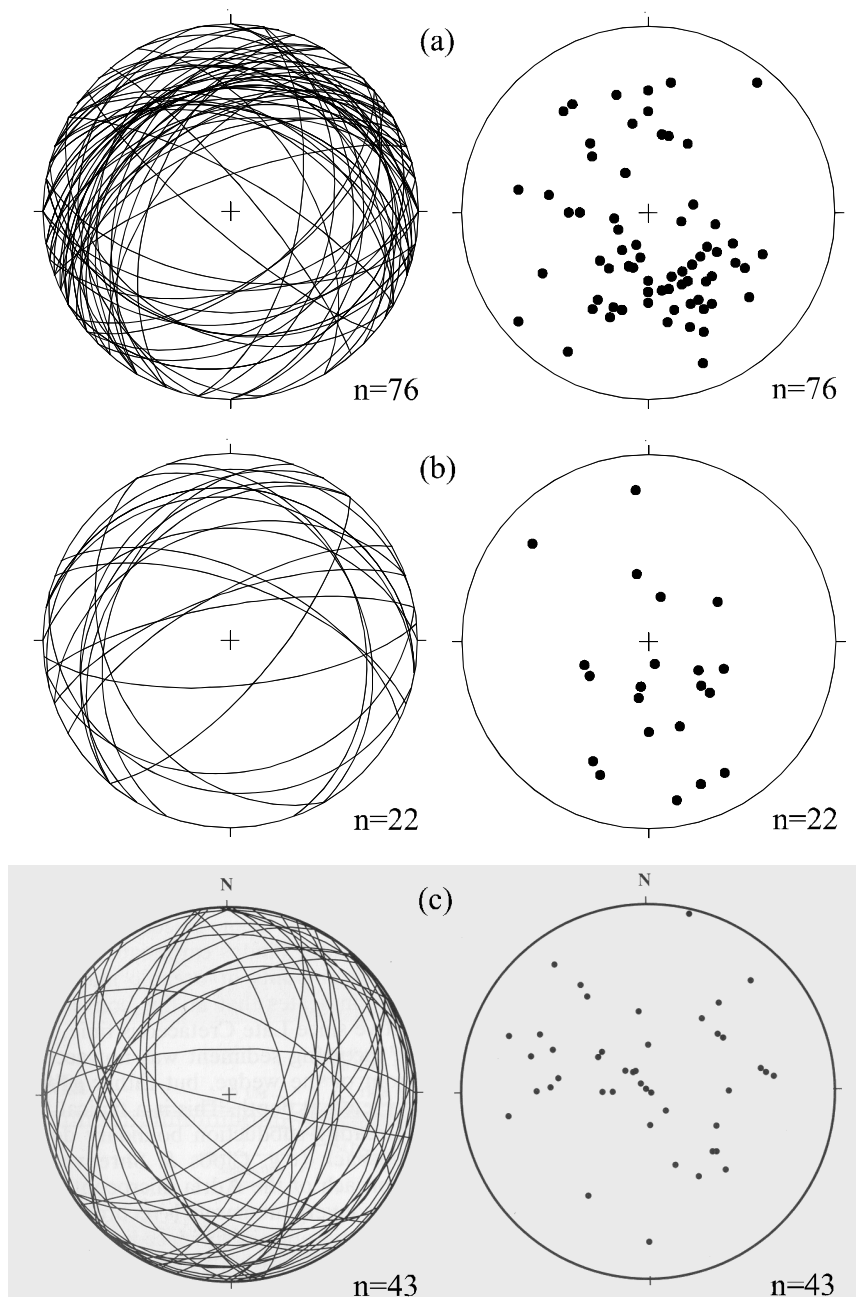


**Figure 42:** The stereographic projection (equal area, lower hemisphere) shows the orientations of main low-angle to moderate-angle brittle normal faults in outcrops of the Phyllite-Quartzite Unit in the working area in western Crete. Note that a slight maximum of faults dipping to northern or southern directions is visible. This implies a weak dominance of north-south directed extension. (a) Along the road from Floria to Kakopetros. (b) Between Sirikari and Kioliana. (c) Stereogram from Thomson et al. (1999) along the western coast of Crete, near Sfinari (west of the working area).

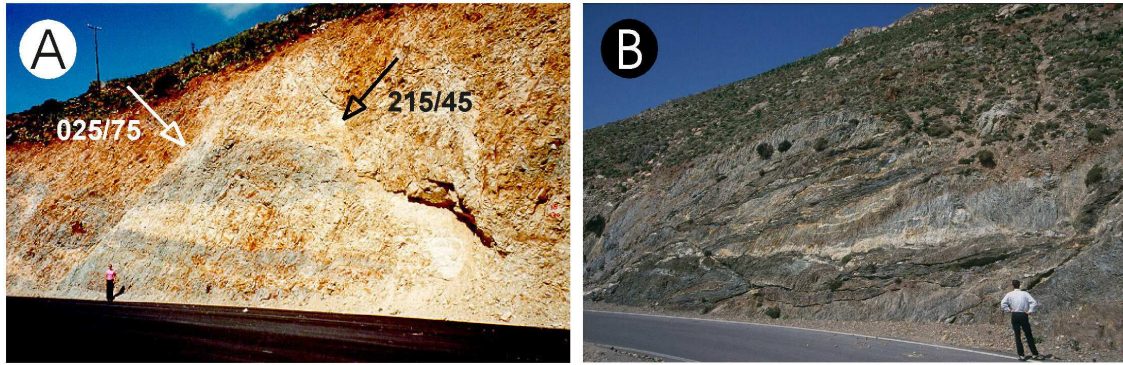


**Figure 43: (a) Horst structure in the Phyllite-Quartzite Unit of western Crete. The normal faults marked by the arrows dip to northern and southern directions. Pass between Kakopetros and Floria. (b) Brittle low-angle normal faults in the Phyllite-Quartzite Unit at the roadside south of Sfinari, western Crete (outside the working area).**

### 3.2.2 Tectono-sedimentary evolution

At the time of late-stage extension the exhumation of the high-pressure rocks was accompanied by disintegration of the brittle upper plate, forming the hangingwall of the extensional detachment fault. This disintegration resulted in W-E trending half-graben structures, which represent supra-detachment basins filled by huge masses of clastic sediments. The mid-Miocene basin fills document continuous extension in the time span between ca. 20-15 Ma (see chapter 4). They are exclusively derived from the pre-Neogene units of the upper plate. This means that the clastic sedimentation took place before the HP-LT metamorphic units were exposed at the surface and subject to erosion. Today at some localities the mid-Miocene breccio-conglomerates are in tectonic contact with the Phyllite-Quartzite Unit. The period of extensional tectonics in lower to middle Miocene times is superseded by a period of high-angle normal faulting and oblique-slip faulting beginning in Tortonian times (ten Veen & Meijer 1998; ten Veen & Postma 1999a, 1999b). Thus, it is suggested that the synorogenic sediments reflect a distinct episode of extension in western Crete.

### 3.2.3 Brittle deformation within the detachment zone

Besides ferruginous alteration (for details see chapter 5), extensional detachment zones of Cordilleran metamorphic core complexes are characterized by intensive brecciation and kinematic structural relationships indicative of sliding and detaching. The rocks in those zones have the appearance of ‘exploded rocks’ as described by Coney (1980): A planar fabric is not developed and the rocks show an exploded microbreccia aspect.

As shown by the photomicrographs in Figure 44 and Figure 45, rocks of the detachment zone in western Crete display similar characteristics. They are in some cases highly brecciated. These tectonic breccias are characterized by a random fabric, i.e. a planar structure is not developed.

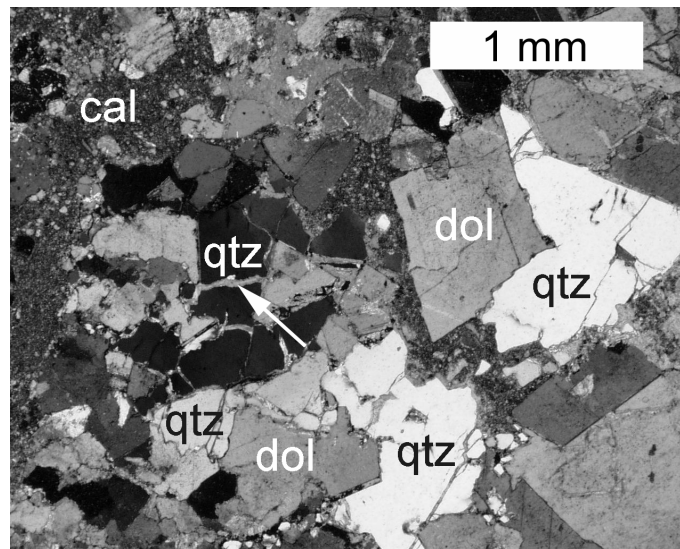


**Figure 44:** Photomicrograph of a brecciated marble (rauhwacke) of the Phyllite-Quartzite Unit. Individual grains are fractured. They break in angular pieces. Fractures (white arrow) are filled with calcite. Partly idiomorphic dolomite crystals grow. At the phase boundaries between dolomite and quartz, the latter is dissolved by pressure solution. In the upper left corner clasts are embedded in a fine-grained calcite matrix. The boundary between individual clasts and the micritic matrix is partly blurred. The breccia shows a random fabric. XPL, M2-40-004.

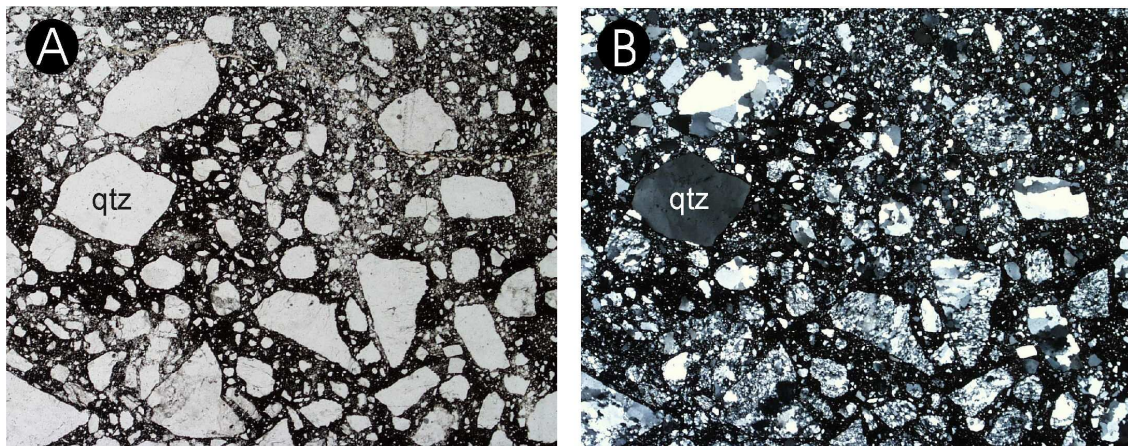


**Figure 45:** Photomicrograph of a brecciated quartzite marking the detachment in the roof of the Phyllite-Quartzite Unit. The clasts are cemented by syntectonic goethite. (A) PPL, 6.5 mm, M2-124-M002. (B) XPL, 6.5 mm, SW of Kakopetros, M2-124-M001.

## 4 Dating of the basin fills

Due to the lack of suitable fossils in the matrix of the deposits of the Topolia alluvial fan complex or in limestones and marls of the Lissos coastal alluvial fan complex an exact dating of the synorogenic sediments is not possible. Thus, the fossils found in the synorogenic sediments can only be used as indicators of the sedimentary environment. At one location within the turbidites of the Lissos coastal alluvial fan complex (see 2.1.3.1) a single shell fragment of a gastropode was observed, whose species or genus could not be determined. Locally, trace fossils are abundant in muddy sediments of the Lissos coastal alluvial fan complex, predominantly in those of the basin plain (see 2.1.3.1). Fracture fills of reddish micritic limestones in conglomeratic mass-flow deposits of the Lissos coastal alluvial fan complex contain *Globigerina* sp. confirming a marine setting.

Clasts (derived from the Tripolitza Unit) containing foraminifers of middle Eocene to upper Eocene age (own observations; cf. Bellas et al. 2000; Keupp & Bellas 2000) indicate that the synorogenic sediments cannot have been deposited prior to the late Eocene (maximum age). A minimum age is given by middle Tortonian (ca. 9 Ma) marine sediments (calcareous nannofossil subzone CN8b according to Frydas & Keupp 1996 and Frydas et al. 1999; CN8a & CN8b, NN10 according to Keupp & Bellas 2000) in northwestern Crete transgressively overlying the breccio-conglomerates. These sediments contain clasts from all units of the Cretan nappe pile.

The marine Neogene is underlain by coarse terrestrial sediments ('geröllführende Rotsedimente' according to Creutzburg 1963; Freudenthal 1969) consisting predominantly of detritus derived from the HP-LT metamorphic Phyllite-Quartzite Unit in the lower part of the Cretan nappe pile. This means that the HP-LT metamorphic rocks were exposed at the latest ca. 10 Ma ago. Rock fragments of the breccio-conglomerates embedded in the terrestrial sediments (e.g. ca. 250 m north of Dromonero, along the road Tavronitis–Paleochora, Roka Formation according to Freudenthal 1969; M<sub>2-3</sub> according to the geological map of Tataris & Christodoulou 1969) give evidence that at this time the synorogenic sediments were already lithified and subject to erosion (Figure 46).

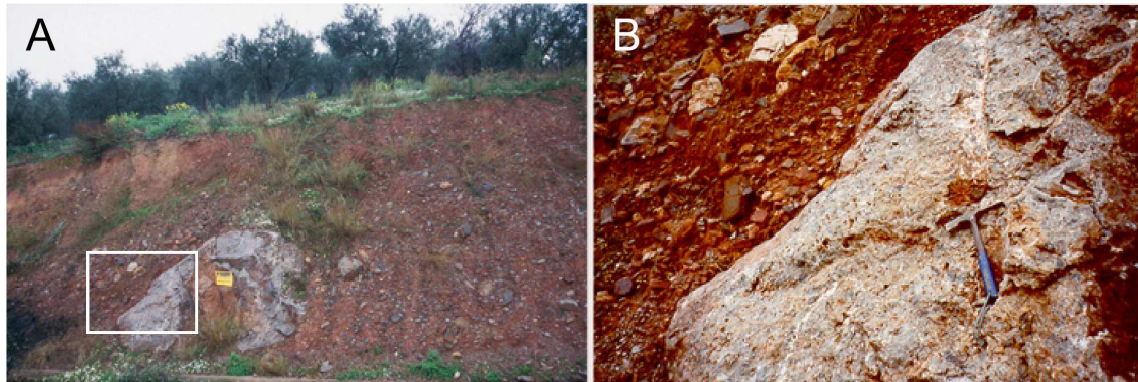


**Figure 46: Fragments of the breccio-conglomerates in upper Miocene terrestrial sediments (=Roka Formation or M<sub>2-3</sub>, cf. text), roadside ca. 250 m north of Dromonero. (A) Outsized clast of breccio-conglomerates in gravel predominantly composed of quartzites and phyllites. (B) Closeup view of the area marked by the frame.**

In the region northeast of Paleochora coral limestones (among others *Matracis* sp. and *Porites* sp.) rest on top of the breccio-conglomerates. The species of the corals could not be determined (see Seidel 1968). At some localities foraminifers are embedded in marly limestones between these corals, among others *Borelis melo* (for detailed information on *Borelis melo* see for instance Loeblich et al. 1964 or Betzler & Schmitz 1997). The stratigraphic distribution of *Borelis melo* (Figure 47) is middle and upper Miocene. *Borelis melo* is superseded by the recent *Borelis pulchra* some time in upper Miocene to Pliocene (Lukas Hottinger, pers. comm., 2001).

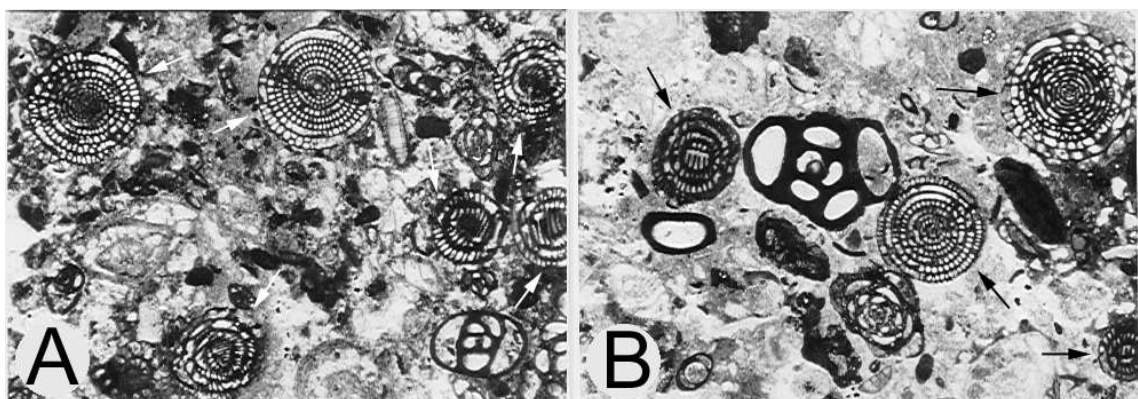


**Figure 47: (A and B) *Borelis melo* (marked by arrows) in thin sections. Width of each photograph 5.2 mm, M2-232.**

In marine Neogene sediments in northwestern Crete *Borelis melo* was erroneously named *Praealveolina* by Keupp et al. (1994, p. 478, Table 2, Fig. 2). But already Christodoulou (1963, in Freudenthal 1969) and Tataris & Christodoulou (1969) noted the appearance of *Nealveolina* (= *Borelis melo*) in Neogene marine sediments of the

Chania province. Due to the occurrence of *Borelis melo* in both regions, it is assumed, that the marly marine Neogene deposits in southwestern Crete (in the region of Paleochora-Lissos) correspond to the deposits of northwestern Crete with regard to age and depositional setting.

Summarized, paleontologic dating (bracketing) suggests a time span between 35 and 10 Ma for the deposition of the synorogenic sediments (Lissos and Topolia alluvial fan complexes).

A further restriction of the age can be given by the thermochronology of the HP-LT metamorphic rocks of the Phyllite-Quartzite Unit in western Crete. Peak P-T conditions were reached between 24-19 Ma. Subsequently the HP-LT rocks were exhumed rapidly. Pervasive brittle extension occurred between 19 and 15 Ma and was concentrated in a detachment fault. Final cooling to below 60°C took place at about 15 Ma indicating near surface position of the Phyllite-Quartzite Unit (Thomson et al. 1998, 1999; cf. Küster & Stöckhert 1997). The formation of iron ores under low-T conditions (ca. 35°C) within the detachment zone (see chapter 5) is related to a period of continuous cooling and decreasing detachment fault activity shortly after 15 Ma. Evidence for a genesis of the iron ore deposits prior to upper Miocene is given by marine Neogene sediments which transgressively overly the iron ore deposits of Ravdoucha and by the occurrence of limonite clasts at the base of these sediments (Kopp & Ott 1977). To go on the assumption that detachment faulting and extension, respectively, triggered simultaneous evolution of half-graben basins and their filling with synorogenic sediments, the age of the breccio-conglomerates can be restricted to the time span between ca. 20 to 15 Ma (Burdigalian – Langhian/Serravallian, i.e. lower to middle Miocene).

For the sake of simplicity, in this work the breccio-conglomerates are loosely termed *middle Miocene* or *mid-Miocene* sediments, deposits, basin fills, etc..

## **5 Iron ore deposits in the detachment zone of western Crete**

### **5.1 Introduction**

Two outcrops of small iron ore deposits occur in western Crete (see Figure 4). They are known for a long time but their genesis is not well understood. The iron ore deposits are located in the upper part of the Phyllite-Quartzite Unit near the detachment fault, one in the vicinity of the small village Ravdoucha in the southern part of Rhodopou peninsula, the other in a mountainous region in the middle of western Crete, south of the village of Kakopetros. The second occurrence was named 'Kakopetros iron ores' by Tataris & Christodoulou (1969) who mapped the sheet Alikianou. The detachment zone is locally tens of meters thick and separates the HP-LT metamorphic Phyllite-Quartzite Unit from the overlying unmetamorphosed units including the breccio-conglomerates. The iron ore deposits are situated underneath the nonmetamorphic rocks which form the 'roof of the iron ores' (cf. Tataris & Christodoulou 1969). They were mined on small scale in open pits until mining ceased in the last century.

In this chapter a first detailed petrographic description of the Kakopetros and the Ravdoucha iron ore deposits is given. Questions to be addressed concern the nature and origin of these deposits and their relation to detachment faulting.

In addition the iron ore deposits in the detachment zone of western Crete are compared with the products of ferruginous alteration and mineralization in detachment zones of metamorphic core complexes in the North American Cordillera.

### **5.2 Setting of the ore deposits**

The ore deposits of Kakopetros and Ravdoucha consist of several lenticular bodies varying in size from decimeter to meter. The ore is hosted by brecciated quartzites, phyllites and marbles in the uppermost part of the Phyllite-Quartzite Unit.

At the top the ore deposits are terminated by the dislocation plane separating the HP-LT metamorphic rocks from the overlying anchi- to nonmetamorphic units. The Kakopetros iron ores are overlain by slivers of the Pindos Unit or by the breccio-conglomerates. The Ravdoucha iron ores are situated below the anchimetamorphic Ravdoucha beds. At the base the ore deposits grade, without a sharp contact, into the country rock of the Phyllite-Quartzite Unit.

The country rock predominantly consists of phyllites, quartzites and marbles. The marbles are heavily altered and have to be classified as rauhewackes. They show a high porosity and easily break in powdery to sandy pieces when hit by hammer. Especially these rocks display impregnation by limonite which give these rocks a yellow to reddish hue, already visible in the field from afar (see Figure 48). It may therefore be assumed

that the formation of the ore deposits is genetically related to the alteration of the marbles. However, the main hosts of the iron ores are quartzites and phyllites. The quartzites and phyllites are intensely brecciated with fractures filled by limonite. The limonite, in turn, is partly brecciated itself. This indicates synchronous brecciation and mineralization.

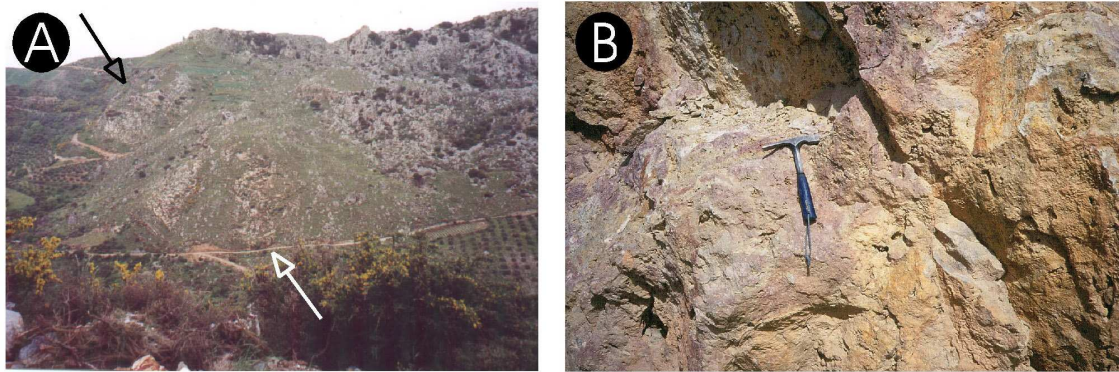


**Figure 48: (A) Photograph of the detachment zone (marked by the arrows) which is characterized by a yellow to reddish hue due to ferruginous alteration. Roadside north of Floria. View to the west. (B) Photograph of rauhewackes within the detachment fault of the Phyllite-Quartzite Unit in western Crete. Roadside north of Floria.**

### 5.3 Mineralogy and petrography

Qualitative powder X-ray diffraction analyses show that the fractures of the tectonic breccias are filled predominantly by goethite. Mn-oxide minerals were identified by ore microscopy. Scanning electron microscopy (SEM), backscattered electron imaging (BSE) and electron microprobe analyses (EPMA) were used for mineral identification and investigations on the internal structure of the ferromanganese ore.

The color of the iron ore varies from typical ochre-brown through dark brownish-grey or nearly black in millimeter to centimeter scale depending on different proportions of ferric iron hydroxides and tetravalent manganese oxides. The ochre-brown ore consists of goethite, whereas the dark, brown to black colored ore is rich in manganese oxides. The goethite occurs as a powdery, friable and porous ore as well as in form of hard crusts. The manganese-rich ores are composed of cryptomelane group minerals. They are usually compact and massive with partly developed botryoidal mm-scaled structures.

BSE imaging revealed that the goethite ore is very finely laminated (Figure 49). The BSE contrast is due to differences in chemical composition, namely variable contents of silica, alumina and manganese (Table 2). The estimated content of water in the goethite rich ore varies between 14 and 20 wt percent.



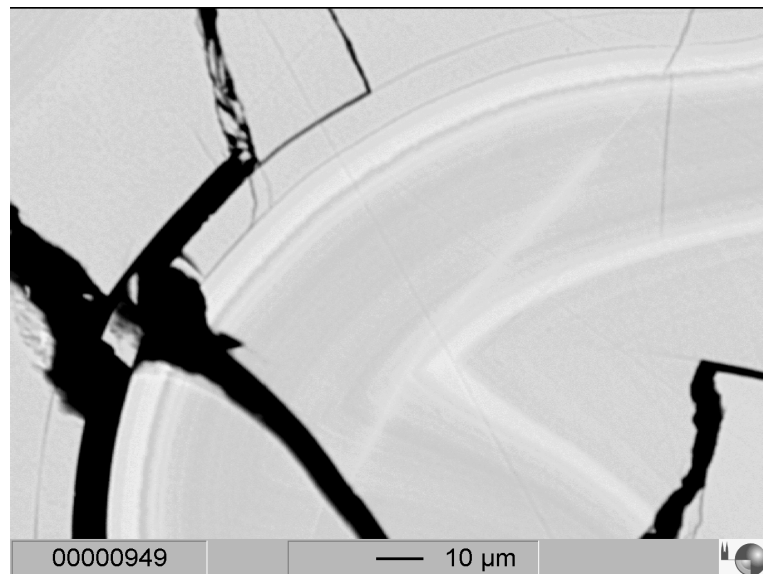
**Table 2: Microprobe analyses of selected goethite samples from the Kakopetros iron ore deposit.**

	M9-17	s	M2-215-1	s	M2-215-2	s	M2-296-1	s	M2-296-2	s
SiO <sub>2</sub> wt%	4.0	0.3	2.2	0.1	2.1	0.1	3.4	0.1	3.9	0.2
MnO <sub>2</sub>	1.1	0.4	0.26	0.04	0.25	0.04	0.9	0.1	0.5	0.1
Al <sub>2</sub> O <sub>3</sub>	1.4	0.2	0.08	0.03	0.07	0.02	1.1	0.1	0.17	0.05
Fe <sub>2</sub> O <sub>3</sub>	79.1	0.7	83.4	0.8	81.1	0.7	74.2	0.7	75.5	0.9
MgO	0.15	0.03	<0.10		<0.10		0.14	0.03	0.12	0.03
CaO	0.40	0.03	<0.10		<0.10		<0.10		0.11	0.02
Subtotal	86.1	0.9	85.9	0.8	83.6	0.8	79.7	0.7	80.3	0.9
H <sub>2</sub> O (calc.)	13.9		14.1		16.4		20.3		19.7	
Total	100.0		100.0		100.0		100.0		100.0	
n	6		248		198		30		56	

Note: In all the analyses manganese is reported as MnO<sub>2</sub> and iron as Fe<sub>2</sub>O<sub>3</sub>.

Water is obtained by difference from 100 wt%. n: number of point analyses s: standard deviation

TiO<sub>2</sub>, BaO, Na<sub>2</sub>O and K<sub>2</sub>O were also measured, but the content of these elements was below the detection limit.

**Figure 49: Electron backscattered photomicrograph of laminated goethite ore. Lamination is due to slight differences in chemical composition. NW of Mesavlia, M2-296.**

EPMA revealed that the laminated hardbands are composed of goethite ore with intercalated bands of manganese oxides on micrometer to millimeter scale (Figure 50 and Figure 51).

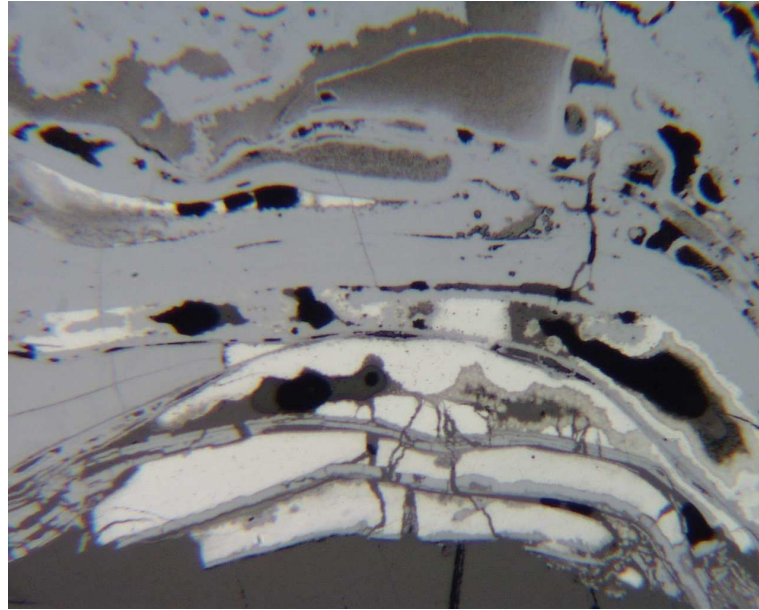


**Figure 50:** Reflected light photomicrograph of laminated hardbands of Ba-rich cryptomelane (white) alternating with goethite (grey). 0.6 mm, NW of Mesavlia, M2-296.

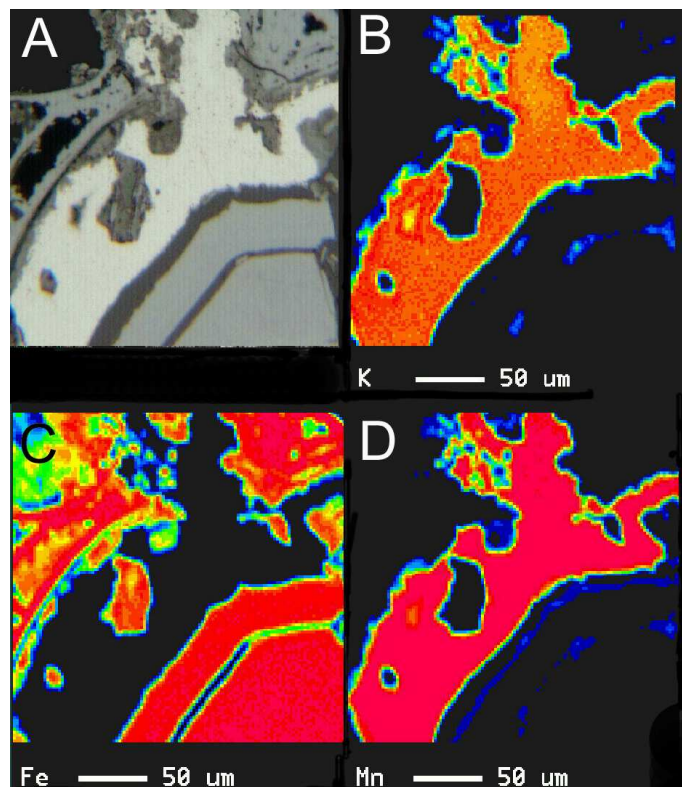


**Figure 51:** (A) Reflected light photomicrograph of laminated hardbands of Ba-rich cryptomelane and goethite. (B, C, D). Electron microprobe maps of the same area showing the relative contents of potassium, iron and manganese. Note, that the cryptomelane is almost free of iron. NW of Mesavlia, M2-296.

Microprobe analyses of Mn-rich laminae and bands in samples of the Kakopetros iron ore deposits are given in Table 3. According to the chemistry, the minerals are referred to the manganomelane group (Ramdohr & Strunz 1978; Frenzel 1980) with the generalized formula  $(\text{Na,K,Ba})_{\leq 2}\text{Mn}^{4+}_8\text{O}_{16}\cdot n\text{H}_2\text{O}$ . Variable contents of Fe may be either related to substitution of Mn by Fe or to cryptocrystalline intergrowth of manganomelane with goethite. The estimated water content of the Mn-minerals varies in a narrow range between 2 to 3.5 wt percent.

K-poor cryptomelane is the most abundant manganomelane group mineral. It is typical of low-*T* manganese oxide mineral assemblages (see Pack et al. 2000).

**Table 3: Microprobe analyses of Mn-rich laminae and bands in samples from the Kakopetros iron ore deposit.**

	M9-17-1	s	M9-17-2	s	M9-17-3	s	M9-17-4	s	M9-17-5	s	M2-296-1	s	M2-296-2	s
SiO <sub>2</sub> wt%	<0.1		<0.1		<0.1		<0.1		<0.1		<0.1		<0.1	
MnO <sub>2</sub>	91.0	0.5	90.0	1.1	89.6	0.9	88.7	0.7	88.3	1.5	89.7	1.0	91.0	0.5
Al <sub>2</sub> O <sub>3</sub>	0.5	0.2	0.5	0.1	0.6	0.1	0.3	0.1	0.4	0.2	0.2	0.1	0.2	0.0
Fe <sub>2</sub> O <sub>3</sub>	0.5	0.2	1.1	0.4	1.4	0.4	1.8	0.6	2.0	1.0	0.6	0.2	0.7	0.3
CaO	0.5	0.1	0.38	0.03	0.42	0.05	0.7	0.1	0.7	0.1	0.6	0.1	0.49	0.03
BaO	0.7	0.3	0.8	0.2	1.0	0.2	0.8	0.3	0.9	0.3	2.5	0.7	1.5	0.2
Na <sub>2</sub> O	0.7	0.1	0.8	0.1	0.7	0.1	0.6	0.1	0.6	0.1	0.7	0.1	0.7	0.1
K <sub>2</sub> O	4.0	0.3	4.4	0.1	4.1	0.2	3.8	0.3	3.7	0.3	2.7	0.3	3.2	0.1
Subtotal	98.0	0.6	97.9	0.9	97.7	0.5	96.7	0.7	96.4	0.6	96.9	0.7	97.7	0.5
H <sub>2</sub> O (calc.)	2.0		2.1		2.2		3.2		3.5		3.1		2.3	
Total	100.0		100.0		100.0		100.0		100.0		100.0		100.0	
Cation proportions based on 32 positive charges per formula unit														
Mn	7.66		7.60		7.58		7.58		7.57		7.69		7.69	
Al	0.07		0.07		0.08		0.05		0.06		0.02		0.03	
Fe <sup>3+</sup>	0.05		0.07		0.12		0.17		0.18		0.05		0.06	
Ca	0.06		0.05		0.06		0.09		0.09		0.08		0.06	
Ba	0.04		0.04		0.05		0.04		0.04		0.12		0.07	
Na	0.17		0.18		0.17		0.15		0.14		0.16		0.16	
K	0.63		0.68		0.65		0.59		0.58		0.42		0.49	
Total	8.68		8.74		8.71		8.68		8.67		8.56		8.58	
n	25		8		25		29		10		7		38	

Note: In all the analyses manganese is reported as MnO<sub>2</sub> and iron is reported as Fe<sub>2</sub>O<sub>3</sub>.

Water is obtained by difference from 100 wt%. n: number of point analyses s: standard deviation

Analyses correspond to chemical composition of cryptomelane.

TiO<sub>2</sub> and MgO were also measured, but the content of these elements was below the detection limit.

## 5.4 Geochemistry

Bulk analyses of the ores, associated breccias and impregnated country rock from the deposits of Kakopetros and Ravdoucha are listed in Table 4. The ore is composed of up to 75 wt percent  $\text{Fe}_2\text{O}_3$  with Mn contents up to 5.7 wt percent ( $\text{Mn}_{\text{tot}}$  given as MnO).  $\text{SiO}_2$  in quartzitic breccias can rise up to 92 wt percent. Concentrations of  $\text{TiO}_2$  are typically between 0.1 and 0.2 wt percent in the hardbands. In the breccias the concentration of  $\text{TiO}_2$  increases up to 1 wt percent due to increase of phyllite fragments.

Mn/Fe ratios in the samples from Kakopetros are generally higher than in those from Ravdoucha. The samples with the highest ratios are enriched in Ba due to incorporation of this element into the manganomelane group minerals (see for comparison Burns & Burns 1981).

**Table 4: Chemical composition of the ore and associated breccias and impregnated country rock of the iron ore deposits of Kakopetros and Ravdoucha as determined by X-ray fluorescence analysis.  $\text{Fe}_{\text{tot}}=\text{Fe}_2\text{O}_3$ ,  $\text{Mn}_{\text{tot}}=\text{MnO}$ .**

		<i>Kakopetros</i>								<i>Ravdoucha</i>		
		M9-17	M9-17A	M2-124	M2-215A	M2-215B	M2-216	M2-296	M2-296A	M1-1A	M1-1A	M1-2
sample from		vein	vein	breccia	vein	vein	breccia	vein	vein	breccia	vein	breccia
$\text{SiO}_2$	wt%	14.0	10.9	92.4	7.06	21.6	58.6	4.97	19.8	60.3	23.4	46.1
$\text{TiO}_2$		0.11	0.16	0.30	0.19	0.16	0.65	0.07	0.36	0.27	0.73	1.00
$\text{Al}_2\text{O}_3$		1.94	2.85	1.47	2.76	1.91	7.26	1.15	5.35	4.18	10.2	11.3
$\text{Fe}_2\text{O}_3$		69.6	70.9	6.63	75.4	60.4	25.5	71.2	59.2	27.4	53.8	30.0
MnO		0.31	0.50	0.02	1.29	3.72	0.07	5.68	1.74	0.01	0.19	0.03
MgO		0.37	0.42	0.44	0.33	0.34	0.43	0.29	0.37	0.23	0.37	0.41
CaO		0.17	0.17	<0.10	<0.10	<0.10	<0.10	0.21	0.13	0.10	0.13	0.28
$\text{Na}_2\text{O}$		<0.10	<0.10	0.16	<0.10	<0.10	0.35	0.15	0.33	0.15	0.34	0.57
$\text{K}_2\text{O}$		0.33	0.48	0.21	0.35	0.38	1.35	0.40	1.01	0.83	2.32	2.67
$\text{P}_2\text{O}_5$		1.74	1.67	0.04	0.07	0.19	0.31	1.25	0.61	0.04	0.27	0.13
L.O.I.		10.4	10.8	0.87	11.6	9.57	5.54	12.3	9.90	5.27	7.24	6.61
Total		<b>99.05</b>	<b>98.75</b>	<b>102.51</b>	<b>99.01</b>	<b>98.34</b>	<b>99.98</b>	<b>97.59</b>	<b>98.80</b>	<b>98.78</b>	<b>98.99</b>	<b>99.22</b>
V	ppm	65	90	36	41	34	68	33	44	<10	98	70
Cr		23	61	<8	57	93	42	109	49	28	105	59
Co		130	170	9	193	6	82	431	101	18	41	13
Ni		456	526	96	229	47	103	348	205	<5	46	<5
Zn		690	656	78	879	50	305	1687	1316	24	64	9
Rb		<5	6	<5	<5	<5	23	<5	16	41	86	84
Sr		17	15	31	25	24	31	112	67	20	76	38
Zr		29	47	187	29	59	313	17	87	170	224	283
Ba		142	200	<18	161	370	199	747	457	92	140	254
Mn/Fe (molar)		0.004	0.008	0.003	0.019	0.068	0.003	0.089	0.033	-	0.004	0.001

## 5.5 Oxygen isotope geochemistry

$\delta^{18}\text{O}$  and  $\delta^{17}\text{O}$  of three goethite-rich ore samples were determined by  $\text{CO}_2$  laser fluorination technique (Table 5). Laser fluorination technique (Sharp 1990) allows precise determination of  $\delta^{17}\text{O}$  along with routine  $\delta^{18}\text{O}$  determination. The three analyzed ore samples plot, within error, on the terrestrial fractionation line (i.e.  $\delta^{17}\text{O}=0.524\cdot\delta^{18}\text{O}$ ). Hence, no mass independent oxygen isotope fractionation effects accompany the formation of the oxide ores.

**Table 5:  $\delta^{17}\text{O}$  and  $\delta^{18}\text{O}$  values of goethite samples from Kakopetros.**

Sample	$\delta^{17}\text{O}_G$	$\delta^{18}\text{O}_G$
M9-17	-0.61	-1.13
M2-215	-0.14	-0.18
M2-296	-0.04	-0.03

Goethite is an indicator mineral for low- $T$ , hydrous and highly oxidizing environments (Langmuir 1971; Murray 1981; Diakonov et al. 1994; Yapp 2001) and is a common mineral in the weathering zone. The oxygen isotope fractionation between water and goethite can be used as low- $T$  geothermometer (Yapp 1987, 1990).  $\delta^{18}\text{O}$  values of goethite samples from Kakopetros range from -1.13 ‰ to -0.03 ‰, the average is ca. -0.6 ‰. Assuming that goethite crystallized in equilibrium with meteoric water, it is possible to estimate the temperature of the formation of goethite as well as the thermal state during late-stage brittle deformation within the detachment zone. The  $\delta^{18}\text{O}$  values for meteoric water are estimated to be similar to the present day annual average value of -8.0 to -4.0 ‰ (Rozanski et al. 1993; IAEA/WMO 2001). The geographic position of Crete island in mid-Miocene times did not differ very much from its present-day position. The existence of Miocene subaerial sediments (mid-Miocene breccio-conglomerates and middle/upper Miocene terrestrial sediments) is evidence for climatic conditions resembling today's conditions.

Yapp (1990) gives a relation between  $1000\ln^{18}\alpha$  ( $^{18}\alpha = \frac{R_{goethite}}{R_{water}}$ ;  $R_{sample} = (^{18}\text{O}/^{16}\text{O})$ ;

$$\delta^{18}\text{O} = \left[ \frac{R_{sample}}{R_{standard}} - 1 \right] \cdot 1000 \text{‰} ; 1000\ln^{18}\alpha \approx \delta^{18}\text{O}_{goethite} - \delta^{18}\text{O}_{water} = \Delta_{goethite-water}; \text{ for further}$$

information see O'Neil (1986)) and temperature based on experimental data (measured for temperatures  $< 100^\circ\text{C}$ ):

$$1000\ln^{18}\alpha_{GW} = \frac{1.63 \cdot 10^6}{T^2} - 12.3$$

The geothermometer published by Zheng (1998) is based on a semi-empirical approach and was calculated for a temperature range of 0–1200°C:

$$1000\ln^{18}\alpha_{GW} = \frac{3.31 \cdot 10^6}{T^2} - \frac{10.39 \cdot 10^3}{T} + 2.74$$

The goethite contains 2–4 wt percent  $\text{SiO}_2$  and 0.1–1.4 wt percent  $\text{Al}_2\text{O}_3$  (cf. Table 2), which, in a first order approach, are assumed to be present as  $\approx 2$  wt percent kaolinite and  $\approx 1$  wt percent quartz/chert. The oxygen isotope fractionation data between water and kaolinite and quartz were taken from Zheng (1993, kaol-H<sub>2</sub>O) and Kawabe (1978, qz-H<sub>2</sub>O). At low temperatures, both quartz and kaolinite concentrate  $^{18}\text{O}$  relative to water.

In a first step, it is assumed that the measured goethite samples are pure ( $\delta^{18}\text{O} = -0.6\text{‰}$  (average value, see above) and that  $\delta^{18}\text{O}$  of water is  $-6.0\text{‰}$  (average value). Using the thermometer of Yapp (1990), a temperature of  $31^\circ\text{C}$  is calculated. Using the thermometer of Zheng (1998), a temperature of  $23^\circ\text{C}$  is calculated.

At a temperature of  $28^\circ\text{C}$  and  $-6.0\text{‰}$  for  $\delta^{18}\text{O}$  of water,  $\delta^{18}\text{O}$  for kaolinite is  $+22\text{‰}$  (Zheng 1993) and for quartz is  $+28\text{‰}$  (Kawabe 1978). Assuming that the goethite samples on average contain 2 wt percent kaolinite and 1 wt percent quartz,  $\delta^{18}\text{O}$  of pure goethite is calculated as  $-1.7\text{‰}$ . With this value, the recalculated temperature of goethite/water equilibration is  $40^\circ\text{C}$  (Yapp 1990) and  $31^\circ\text{C}$  (Zheng 1998). On the basis of this new temperature estimate of  $36^\circ\text{C}$  (average value),  $\delta^{18}\text{O}$  of the pure goethite is  $-1.6\text{‰}$  (calculated in a second iteration cycle). With this value temperatures of  $39^\circ\text{C}$  (Yapp 1990) and  $31^\circ\text{C}$  (Zheng 1998) result which within error are identical to the values calculated in the first iteration cycle. A temperature range between 31 and  $40^\circ\text{C}$  is in agreement with the presumed low- $T$  formation of the iron ores in the detachment zone of western Crete. Under normal geothermal gradient, a maximum burial depth of 1200 m is indicated.

The data presented here give evidence for low- $T$  precipitation of the ferromanganese ores. The occurrence of goethite as fracture infilling and, in turn, fractured ores proof the syntectonic origin of the ferromanganese ores. Hence, the ore mineralization documents brittle deformation in the detachment zone during late-stage extension, before deformation ceased with the final exhumation of the HP-LT metamorphic Phyllite-

Quartzite Unit which took place around 15 Ma. At this time the HP-LT Phyllite-Quartzite Unit was cooled down below 60°C (Thomson et al. 1998, 1999). This temperature is in good agreement with the temperature range calculated for the formation of the iron ores in the detachment zone of western Crete implying a depth of ca. 1200 m under normal geothermal gradient. Evidence for a genesis of the iron ore deposits prior to upper Miocene is given by limonite clasts in basal conglomerates of Tortonian sediments and by marine Neogene sediments transgressively overlying the ore deposits (Kopp & Ott 1977).

## 5.6 Fluid flow patterns

The fractured and brecciated rocks within the detachment zone are characterized by a high permeability. These breccias are thus feeder channels for hydrothermal solutions (cf. Tobin et al. 2001). In the phyllite and quartzite breccias goethite was predominantly precipitated in fissures between the rock fragments (Figure 52) whereas the altered marbles (rauhwackes) were pervasively impregnated by goethite (Figure 48b).

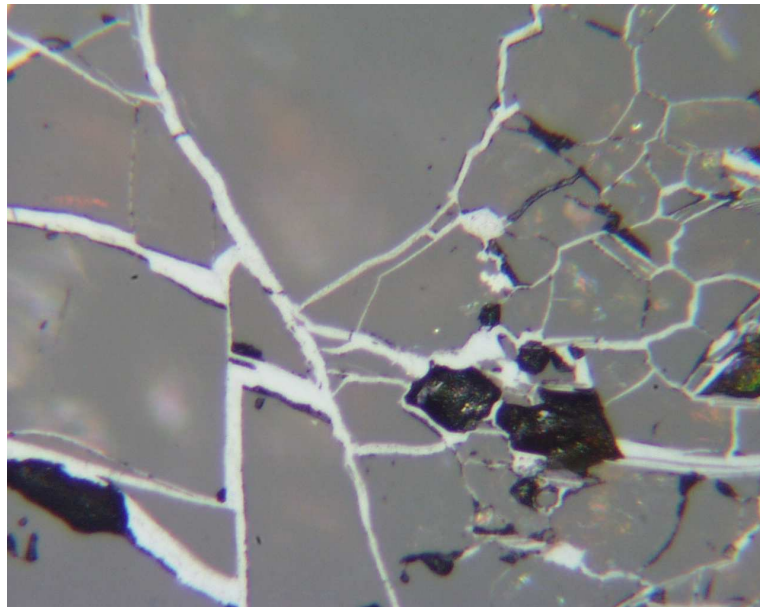


**Figure 52: Reflected light photomicrograph showing a quartzite breccia with angular clasts. The veins are filled predominantly by goethite. 0.3 mm, M2-215-2.**

The different kind of ore mineralization in the quartzite and phyllite breccias and in the rauhwackes is explained by differences in the permeability caused by different mechanical behaviour of the host rocks (Figure 53). The highest fluid transport took place within the phyllite and quartzite breccias beneath the dislocation plane. The massive iron ore deposits are therefore restricted to this domain. In the rauhwackes reduced fluid transport was active. This is attributed to significant reduction of open joints in the rauhwackes compared to the quartzite and phyllite breccias.

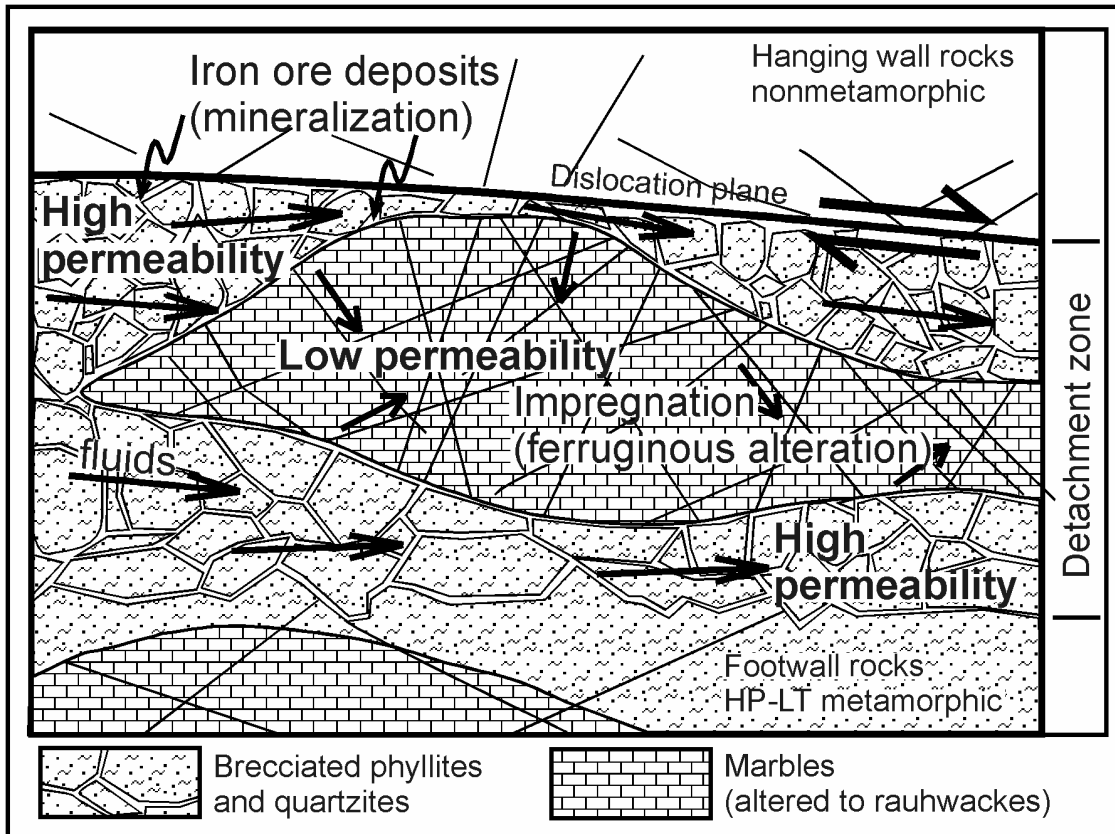


**Figure 53: Fluid flow pattern within the detachment zone. High fluid flow is restricted to intensely brecciated rocks leading to precipitation of vein-filling iron ore deposits. By contrast, the relative smooth marbles are pervasively impregnated by fine-grained goethite due to lower permeability.**



## 5.7 A comparison with metamorphic core complexes of Cordilleran type

The iron ore deposits in the detachment zone of western Crete resemble the so called 'ferruginous alteration' (Davis & Hardy 1981) typical of extensional detachment zones of metamorphic core complexes of Cordilleran type (see Coney 1980).

In general, two categories of metamorphic core complexes can be distinguished: The metamorphic core complex in the usual sense is a domelike exposure of the metamorphosed, mylonitic footwall of the regional detachment fault beneath a wide continental rift. Several examples are known from a belt along the eastern edge of the Basin and Range Province in the North American Cordillera. A metamorphic core complex in the broader sense is any metamorphic complex that occurs in the 'core' (internal region) of an orogen (cf. Jackson 1997). The complexes of Cordilleran type are characterized by a particular internal architecture (Davis & Coney 1979; Coney 1980; Davis 1980): The centers are domes of granite or gneiss, followed by a metamorphic carapace, which shows foliation, and an overlying nonmetamorphic cover, named detachment, consisting of allochthonous, rotated hangingwall rocks (Davis & Hardy 1981). The lower rocks are separated from the upper rocks by a sharp discontinuity or zone, termed detachment fault (Davis et al. 1980), marking an abrupt change in rock type, structure, fabric and grade of metamorphism. The detachment fault is considered to be a low-angle normal fault (Wernicke 1981). In addition, every of these four internal units (core, metamorphic carapace, detachment fault, cover) displays typical structural features. For example, rocks within the broad detachment zone are usually brecciated and extensively altered. Retrograde chlorite is very common in these rocks, and development of a distinctive red-stained fracture filling is ubiquitous, caused by precipitation of iron compounds between rock fragments (the so-called ferruginous alteration of Davis & Hardy 1981). Already Heidrick & Wilkens (1980) noted, that in the Buckskin mountains (Arizona) loci of intense alteration are positioned along the keel of the detachment fault due to vulnerability to migration of hydrothermal solutions along the detachment strata. The tectono-hydrologic state of the detachment fault in the Buckskin mountains is comparable with the situation in western Crete. Along-fault migration of ground water predominantly in the highly permeable fracture zone leads to precipitation of the iron ore deposits and ferruginous alteration which is painting the detachment zone in a yellow to red color.

Ferruginous alteration seems to be a typical feature of detachment zones in general. It is not restricted to metamorphic core complexes of Cordilleran type but may also occur in metamorphic core complexes in the broader sense like Crete.

## 6 Lineament analyses on satellite images and aerial photographs of western Crete

Lineament analyses were applied on a satellite (SPOT) image and on aerial photographs of Western Crete. The lineaments detected on the images are shown in Figure 54.

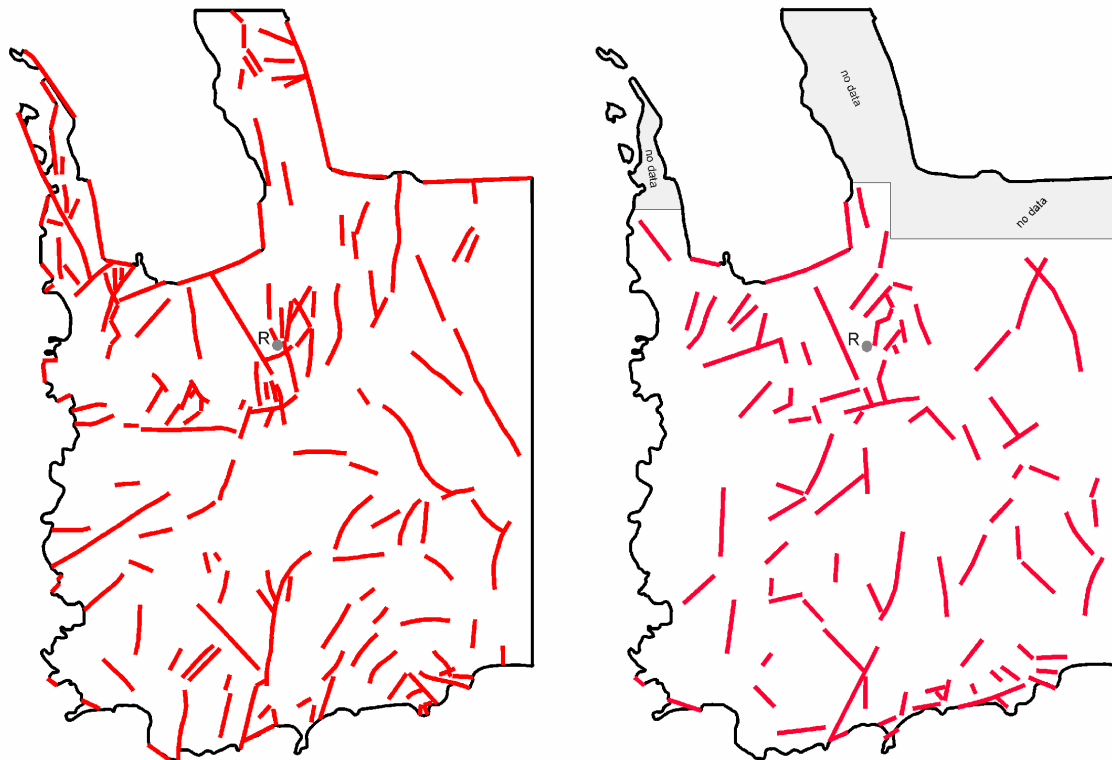


**Figure 54: Results of lineament analyses for western Crete. (A) SAT image. (B) Aerial photograph. R: Roka**

The number of detected lineaments is 161 in the SPOT image and 97 in the aerial photographs. The rose diagrams (Figure 55) show, that lineament patterns of SPOT image and aerial photographs are similar. Most lineaments fall into 4 dominant fault groups with approximate azimuths ranging from N010E to N050E and N080E to N100E and with an azimuth of N135E as well as an azimuth ranging from N165E to N175E. The lineaments detected in the SPOT image are concentrated in the northwestern part of Crete, which can be correlated with the tectonically controlled development of the marine Neogene sedimentary basins (e.g. Kontopoulos et al. 1996). The Roka ridge (Meulenkamp 1979), part of the Topolia alluvial fan complex, is accentuated by an increased number of lineaments on both images. It is interpreted as a NNE-SSW trending horst structure bound by steep normal faults.

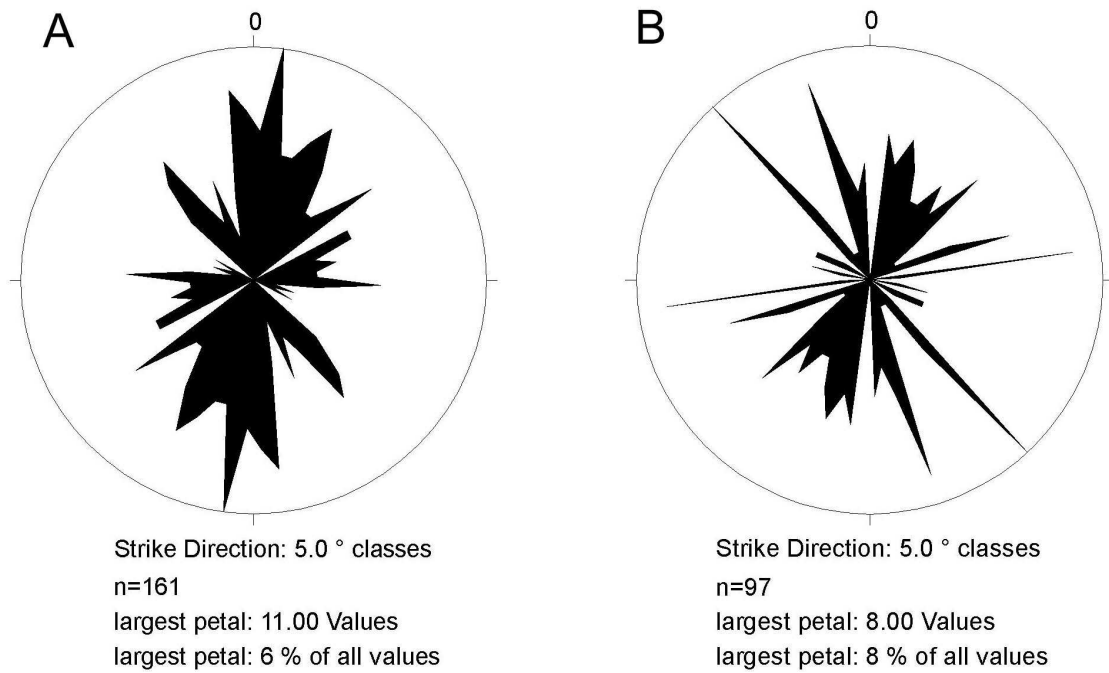


**Figure 55: Rose diagrams of (A) SPOT image and (B) aerial photograph.**

Many lineaments detected in the SPOT image and in the aerial photographs correspond to faults and fault zones identified in the field and documented in the geological maps. Thus, the structural patterns obtained from lineament analyses reflect the actual distribution and orientation of tectonic features in western Crete.

## 7 Comparison with basin fills in eastern and central Crete

### 7.1 Neogene basin fills in the Ierapetra region (eastern Crete)

#### 7.1.1 Geology of the Ierapetra basin

The stratigraphy and the sedimentary history of the Neogene deposits of the Ierapetra region, located east of the Lassithi mountains, are described in Fortuin's PhD-thesis (1977). Fortuin & Peters (1984) report on the Prina Complex, which represents a distinct rock unit within the Ierapetra basin and is regarded as a possible equivalent of the breccio-conglomerates in western Crete (Aubouin & Dercourt 1965; Kopp & Richter 1983).

Aubouin & Dercourt (1965) regarded 'les brèches de la Crète occidentale' (=Topolia alluvial fan complex) as an equivalent of the breccias in the region of Kritsa-Kopraki in the Ierapetra basin. Based on the finding of *Clypeina jurassica* FAVRE they suggested an Upper Jurassic age leading to the hypothesis, that the breccias in western Crete and in the Ierapetra area represent a lower part of the Tripolitza Unit. But obviously, the fossil came from a clast within the breccio-conglomerates.

In the following, the sedimentary evolution of the Ierapetra Basin is summarized according to Fortuin (1977), Fortuin & Peters (1984), Postma & Drinia (1993) and Postma et al. (1993). The older formations (?Serravallian) mainly consist of coarse clastic continental deposits (Mithi and Males Formation). The stratigraphy is complicated by tectonic movements during sedimentation, especially in the initial period of subsidence and submergence during the late Serravallian, leading to the deposition of brackish to shallow marine sediments (Parathiri Member of the Males Formation). During this period the Ierapetra region, located at the southern margin of the Southern Aegean Landmass, was a continental borderland, which began to subside after strong blockfaulting due to crustal tension. Elevated blocks in the north were bound by W-E faults, and a N-S trending graben-like depression was formed in the central part of the region, which was open to the south and rapidly filled up with clastics from north and northeast. At this time, the sedimentation is characterized by gravity sliding of rock slabs and by discharge of coarse clastics from the uplifted blocks towards the central depression resulting in the deposition of breccio-conglomerates with megaliths and sandy boulder conglomerates (Prina Complex). Calcareous sandstones and marls were deposited further to the south and are attributed to a subsea fan environment (Kalamavka Formation). Since the beginning of Tortonian, in the deepest part in the south, a poorly defined turbidite basin existed, characterized by a high sedimentation rate (Makrilia Formation). During this time, also the northern parts of the area may have been submerged. In the middle Tortonian, limestone sedimentation became more pronounced, due to gradual

shallowing. This is observed all over Crete. The shallowing tendency resulted in the Messinian facies with gypsum, which is related to the late Miocene salinity crisis.

The tectonic evolution of the Ierapetra basin - as suggested by Fortuin & Peters (1984) - is caused by sinistral strike-slip movements (sinistral oblique-slip, Postma & Drinia 1993) along a NE-SW-oriented fault zone. Investigations of Postma et al. (1993) and Postma & Drinia (1993) showed, that the basin fill architecture of the Ierapetra basin was tectonically controlled. They suggest, that the time around the middle and late Miocene boundary was a period of compression leading to rapid tectonic uplift, folding and steepening of a relief along a fault zone bordering the basin to the north (formation of the Prina Complex). This compressional phase is followed by NNE-SSW extension during the Tortonian. The time around the Miocene/Pliocene boundary was again a period of compression (see also ten Veen & Postma 1999b). The Pliocene was dominated by extension with northward tilting of fault blocks (Postma et al. 1993; ten Veen & Postma 1999a).

The pebble spectrum of the basal Neogene deposits, unconformably overlying the nappe pile, shows a close relationship to the lithologies of the pre-Neogene rocks. From old to young, the Neogene clastics reflect the progressive erosion and denudation of the nappe pile (Fortuin & Peters 1984). The basal Mithi Formation consists almost exclusively of components derived from the Uppermost Unit. Large amounts of components derived from the Pindos Unit are typical of the Males Formation. In contrast, slabs and coarse clastics derived from the Tripolitza Unit predominate in the lower parts of the Prina Complex. In higher structural levels of the Prina Complex, clasts from the HP-LT metamorphic units at the base of the nappe pile (Phyllite-Quartzite Unit, Plattenkalk Unit) appear. Own observations along the road from Kritsa to the Katharo Plateau confirmed the widespread occurrence of coarse crystalline marbles with cherts from the Plattenkalk Unit in conglomerates of the Prina Complex.

### 7.1.2 Discussion

The age of the oldest, continental sediments (Mithi and lower part of the Males Formation) of the Ierapetra Basin cannot be determined exactly (cf. Fortuin 1977; Fortuin & Peters 1984). These sediments were deposited prior to the late Serravallian at the latest. The Prina Complex is of late Serravallian (Fortuin 1977; Fortuin & Peters 1984) to early Tortonian (Postma & Drinia 1993) age. The ages estimated for the Mithi and Males Formations and for the Prina Complex match fairly well the time span supposed for the deposition of the Topolia and Lissos complexes in western Crete (see 4). In respect to sedimentology, the breccio-conglomerates in western Crete best compare to the Prina Complex in the Ierapetra area.

The Prina Complex is a heterogenous association of sediments or a sedimentary *mélange* (Fortuin & Peters 1984), put up by a number of lithological units. Especially the Breccia Series (Postma & Drinia 1993), representing sediment gravity flow deposits with megaclasts derived from the Tripolitza Unit, resembles the mid-Miocene basin fills in western Crete, in particular the Lissos coastal alluvial fan complex. But in contrast to western Crete, the Prina Complex consists of debris derived from all units of the pre-Neogene nappe pile forming a 'hinterland' in which the HP-LT metamorphic rocks had already been exhumed at this time and were subject to erosion (Fortuin 1977; Fortuin & Peters 1984), whereas the Topolia and Lissos fan complexes exclusively contain clasts from the upper units atop the detachment fault. Therefore, the Prina Complex in the Ierapetra area and the basin fills of western Crete reflect different tectonic scenarios, with steep faulting and rapid tectonic uplift in the Ierapetra region during a compressional stage (see above) and with detachment faulting in western Crete during extension.

## 7.2 Neogene graben fills in the Iraklion area (central Crete)

### 7.2.1 Geological setting

In the General Geological Map of Crete (Creutzburg et al. 1977), 10 km west of Iraklion, a small occurrence of clastic sediments is marked in with the same signature as the breccio-conglomerates in the area of Topolia and Paleochora in western Crete (Figure 56). Kopp & Richter (1983) assigne these breccio-conglomerates to their 'Topolia Formation', due to the lack of clasts of the Phyllite-Quartzite Unit. According to these authors, the sediments west of Iraklion are deposited on volcanites of the Pindos Unit from which the numerous green components in the outcrops along the old road from Iraklion to Rethimnon are derived.

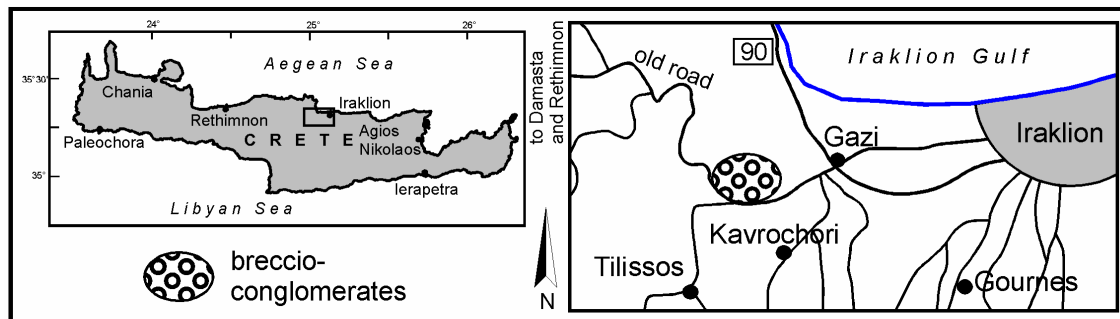


**Figure 56:** General map showing the geographical position of the outcrop of breccio-conglomerates west of Iraklion.

### 7.2.2 Discussion

Own studies showed that the clastic deposits west of Iraklion are built up by fluvial sandstones and breccio-conglomerates only poorly lithified. The grain size ranges from sand to fine cobble. Clasts are subangular to poorly rounded. The clastic sediments rest on amphibolites (Figure 57), which were mistaken for Pindos volcanic rocks by Kopp & Richter (1983). These amphibolites can be attributed to the Uppermost Unit.

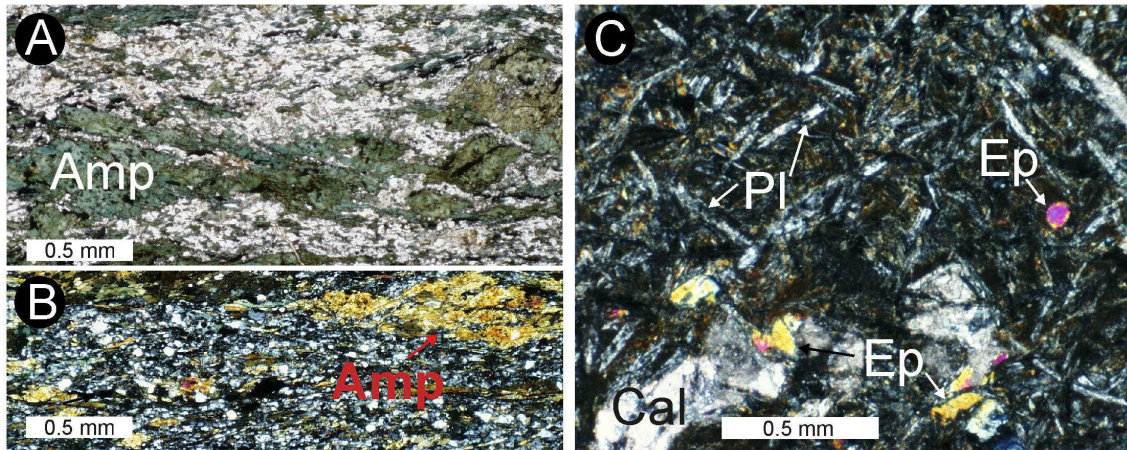


**Figure 57: Rock samples in thin section. (A, B) Photomicrographs of an amphibolite underlying the breccio-conglomerates west of Iraklion. (A) PPL, M1-66. (B) XPL, M1-66. (C) Photomicrograph of a volcanic clast in the graben fill. XPL, M1-60. For mineral abbreviations see appendix.**

As already noted by Kopp & Richter (1983), the breccio-conglomerates mainly contain components from the Tripolitza and Pindos Units. Outcrops of both units are found nearby. The source of the volcanite clasts (Figure 57) cannot be addressed definitely. In their fabric and chemical composition (Table 6) they correspond to basalts. Such volcanites locally occur within the Pindos Unit, but are widespread in the Uppermost Unit. A small body of basaltic rocks of the Uppermost Unit is exposed some kilometers to the south (Creutzburg et al. 1977).

**Table 6: Chemical composition of volcanite clasts as determined by X-ray fluorescence analysis.**

	M1-60	M1-62
SiO <sub>2</sub> (wt%)	43.3	45.7
TiO <sub>2</sub>	1.07	1.34
Al <sub>2</sub> O <sub>3</sub>	15.4	13.7
Fe <sub>2</sub> O <sub>3</sub>	8.78	8.99
MnO	0.12	0.12
MgO	5.01	5.26
CaO	13.8	12.3
K <sub>2</sub> O	0.30	1.11
Na <sub>2</sub> O	3.73	3.79
P <sub>2</sub> O <sub>5</sub>	0.10	0.23
L.O.I.	8.30	6.96
Total	99.90	99.56
Sc (ppm)	41	43
V	141	202
Cr	267	400
Ni	109	119
Rb	<2	21
Sr	308	142
Y	20	21
Zr	72	93
Nb	12	22

The breccio-conglomerates in the occurrence west of Iraklion are considered local deposits bound to the western shoulder of the Iraklion graben. The spectrum of clasts reflects the local lithology of the surrounding pre-Neogene units. There is no reason to see the formation of these clastics in context with detachment faulting.



## 8 Synthesis

The exhumation of the high-pressure/low temperature metamorphic units during lower to middle Miocene times was accompanied by structural disintegration of the hangingwall, leading to formation of sedimentary basins on top of the nappe pile. The tectono-sedimentary evolution of these supra-detachment basins provides information on the state of the Hellenic fore arc at that time.

The basins are half-graben structures filled by huge masses of clastic sediments exclusively derived from the tectonostratigraphic units atop the detachment fault which separates the HP-LT metamorphic units from the nonmetamorphic units. This means that sedimentation of the breccio-conglomerates took place before the exposure of the high-pressure metamorphic units at the surface and their accessibility to erosion.

Facies analysis shows that the lower to middle Miocene basin fills of the half grabens vary from alluvial fan deposits in a terrestrial environment to turbiditic successions reflecting a marine environment. The Topolia alluvial fan complex in northwestern Crete is debris-flow-dominated, with poor sorting and clast-rich to matrix-supported deposits. SEM- and CL-studies reveal the high degree of compaction and cementation after deposition. The Lissos coastal alluvial fan complex in southwestern Crete, a thick fault scarp related wedge of sediments, includes subaerial waterlaid and debris-flow deposits as well as marine debris-flow and turbidite deposits.

Predominant clastic components in the basin fills are limestones and dolomites with microfacies and fossil assemblages corresponding to members of the Tripolitza Unit. Limestones with chert, radiolarites, sandstones and calcarenites can easily be derived from the Pindos Unit, whereas the provenance of some pebbles to slabs of marbles remains enigmatic.

Due to progressive extension, in places the western Cretan basin fills and the nonmetamorphic units are now in tectonic contact along the detachment zone with the high-pressure/low-temperature metamorphic Phyllite-Quartzite Unit. Combining observations and informations from field, laboratory and literature results in a simplified model for the tectonic evolution of western Crete during Burdigalian to Langhian/Serravallian which is shown in Figure 58.

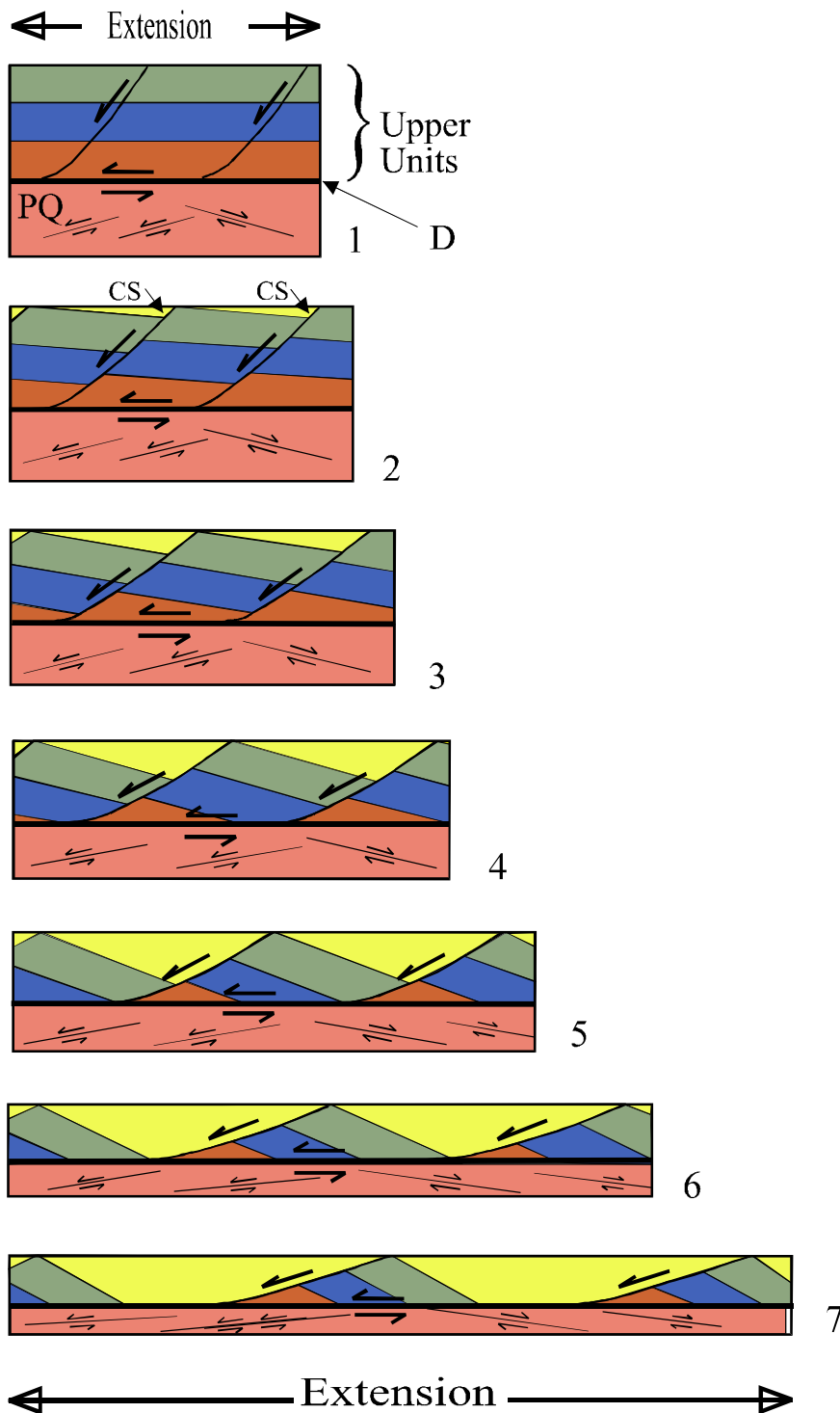


**Figure 58:** Schematic cross sections (1-7) showing progressive stretching of the brittle upper crust (upper tectonic units, not affected by late Oligocene/early Miocene HP-LT metamorphism) with evolution of half-graben structures. The upper units are separated by a low-angle detachment fault (D) from the HP-LT metamorphic rocks of the Phyllite-Quartzite-Unit (PQ). Note tectonic erosion at the base of the upper units. The half grabens are filled with clastic sediments (CS) derived exclusively from the upper units (footwall blocks). Stretching within the Phyllite-Quartzite Unit results in low- to moderate-angle normal faults. The scenario corresponds to a geometrical model of crustal stretching along spaced, discrete faults proposed by Le Pichon & Sibuet (1981) and to the shear-zone model for metamorphic core complexes proposed by Davis (1983).

The detachment zone is a brecciated layer, locally tens of meters thick, and is characterized by ferruginous alteration with fracture- and vug-filling goethite.  $\delta^{18}\text{O}$  data of goethite give evidence for low-temperature precipitation of the ores. The genesis of the two major iron ore deposits in western Crete (Kakopetros and Ravdoucha) may thus be related to the extensional detachment fault. A comparison of the Cretan iron ores with products of ferruginous alteration and mineralization in detachment zones of Cordilleran metamorphic core complexes in North America indicates that the genesis of iron ores is a typical feature of detachment zones in general.

The lower to middle Miocene basin fills of the half graben structures in western Crete document the history of continuous extension in the fore arc of the roll back controlled Hellenic subduction zone and allow a reconstruction of the paleogeographic evolution for a period of time (20 to 15 Ma, Burdigalian – Langhian/Serravallian) otherwise not well recorded (Figure 59, Figure 60).

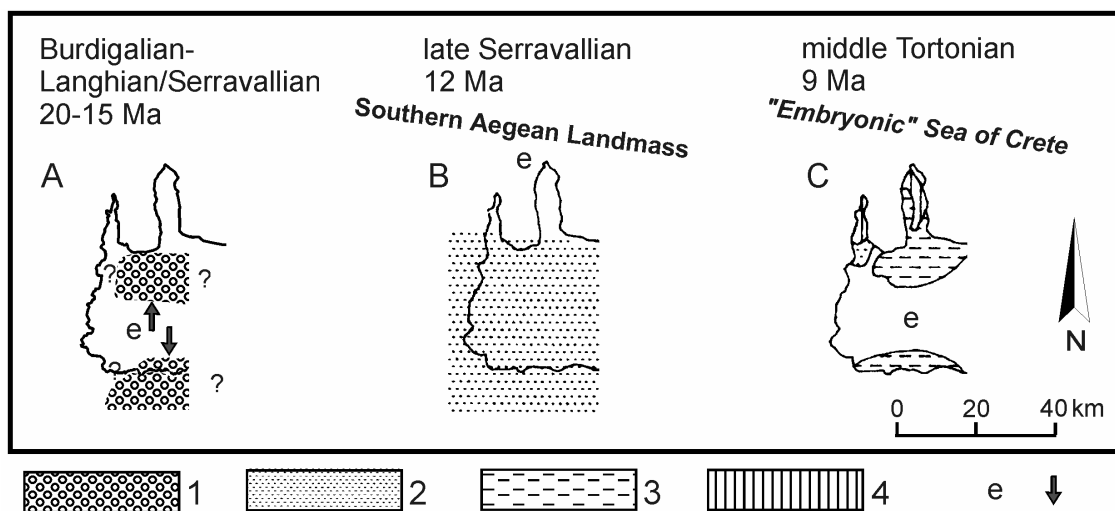


**Figure 59: Successive steps in the paleogeographic evolution of Crete since the Burdigalian. (A) lower and middle Miocene. (B) late middle Miocene. (C) upper Miocene (steps B and C are modified after Meulenkamp 1985 and Meulenkamp et al. 1994). 1: deposition of breccioconglomerates. 2: fluvio-lacustrine sediments (with clasts derived from the HP-LT Phyllite-Quartzite Unit). 3: marine and nonmarine terrigenous-clastic sequences. 4: areas included in the subsidence in late Tortonian time. e: areas subject to erosion. ↓: direction of sediment transport during lower and middle Miocene.**

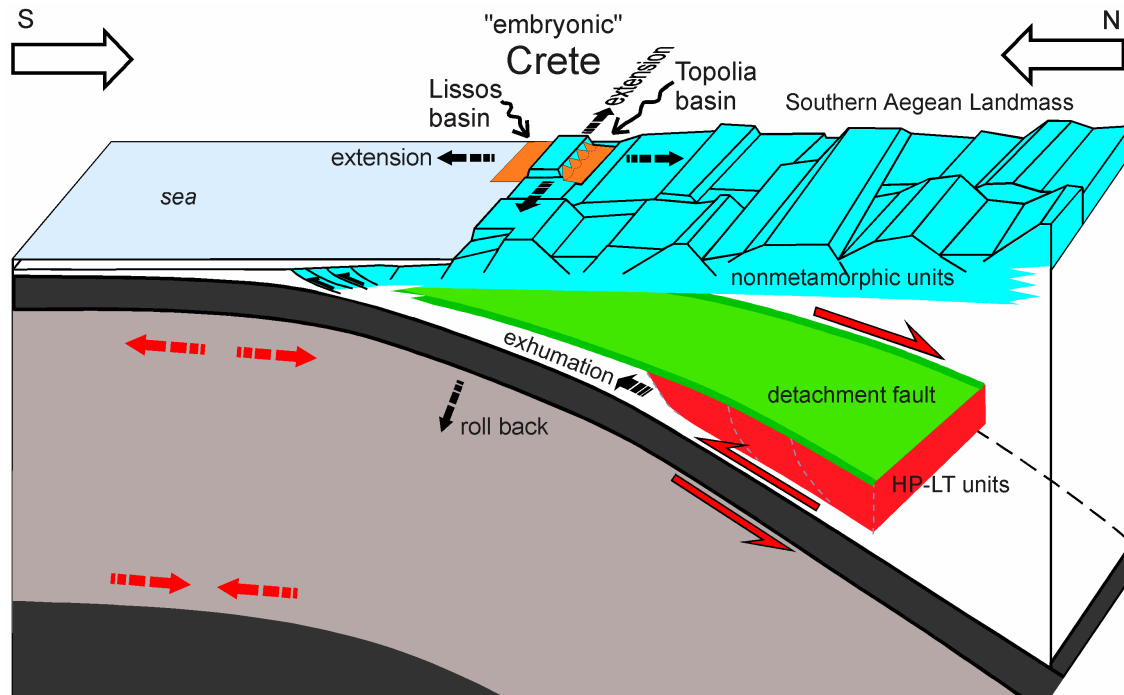


**Figure 60:** Cartoon showing a schematic cross section of the Hellenic subduction zone and the southern Aegean region during lower to middle Miocene times. The supra-detachment basins are situated in the hanging wall of the detachment fault (green). The HP-LT units (red) are being exhumed due to extension tectonics caused by roll back. The clasts of the lower to middle Miocene basin fills (orange) in western Crete are exclusively derived from the nonmetamorphic units (blue).

Contrary to the lower to middle Miocene basin fills in western Crete, clastic sediments of similar facies and age in the Ierapetra region reflect blockfaulting during a compressional stage.

## 9 Analytical techniques and laboratory equipment

### STAINING OF THIN SECTIONS

In order to distinguish calcite from dolomite in thin sections Alizarin red *S*, and in some cases, in order to distinguish carbonate minerals containing Fe<sup>2+</sup> (ferroan minerals) from those with little or no iron potassium ferricyanide were used. For further information the reader is referred to Dickson (1965).

### BULK ROCK ANALYSIS

**X-ray fluorescence analysis (XRF):** This technique was used to analyse major elements and some trace elements. A Philips PW 2400 X-ray fluorescence spectrometer equipped with a Rh tube was used for the analyses of glass discs which were made from 0.600 g sample powder and 3.6 g lithium tetraborate. The mixture was melted in a platinum crucible. Loss on ignition (L.O.I.) was determined in a muffle furnace at 1000°C.

### MICROANALYTICAL METHODS

**Powder X-ray diffraction (XRD):** All samples for X-ray diffraction were ground in order to obtain a homogenous powder. A Philips PW 1800 X-ray powder diffractometer with Cu-K $\alpha$  radiation was used for qualitative phase analyses.

**Electron probe microanalysis (EPMA):** This technique was used to determine major and trace element compositions of minerals. Compositions were determined by wavelength dispersive analytical techniques on a JEOL JXA 8900 (superprobe) electron microprobe, using standard operating conditions of 15 kV accelerating voltage and 20 nA probe current (absorbed current on brass). Data were automatically processed by ZAF method.

Electron microprobe mapping has been carried out on carbon- or gold-coated polished thin sections. Elemental distribution maps have been obtained at 20 keV beam energy,  $4.0 \times 10^{-8}$  A beam-current density, 1  $\mu\text{m}$  probe diameter, 20 s dwell time and 2  $\mu\text{m}$  point distance.

**Cathodoluminescence (CL):** Polished gold- or carbon-coated thin sections of rock samples were bombarded by a scanning energetic electron beam resulting in the emission of light of various wavelengths. The wavelengths and the intensity of the light emission are characteristic of a specific mineral and its integration of trace elements in the structure resulting in additional information on the sample. Cathodoluminescence studies were carried out in Cologne using a HC2-LM and in Bochum using a HC1-LM cathodoluminescence apparatus. At both instruments standard operating conditions were

14 kV accelerating voltage and 0.1 mA beam current, using a hot cathode (HC) electron gun. In Bochum pictures were taken with a KAPPA DX 10 digital camera.

**Scanning electron microscopy (SEM) and energy dispersive X-ray spectroscopy (EDX/EDS):** Scanning electron microscopy studies (with backscattered electron (BSE) detector) provide information on the spatial distribution of minerals in rock samples. SEM was carried out in Cologne on a JEOL JXA 8900 (superprobe) electron microprobe. Additional analyses were performed in Bochum on a LEO 1530 Gemini (equipped with a field emission cathode). SEM was carried out on mm-sized rock fragments, which were sputtered with gold, and on gold- or carbon-coated thin sections. The chemical composition of minerals imaged in the SEM was identified by energy dispersive X-ray spectroscopy (EDX/EDS).

**Electron backscattered diffraction (EBSD):** Electron backscattered diffraction (EBSD) in the scanning electron microscope (SEM) allows the exact determination of the crystallographic orientation of minerals. EBSD measurements were carried out at the Ruhr-Universität Bochum with a LEO 1530 Gemini equipment.

**Oxygen isotope analysis:** Oxygen isotope analyses were performed on 1–2 mg sized samples using IR-laser fluorination technique with  $\text{BrF}_5$  as oxidizing agent (Sharp 1990). The samples were loaded along with laboratory mineral standards in a Ni-sample holder and put into a vacuum sample chamber. Samples were pre-fluorinated ( $\approx 100$  mbar) over night in order to remove moisture and surface absorbed impurities. Fluorination of the samples was performed by laser heating using a 25 W IR  $\text{CO}_2$ -gas laser ( $\lambda = 10500 \mu\text{m}$ ) in a 100 mbar  $\text{BrF}_5$  atmosphere. Liberated oxygen was cleaned from excess oxidation agent by conducting the gas mixture over heated KCl.  $\text{Cl}_2$  was separated from the sample  $\text{O}_2$  in a cold trap. The  $\text{O}_2$  was collected on two successive molecular sieve traps ( $5\text{\AA}$ ) before it was expanded into the bellow of the dual inlet system of a Finnigan Delta Plus XL gas mass spectrometer. A correction of  $-0.3\text{‰}$  had to be applied on the measured  $\delta^{17}\text{O}$  value as result of an  $^{17}\text{O}$  excess in the bottled reference oxygen gas. Accuracy and precision of  $\delta^{17}\text{O}$  and  $\delta^{18}\text{O}$  is within  $\pm 0.2\text{‰}$ . Due to the correlation between error of  $\delta^{17}\text{O}$  and  $\delta^{18}\text{O}$ , is the error of  $\Delta^{17}\text{O}$  very low, i. e. smaller than  $\pm 0.01\text{‰}$ . All data are reported relative to V-SMOW (Gonfiantini 1978). Oxygen isotope analyses were carried out by A. Pack at the University of New Mexico in Albuquerque.

## 10 References

- ANOVITZ, L.M. & ESSENE, E.J., 1987, Phase equilibria in the system  $\text{CaCO}_3\text{-MgCO}_3\text{-FeCO}_3$ . *J. Petrol.*, 28, 389-414.
- AUBOUIN, J. & DERCOURT, J., 1965, Sur la géologie de l'Egée: regard sur la Crète. *Bull. Soc. Géol. France*, 7, 787-821.
- BARBER, D.J., 1985, Dislocations and microstructures. *in* WENK, H.-R., ed., Preferred orientation in deformed metals and rocks: An introduction to modern texture analyses. Academic Press, Orlando, 149-182.
- BARKER, C.E. & KOPP, O.C., eds., 1991, Luminescence microscopy and spectroscopy: Qualitative and quantitative Applications. SEPM, Tulsa, 195 pp.
- BELLAS, S., HÖRNIG, A. & KEUPP, H., 2000, Contribution to the geology-sedimentology of the Breccia Member, Topolia Formation, NW Crete, Greece. *Mitt. Ges. Geol. Bergbaustud. Österr.*, 43, 25.
- BETZLER, C. & SCHMITZ, S., 1997, First record of *Borelis melo* and *Dendritina* sp. in the Messinian of SE Spain (Cabo de Gata, Province Almeria). *Paläont. Z.*, 71, 211-216.
- BIZON, G. & THIEBAULT, F., 1974, Données nouvelles sur l'âge des marbres et quartzites du Taygète (Péloponnèse méridional, Grèce). *C.R. Acad. Sci. Paris, D* 278, 9-12.
- BLAIR, T.C., 1999a, Sedimentary processes and facies of the waterlaid Anvil Spring Canyon alluvial fan, Death Valley, California. *Sedimentology*, 46, 913-940.
- BLAIR, T.C., 1999b, Sedimentology of the debris-flow-dominated Warm Spring Canyon alluvial fan, Death Valley, California. *Sedimentology*, 46, 941-965.
- BLAIR, T.C., 1999c, Cause of dominance by sheetflood vs. debris-flow processes on two adjoining alluvial fans, Death Valley, California. *Sedimentology*, 46, 1015-1028.
- BLAIR, T.C. & MCPHERSON, J.G., 1992, The Trollheim alluvial fan and facies model revisited. *Geol. Soc. Am. Bull.*, 104, 762-769.
- BLAIR, T.C. & MCPHERSON, J.G., 1994, Alluvial fans and their natural distinction from rivers based on morphology, hydraulic processes, sedimentary processes, and facies assemblages. *J. Sed. Res.*, A64, 450-489.
- BLAIR, T.C. & MCPHERSON, J.G., 1998, Recent debris flow processes and resultant form and facies of the dolomite alluvial fan, Owens Valley, California. *J. Sed. Res.*, 68, 800-818.
- BONNEAU, M., 1973, Sur les affinités ioniennes des "calcaires en plaquettes" épimétamorphiques de la Crète, la charriage de la série de Gavrovo-Tripolitza et la structure de l'arc Égéen. *C.R. Acad. Sci. Paris, D* 227, 2453-2456.
- BOUMA, A.H., 1962, Sedimentology of some flysch deposits. Elsevier, Amsterdam, 168 pp.
- BRADY, J.B., MARKLEY, M.J., SCHUMACHER, J.C., CHENEY, J.T. & BIANCIARDI, G.A., subm., Aragonite pseudomorphs in high pressure marbles of Syros, Greece. *Geology*.
- BURKHARD, M., 1993, Calcite twins, their geometry, appearance and significance as stress-strain markers and indicators of tectonic regime: a review. *J. Struct. Geol.*, 15, 351-368.
- BURNS, R.G. & BURNS, V.M., 1981, Manganese oxides. *in* BURNS, R.G., ed., Marine minerals. *Rev. Mineral.*, 6, 1-46.
- CHOE, M.Y. & CHOUGH, S.K., 1988, The Hunghae Formation, SE Korea: Miocene debris aprons in a back-arc intraslope basin. *Sedimentology*, 35, 239-255.

- CHRISTODOULOU, G.E., 1963, Geological and micropaleontological investigations of the Neogene of the isle of Crete (in Greek, with an English and German summary). Author's ed., Athens, 157 pp.
- COCARD, M., KAHLE, H.G., PETER, Y., GEIGER, A., VEIS, G., FELEKIS, S., PARADISSIS, D. & BILLIRIS, H., 1999, New constraints on the rapid crustal motion of the Aegean region: recent results inferred from GPS measurements (1993-1998) across the West Hellenic Arc, Greece. *Earth Planet. Sci. Lett.*, 172, 39-47.
- CONEY, P.J., 1980, Cordilleran metamorphic core complexes: An overview. *in* CRITTENDEN, M.D., CONEY, P.J. & DAVIS, G.H., eds., *Cordilleran Metamorphic Core Complexes*. *Geol. Soc. Am. Mem.*, 153, 7-31.
- CREUTZBURG, N., 1963, Geröllführende Rotsedimente auf der Insel Kreta. *Ann. Geol. Pays Hellen.*, 14, 357-404.
- CREUTZBURG, N., DROOGER, C.W., MEULENKAMP, J.E., PAPASTAMATIOU, J., SANNEMANN, W., SEIDEL, E. & TATARIS, A., 1977, General Geological Map of Crete 1:200,000. Institute of Geological and Mining Research, Athen.
- DAMANTI, J.F., 1993, Geomorphic and structural controls on facies patterns and sediment composition in a modern foreland basin. *in* MARZO, M., & PUIGDEFABREGAS, C., eds., *Alluvial Sedimentation*. *Spec. Publ. Int. Ass. Sediment.*, 17, 221-233.
- DAVIS, G.A., ANDERSON, J.L., FROST, E.G. & SHACKELFORD, T.J., 1980, Mylonitization and detachment faulting in the Whipple-Buckskin-Rawhide Mountains terrane, southeastern California and western Arizona. *in* CRITTENDEN, M.D., CONEY, P.J. & DAVIS, G.H., eds., *Cordilleran Metamorphic Core Complexes*. *Geol. Soc. Am. Mem.*, 153, 79-129.
- DAVIS, G.H., 1980, Structural characteristics of metamorphic core complexes, southern Arizona. *in* CRITTENDEN, M.D., CONEY, P.J. & DAVIS, G.H., eds., *Cordilleran Metamorphic Core Complexes*. *Geol. Soc. Am. Mem.*, 153, 35-77.
- DAVIS, G.H., 1983, Shear-zone model for the origin of metamorphic core complexes. *Geology*, 11, 342-347.
- DAVIS, G.H. & CONEY, P.J., 1979, Geologic development of the Cordilleran metamorphic core complexes. *Geology*, 7, 120-124.
- DAVIS, G.H. & HARDY, J.J., 1981, The Eagle Pass detachment, southeastern Arizona: Product of mid-Miocene listric(?) normal faulting in the southern Basin and Range. *Geol. Soc. Am. Bull.*, 92/1, 749-762.
- DE BRESSER, J.H.P., 1991, Intracrystalline deformation of calcite. *Geol. Utraiectina*, 79, 191 pp.
- DEER, W.A., HOWIE, R.A. & ZUSSMAN, J., An introduction to the rock-forming minerals. 2<sup>nd</sup> ed., Longman, Essex, 696 pp.
- DIKONOV, I., KHODAKOVSKY, I., SCHOTT, J., SERGEEVA, E., 1994, Thermodynamic properties of iron oxides and hydroxides. I. Surface and bulk thermodynamic properties of goethite ( $\alpha$ -FeOOH) up to 500 K. *Eur. J. Mineral.*, 6, 967-83.
- DICKSON, J.A.D., 1965, A modified staining technique for carbonates in thin section. *Nature*, 205, 587.
- EINSELE, G., 2000, *Sedimentary Basins*. Springer, Berlin, 792 pp.
- FASSOULAS, C., KILIAS, A. & MOUNTRAKIS, D., 1994, Postnappe stacking extension and exhumation of high-pressure/low-temperature rocks in the island of Crete, Greece. *Tectonics*, 13, 127-138.



- FERRILL, D.A., 1991, Calcite twin widths and intensities as metamorphic indicators in natural low-temperature deformation of limestone. *J. Struct. Geol.*, 13, 667-675.
- FORTUIN, A.R., 1977, Stratigraphy and sedimentary history of the Neogene deposits in the Ierapetra region, eastern Crete. GUA Paper of Geology, Amsterdam, 164 pp.
- FORTUIN, A.R. & PETERS, J.M., 1984, The Prina Complex in eastern Crete and its relationship to possible Miocene strike-slip tectonics. *J. Struct. Geol.*, 6, 459-476.
- FRENZEL, G., 1980, The manganese ore minerals. *in* ANNHAUSSER, C.R. & MASKE, S.S., eds., *Geology and geochemistry of manganese*. Schweizerbart, Stuttgart, 25-157.
- FREUDENTHAL, T., 1969, Stratigraphy of Neogene deposits in the Khandia Province, Crete. *Utrecht micropaleont. Bull.*, 1, 1-208.
- FROSTIK, L.E. & STEEL, R.L., eds., 1993, *Tectonic Controls and Signatures in Sedimentary Successions*. Spec. Publ. Int. Ass. Sediment., 20, 520 pp.
- FRYDAS, D. & KEUPP, H., 1996, Biostratigraphical results in Late Neogene deposits of NW Crete, Greece, based on calcareous nannofossils. *Berliner geowiss. Abh.*, E 18, 169-189.
- FRYDAS, D., KEUPP, H. & BELLAS, S., 1999, Biostratigraphical research in Late Neogene marine deposits of the Chania Province, western Crete, Greece. *Berliner geowiss. Abh.*, E 30, 55-67.
- FYTROLAKIS, N., 1972, Die Einwirkungen gewisser orogener Bewegungen und die Gipsbildung in Ostkreta (Prov. Sitia). *Bull. Geol. Soc. Greece*, 9, 81-100.
- GONFIANTINI, R., 1978, Standards for stable isotope measurements in natural compounds. *Nature*, 271, 534-536.
- GROSHONG, R.H., PFIFFNER, O.A. & PRINGLE, L.R., 1984, Strain partitioning in the Helvetic thrust belt of eastern Switzerland from the leading edge to the internal zone. *J. Struct. Geol.*, 6, 19-32.
- HEIDRICK, T.L. & WILKENS, J.W., 1980, Field guide to the geology and ore deposits of the Buckskin Mountains, Arizona. *in* HEIDRICK, T.L., coord., *Mylonitization, detachment faulting, and associated mineralization, Whipple Mountains, California and Buckskin Mountains, Arizona*. Arizona Geological Society, Spring field trip guide, 31-45.
- HOOKE, R.L., 1967, Processes on arid-region alluvial fans. *J. Geol.*, 75, 438-460.
- HOOKE, R.L., 1987, Mass movements in semi-arid environments and the morphology of alluvial fans. *in* ANDERSON, M.G. & RICHARDS, K.S., eds., *Slope stability*. Wiley, Chichester, 505-529.
- HWANG, I.G. & CHOUGH, S.K., 2000, The Maesan fan delta, Miocene Pohang Basin, SE Korea: architecture and depositional processes of a high-gradient fan-delta-fed slope system. *Sedimentology*, 47, 995-1010.
- IAEA/WMO, 2001, Global Network for Isotopes in Precipitation. The GNIP Database. Accessible at: <http://isohis.iaea.org>
- JACKSON, J., 1994, Active tectonics of the Aegean region. *Annu. Rev. Earth Planet. Sci.*, 22, 239-271.
- JACKSON, J.A., ed., 1997, *Glossary of Geology*. 4<sup>th</sup> ed., American Geological Institute, Alexandria/Va., 769 pp.
- JACOBESHAGEN, V., ed., 1986, *Geologie von Griechenland*. Bornträger, Stuttgart, 363 pp.
- JOHNSON, A.M. & RODINE, J.R., 1984, Debris flow. *in* BRUNSDEN, D. & PRIOR, D.B., eds., *Slope Instability*. Wiley, Chichester, 257-361.

- JOLIVET, L., DANIEL, J.M., TRUFFERT, C. & GOFFE, B., 1994, Exhumation of deep crustal metamorphic rocks and crustal extension in arc and back-arc regions. *Lithos*, 33, 3-30.
- JOLIVET, L., GOFFE, B., MONIE, P., TRUFFERT-LUXEY, C. & BONNEAU, M., 1996, Miocene detachment in Crete and exhumation P-T-t paths of high-pressure metamorphic rocks. *Tectonics*, 15/6, 1129-1153.
- KAWABE, I., 1978, Calculation of oxygen isotope fractionation in quartz-water system with special reference to the low temperature fractionation. *Geochim. Cosmochim. Acta*, 42, 613-621.
- KEUPP, H. & BELLAS, S.M., FRYDAS, D. & KOHRING, R., 1994, Aghia Irini, ein Neogenprofil auf der Halbinsel Gramvousa/NW-Kreta. *Berliner geowiss. Abh.*, E 13, 469-481.
- KEUPP, H. & BELLAS, S.M., 2000, Neogene development of the sedimentary basins of NW Crete island, Chania Prefecture, South Aegean Arc System, Greece. *Berliner geowiss. Abh.*, E 34, 3-117.
- KILIAS, A., FASSOULAS, C. & MOUNTRAKIS, D., 1994, Tertiary extension of continental crust and uplift of Psiloritis metamorphic core complex in the central part of the Hellenic Arc, Crete, Greece. *Geol. Rundsch.*, 83, 417-430.
- KÖNIG, H. & KUSS, S.E., 1980, Neue Daten zur Biostratigraphie des permotriadischen Autochthons der Insel Kreta (Griechenland). *N. Jb. Geol. Paläont. Mh.*, 1980/9, 525-540.
- KONTOPOULOS, N., ZELILIDIS, A. & FRYDAS, D., 1996, Late Neogene sedimentary and tectonostratigraphic evolution of northwestern Crete island, Greece. *N. Jb. Geol. Paläont. Abh.*, 202/3, 287-311.
- KOPP, K.-O. & OTT, E., 1977, Spezialkartierungen im Umkreis neuer Fossilfunde in Trypali- und Tripolitza-Kalken Westkretas. *N. Jb. Geol. Paläont. Mh.*, 1977/4, 217-238.
- KOPP, K.-O. & RICHTER, D., 1983, Synorogenetische Schuttbildungen und die Eigenständigkeit der Phyllit-Gruppe auf Kreta. *N. Jb. Geol. Paläont. Abh.*, 165/2, 228-253.
- KOSTASCHUK, R.A., MACDONALD, G.M. & PUTNAM, P.E., 1986, Depositional processes and alluvial fan-drainage basin morphometric relationships near Banff, Alberta, Canada. *Earth Surf. Proc.*, 11, 471-484.
- KOSTER, E.H. & STEEL, eds., 1984, *Sedimentology of gravels and conglomerates*. Can. Soc. Petrol. Geol. Mem., 10, Calgary, 441 pp.
- KRAHL, J., KAUFFMANN, G., KOZUR, H., RICHTER, D., FÖRSTER, O. & HEINRITZI, F., 1983, Neue Daten zur Biostratigraphie und zur Lagerung der Phyllit-Gruppe und der Trypali-Gruppe auf der Insel Kreta (Griechenland). *Geol. Rundsch.*, 72, 1147-1166.
- KÜSTER, M. & STÖCKHERT, B., 1997, Density changes of fluid inclusions in high-pressure low-temperature metamorphic rocks from Crete: A thermobarometric approach based on the creep strength of the host minerals. *Lithos*, 41, 151-167.
- LANGMUIR, D. 1971, Particle size effect on the reaction goethite = hematite + water. *Am. J. Sci.*, 271, 147-156.
- LANGMUIR, D. 1971, Correction: particle size effect on the reaction goethite = hematite + water. *Am. J. Sci.*, 272, 972.
- LEEDER, M.R. & GAWTHORPE, R.L., 1987, Sedimentary models for extensional tilt-block/half-graben basins. *in* COWARD, M.P., DEWEY, J.F. & HANCOCK, P.L., eds., *Continental extension tectonics*. Geol. Soc. Lond. Spec. Publ., 28, 139-152.
- LE PICHON, X. & SIBUET, J., 1981, Passive margins: A model of formation. *J. Geophys. Res.*, 86/B5, 3708-3720.

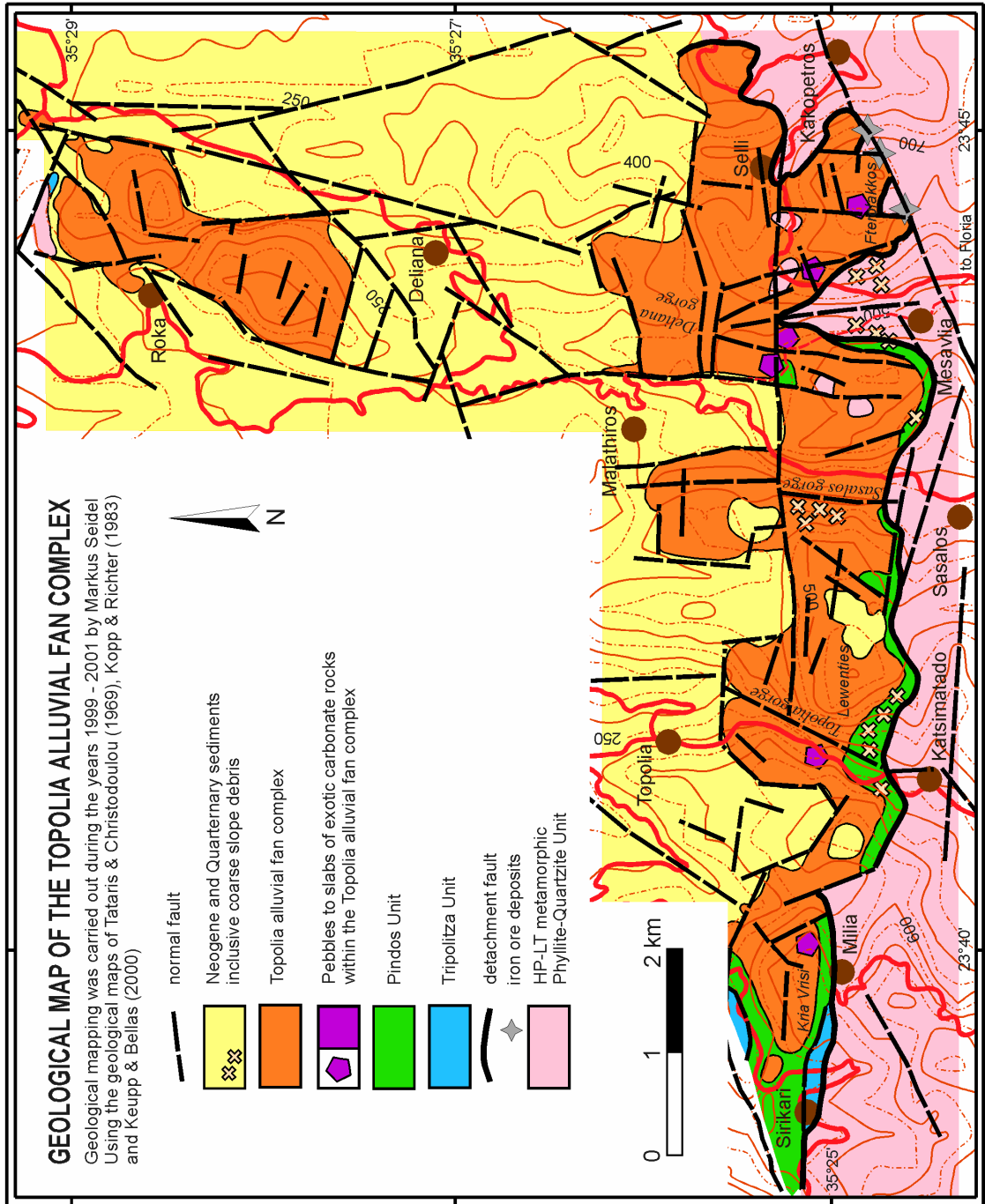
- 
- LE PICHON, X., CHAMOT-ROOKE, N., LALLEMANT, S., NOOMEN, R. & VEIS, G., 1995, Geodetic determination of the kinematics of central Greece with respect to Europe: Implications for eastern Mediterranean tectonics. *J. Geophys. Res.*, 100, 12675-12690.
- LEPPIG, U., 1974, Die Mikrofauna der Tripolitza-Kalke im nördlichen Mittelkreta (Griechenland). Diss., Albert-Ludwigs-Univ., Freiburg i. Br., 142 pp.
- LLOYD, G.E., 1987, Atomic number and crystallographic contrast images with the SEM: a review of backscattered electron techniques. *Mineralogical Magazine*, 51, 3-19.
- LLOYD, G.E., 1994, An appreciation of the SEM electron channelling technique for microstructural analysis of geological materials. *in* BUNGE, H.-J. & WEBER, K., eds., *Textures of Geological Materials*. German Society of Materials Science, 109-126.
- LOEBLICH, A.R., TAPPAN, H., BARKER, R.W., COLE, W.S., DOUGLASS, R.C., REICHEL, M. & THOMPSON, M.L., 1964, Part C Protista 2 Sarcodina chiefly "Thecamoebians" and Foraminiferida. *in* MOORE, R.C., ed., *Treatise on Invertebrate Paleontology*. Geological Society of America, New York, C1-C510a pp.
- LOWE, D.R., 1976, Grain flow and grain flow deposits. *J. Sed. Petrol.*, 46, 188-199.
- MACHEL, H.G. & BURTON, E.A., 1991, Factors governing cathodoluminescence in calcite and dolomite, and their implications for studies of carbonate diagenesis. *in* BARKER, C.E. & KOPP, O.C., eds., *Luminescence microscopy and spectroscopy: Qualitative and quantitative applications*. SEPM Short Course, 25, 37-57.
- MAKRIS, J. & RÖWER, P., 1986, Struktur und heutige Dynamik der Lithosphäre in der Agäis. *in* Jacobshagen, V., ed., *Geologie von Griechenland*. Gebrüder Bornträger, Berlin, 241-256.
- MARSHALL, D.J., 1988, Cathodoluminescence of geologic materials. Unwin Hyman, Boston, 146 pp.
- MASCLE, J. & CHAUMILLON, E., 1997, Pre-collisional geodynamics of the Mediterranean Sea: the Mediterranean Ridge and the Tyrrhenian Sea. *Annali di Geofisica*, XL 3, 569-586.
- MCKENZIE, D.P., 1978, Active tectonics of the Alpine-Himalayan belt: the Aegean Sea and surrounding regions. *Geophys. J. R. Astron. Soc.*, 55, 217-254.
- MCPHERSON, J.G., SHANMUGAN, G. & MOIOLA, R., 1987, Fan-deltas and braid deltas: Varieties of coarse-grained deltas. *Geol. Soc. Am. Bull.*, 99, 331-340.
- MEULENKAMP, J.E., 1979, Field guide to the Neogene of Crete. Dept. Geol. Pal. University of Athens, A32, 1-31.
- MEULENKAMP, J.E., 1985, Aspects of the Late Cenozoic Evolution of the Aegean Region. *in* STANLEY, D.J. & WEZEL, F.C., eds., *Geological evolution of the Mediterranean Basin*. Springer, New York, 307-321.
- MEULENKAMP, J.E., VAN DER ZWAAN, G.J. & VAN WAMEL, W.A., 1994, On Late Miocene to Recent vertical motions in the Cretan segment of the Hellenic arc. *Tectonophysics*, 234, 53-72.
- MEYERS, W.J., 1991, Calcite cement stratigraphy: an overview. *in* BARKER, C.E. & KOPP, O.C., eds., *Luminescence microscopy and spectroscopy: Qualitative and quantitative applications*. SEPM Short Course, 25, 133-148.
- MIALL, A.D., 1996, *The Geology of Fluvial Deposits: sedimentary facies, basin analysis and petroleum geology*. Springer, Berlin, 582 pp.
- MILLER, J., 1988, Cathodoluminescence Microscopy. *in* TUCKER, M., ed., *Techniques in Sedimentology*. Blackwell, Oxford, 394 pp.

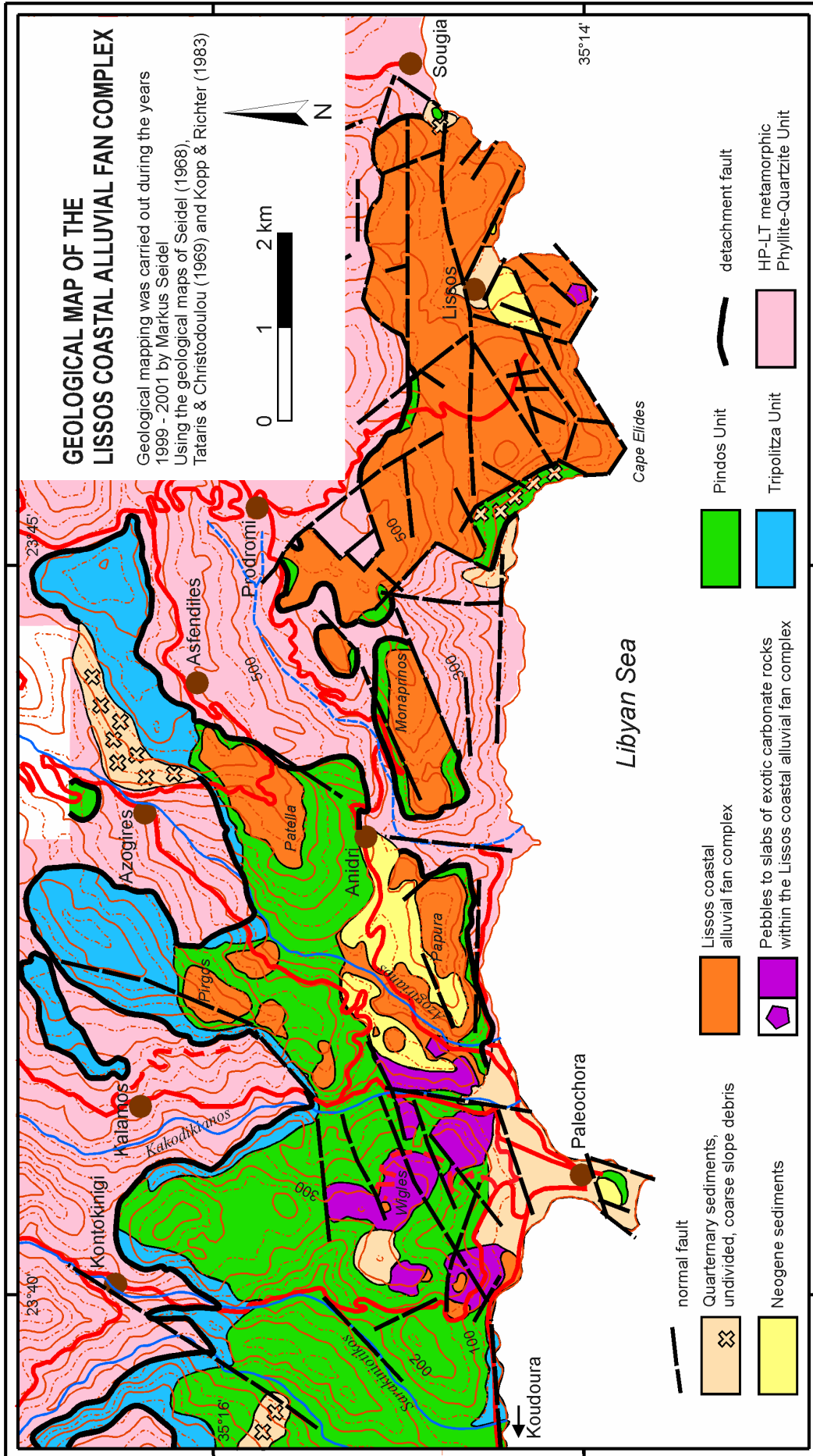
- MURRAY, J.W., 1981, Iron oxides. *in* BURNS, R.G., ed., Marine minerals. *Rev. Mineral.*, 6, 47-98.
- NEMEC, W., 1990, Deltas – remarks on terminology and classification. *in* COLELLA, A. & PRIOR, D.B., eds., Coarse-Grained Deltas. *Spec. Publ. Int. Ass. Sediment.*, 10, 3-12.
- O'NEIL, J.R., 1986, Appendix: Terminology and Standards. *in* VALLEY, J.W., TAYLOR, H.P. & O'NEIL, J.R., eds., Stable Isotopes. *Rev. Mineral.*, 16, 561-570.
- PACK, A., GUTZMER, J., BEUKES, N.J., VAN NIEKERK, H.S. & HOERNES, S., 2000, Supergene ferromanganese wad deposits derived from Permian Karroo strata along the late Cretaceous-mid-Tertiary African land surface, Ryedale, South Africa. *Economic Geology*, 95, 203-220.
- PAPANIKOLAOU, D. & STÖCKHERT, B., 1998, ICDP Workshop on a Drilling Projekt in the Forearc of the Hellenic Subduction Zone, Crete, Greece. ICDP-Report.
- PASSCHIER, C.W. & TROUW, R.A.J., 1996, *Microtectonics*. Springer, Berlin, 289 pp.
- POSTMA, G., 1990, Depositional architecture and facies of river and fan deltas: a synthesis. *in* COLELLA, A. & PRIOR, D.B., eds., Coarse-Grained Deltas. *Spec. Publ. Int. Ass. Sediment.*, 10, 13-27.
- POSTMA, G. & DRINIA, H., 1993, Architecture and sedimentary facies evolution of a marine, expanding outer-arc half-graben (Crete, late Miocene). *Basin Res.*, 5, 103-124.
- POSTMA, G., FORTUIN, A.R. & VAN WAMEL, W.A., 1993, Basin-fill patterns controlled by tectonics and climate: the Neogene 'fore-arc' basins of eastern Crete as a case history. *in* FROSTIK, L.E. & STEEL, R.L., eds., Tectonic Controls and Signatures in Sedimentary Successions. *Spec. Publ. Int. Ass. Sediment.*, 20, 335-362.
- POWELL, R., CONDLIFFE, D.M. & CONDLIFFE, E., 1984, Calcite-dolomite geothermometry in the system  $\text{CaCO}_3\text{-MgCO}_3\text{-FeCO}_3$ : an experimental study. *J. Metamorphic Geology*, 2, 33-41.
- PRIOR, D.B. & BORNHOLD, B.D., 1990, The underwater development of Holocene fan deltas. *in* COLELLA, A. & PRIOR, D.B., eds., Coarse-Grained Deltas. *Spec. Publ. Int. Ass. Sediment*, 10, 75-90.
- PRIOR, D.J., BOYLE, A.B., BRENKER, F., CHEADLE, M.C., DAY, A., LOPEZ, G., PERUZZO, L., POTTS, G.J., REDDY, S., SPIES, R., TIMMS, N.E., TRIMBY, P., WHEELER, J. & ZETTERSTRÖM, L., 1999, The application of electron backscatter diffraction and orientation contrast imaging in the SEM to textural problems in rocks. *Am. Mineral.*, 84, 1741-1759.
- RAMDOHR, P. & STRUNZ, H., 1978, *Klockmanns Lehrbuch der Mineralogie*. Stuttgart, Ferdinand Enke Verlag, 875 pp.
- RING, U., LAYER, P.W. & REISCHMANN, T., 2001, Miocene high-pressure metamorphism in the Cyclades and Crete, Aegean Sea, Greece: Evidence for large-magnitude displacement on the Cretan detachment. *Geology*, 29, 395-398.
- ROWE, K.J. & RUTTER, E. H., 1990, Paleostress estimation using calcite twinning: experimental calibration and application to nature. *J. Struct. Geol.*, 12, 1-17.
- ROZANSKI, K., ARAGUAS-ARAGUAS, L., GONFIANTINI, R., 1993, Isotope Patterns in Modern Global Precipitation. *in* American Geophysical Union, ed., *Climate Change in Continental Isotope Records*. Geophysical Monograph, 78, 1-36.
- SANNEMANN, W. & SEIDEL, E., 1976, Die Trias-Schichten von Rawdoucha/NW-Kreta. Ihre Stellung im kretischen Deckenbau. *N. Jb. Geol. Paläont. Mh.*, 1976/4, 221-228.
- SAUVAGE, M. & AUTHIER, A., 1965, Etude des bandes de croissance et dislocations de macles dans la calcite. *Bull. Soc. fr. Mineral. Cristal.*, 88, 379-388.

- SEIDEL, E., 1968, Die Tripolitza- und die Pindos-Serie im Raum von Paleochora, SW-Kreta, Griechenland. Diss., Univ. Würzburg, 102 pp.
- SEIDEL, E., 1971, Die Pindos-Serie in Westkreta, auf der Insel Gavdos und im Kedros-Gebiet (Mittelkreta). N. Jb. Geol. Paläont. Abh., 137, 443-460.
- SEIDEL, E., 1978, Zur Petrologie der Phyllit-Quarzit-Serie Kretas. Habil.-Schrift, Univ. Braunschweig, 145 pp.
- SEIDEL, E. & THEYE, T., 1993, High-pressure/low-temperature metamorphism in the external Hellenides, Crete, Peloponnes. Bull. Geol. Soc. Greece, 28, 49-55.
- SEIDEL, E. & WACHENDORF, H., 1986, Die südägäische Inselbrücke. in JACOBSHAGEN, V., ed., Geologie von Griechenland. Gebrüder Bornträger, Berlin, 54-80.
- SEIDEL, E., KREUZER, H. & HARRE, W., 1982, A late Oligocene/early Miocene high pressure belt in the external Hellenides. Geol. Jb., E 23, 165-206.
- SEIDEL, E., OKRUSCH, M., KREUZER, H., RASCHKE, H. & HARRE, W., 1981, Eo-alpine metamorphism in the uppermost unit of the Cretan nappe system – petrology and geochronology. Part 2. Synopsis of the high-temperature metamorphics and associated ophiolites. Contrib. Mineral. Petrol., 76, 351-361.
- SELBY, M.J., 1994, Hillslope sediment transport and deposition. in PYE, K., ed., Sediment transport and depositional processes. Blackwell, Cambridge, 61-87.
- SHARP, Z.D., 1990, A laser-based microanalytical method for the in-situ determination of oxygen isotope ratios of silicates and oxides. Geochim. Cosmochim. Acta, 54, 1353-1357.
- STÖCKHERT, B., 2001, Insight into the mechanics of subduction roll back - significance, status, and perspectives of an integrated onshore-offshore drilling project in the Hellenic subduction zone, ICDP-SPP Kolloquium 2001 (DFG), Bochum 7./8.7.2001, Abstracts, 201-207.
- STÖCKHERT, B., WACHMANN, M., KÜSTER, M. & BIMMERMANN, A., 1999, Low effective viscosity during high pressure metamorphism due to dissolution precipitation creep: the record of HP-LT metamorphic carbonates and siliciclastic rocks from Crete. Tectonophysics, 303, 299-319.
- TATARIS, A. & CHRISTODOULOU, G., 1969, Geological Map of Greece 1:50,000, Sheet Alikianou. IGME, Athen.
- TAYMAZ, T., JACKSON, J. & WEATAWAY, R., 1990, Earthquake mechanisms in the Hellenic Trench near Crete. Geophys. J. Int., 102, 695-731.
- TEN VEEN, J.H. & MEIJER, P.T., 1998, Late Miocene to Recent tectonic evolution of Crete, Greece, geological observations and model analysis. Tectonophysics, 298, 191-208.
- TEN VEEN, J.H. & POSTMA, G., 1999a, Neogene tectonics and basin fill patterns in the Hellenic outer-arc, Crete, Greece. Basin Res., 11, 223-241.
- TEN VEEN, J.H. & POSTMA, G., 1999b, Roll-back controlled vertical movements of outer-arc basins of the Hellenic subduction zone, Crete, Greece. Basin Res., 11, 243-266.
- THEYE, T., 1988, Aufsteigende Hochdruckmetamorphose in den Sedimenten der Phyllit-Quarzit-Einheit Kretas und des Peloponnes. Diss., Univ. Braunschweig, 224 pp.
- THEYE, T. & SEIDEL, E., 1993, Uplift-related retrogression history of aragonite marbles in Western Crete (Greece). Contrib. Mineral. Petrol., 114, 349-356.
- THEYE, T. & SEIDEL, E., 2001, Bauxite in hochdruckmetamorphen Einheiten der externen Helleniden. Braunschweiger geowiss. Arb., 24, 225-233.

- THOMSON, S.N., STÖCKHERT, B. & BRIX, M.R., 1998, Thermochemistry of the high-pressure metamorphic rocks on Crete, Greece: Implications for the speed of tectonic processes. *Geology*, 26, 259-262.
- THOMSON, S.N., STÖCKHERT, B. & BRIX, M.R., 1999, Miocene high-pressure metamorphic rocks of Crete, Greece: rapid exhumation by buoyant escape. *in* RING, U., BRANDON, M.T., LISTER, G.S. & WILLET, S.D., eds., 1999, Exhumation Processes: Normal faulting, Ductile Flow and Erosion. *Geol. Soc. Lond. Spec. Publ.*, 154, 87-108.
- TOBIN, H., VANNUCCHI, P. & MESCHEDÉ, M., 2001, Structure, inferred mechanical properties, and implications for fluid transport in the décollement zone, Costa Rica convergent margin. *Geology*, 29, 907-911.
- TRUFFERT, C., CHAMOT-ROOKE, N., LALLEMANT, S., DE VOOGD, B., HUCHON, P. & LE PICHON, X., 1993, The crust of the western Mediterranean ridge from deep seismic data and gravity modelling. *Geophys. J. Int.*, 114, 360-372.
- TURNER, F. J. & OROZCO, M., 1976, Crystal bending in metamorphic calcite and its relations to associated twinning. *Contrib. Mineral. Petrol.*, 57, 83-97.
- VERNON, R.H., 1981, Optical microstructure of partly recrystallized calcite in some naturally deformed marbles. *Tectonophysics*, 78, 601-612.
- WACHENDORF, H., GRALLA, P., KOLL, J. & SCHULZE, I., 1980, Geodynamik des mittelmittelkretischen Deckenstapels (nördliches Dikti-Gebirge). *Geotekt. Forsch.*, 59, 1-72.
- WACHMANN, M., 1997, Die strukturelle Entwicklung hochdruckmetamorpher Karbonatgesteine bei Agios Theodori, SW Kreta. *Bochumer Geol. Geotech. Arb.*, 48, 168 pp.
- WEISS, L.E., 1954, A study of tectonic style: Structural investigations of a marble quartzite complex in southern California. *Univ. Calif. Publ. Geol. Sci.*, 30, 1-102.
- WENK, H.-R., 1985, Carbonates. *in* WENK, H.-R., ed., Preferred orientation in deformed metals and rocks: An introduction to modern texture analyses. Academic Press, Orlando, 361-384.
- WERNICKE, B., 1981, Low-angle normal faulting in the Basin and Range Province: Nappe tectonics in an extending orogen. *Nature*, 291, 645-648.
- WESCOTT, W.A., & ETHRIDGE, F.G., Fan-delta sedimentology and tectonic setting – Yallahs fan delta, southeast Jamaica. *Bull. Am. Assoc. Petrol. Geol.*, 64, 374-399.
- WORTEL, M.J.R., GOES, S.B. & SPAKMAN, W., 1990, Structure and seismicity of the Aegean subduction zone. *Terra Nova*, 2, 554-562.
- YAPP, C.J., 1987, Oxygen and hydrogen isotope variations among goethites,  $\alpha$ -FeOOH, and the determination of paleotemperatures. *Geochim. Cosmochim. Acta*, 51, 355-364.
- YAPP, C.J., 1990, Oxygen isotopes in iron, III, oxides. 1. Mineral-water fractionation factors. *Chem. Geol.*, 85, 329-335.
- YAPP, C.J., 2001, Rusty relics of earth history: Iron (III) Oxides, Isotopes, and Surficial Environments. *Annu. Rev. Earth Planet. Sci.*, 29, 165-199.
- ZAGER, D., 1972, Sedimentologie der Tripolitzakarbonate im nördlichen Mittelkreta (Griechenland). *Diss., Albert-Ludwigs-Universität, Freiburg i. Br.*, 131 pp.
- ZHENG, Y.-F., 1993, Calculation of oxygen isotope fractionation in hydroxyl-bearing silicates. *Earth Planet. Sci. Lett.*, 120, 247-263.
- ZHENG, Y.-F., 1998, Oxygen isotope fractionation between hydroxide minerals and water. *Phys. Chem. Mineral.*, 25, 213-221.

# 11 Geological maps







## **Ausführliche Zusammenfassung**

Die Hellenische Subduktionszone am Südrand der Ägäis stellt mit dem Zurückrollen der abtauchenden afrikanischen Platte und der damit einhergehenden Dehnung im Frontbereich der hangenden eurasischen Platte ein interessantes Studienobjekt dar. Im zentralen Forearc der Hellenischen Subduktionszone liegt als Horst die Insel Kreta. Ihre geologische Geschichte dokumentiert die Entwicklung der Plattengrenze zwischen Afrika und Eurasien während der letzten 35 Ma.

Kreta besteht aus einem oligozän/miozänen Akkretionskomplex, in dem unter erheblicher Krustendehnung im Zeitraum zwischen 23 und 15 Ma vor heute Krustenteile aus über 30 km Tiefe exhumiert wurden. Diese hochdruckmetamorphen Einheiten (Plattenkalk-Einheit, Phyllit-Quarzit-Einheit) befinden sich heute unmittelbar unter nicht metamorphen Einheiten (Tripolitza-Einheit, Pindos-Einheit). Dazwischen liegt eine tektonische Trennfläche, die analog zur Situation in einem „metamorphic core complex“ als flache Abschiebung (low-angle normal fault oder detachment fault) interpretiert wird. Der gesamte Deckenstapel ist heutzutage nur wenige Kilometer mächtig, sein Unterbau ist unbekannt.

Informationen über die frühere Entwicklung der Hellenischen Subduktionszone liefern neben den hochdruckmetamorphen Einheiten im Liegenden unter- bis mittelmiozäne Beckenfüllungen (Konglomerat- und Brekzienkalke) im Hangenden des kretischen Deckenstapels, die in Halbgräben abgelagert wurden. Diese nur in Westkreta vorkommenden synorogenen Schuttbildungen entstanden bei der Disintegration der Hangendplatte im Zusammenhang mit der dehnungsbedingten Exhumierung der hochdruckmetamorphen Einheiten. Sie werden ebenso wie die Pindos-, Tripolitza- und Phyllit-Quarzit-Einheit diskordant von marinen Sedimenten des Obermiozäns überlagert.

Die lithologische und strukturelle Charakterisierung der unter- bis mittelmiozänen Beckenfüllungen in Westkreta war Gegenstand der vorliegenden Arbeit. Das Arbeitsgebiet liegt westlich der weißen Berge (Levka Ori) und ist zweigeteilt. Ein Areal befindet sich im Nordwesten der Insel in der Umgebung der Ortschaften Sirikari, Topolia und Kakopetros, das andere im Südwesten zwischen Paleochora und Sougia.

Das Geröllspektrum der unter- bis mittelmiozänen Beckenfüllungen wird von Flachwasserkalken dominiert, die in ihrer Mikrofazies und ihrem Fossilinhalt (Rudisten, Nummuliten) kretazischen und eozänen Abschnitten der Tripolitza-Einheit entsprechen. Komponenten, die dem Faziesbereich der Pindos-Einheit zugeordnet werden können (Radiolarite, pelagische Kalke mit Hornsteinknollen, Kalkarenite, Flyschsandsteine) treten stark zurück. Die Herkunft einiger Marmor-komponenten bleibt rätselhaft (exotische Komponenten). Fragmente aus den hochdruckmetamorphen Einheiten Kretas konnten weder im Gelände noch im Labor nachgewiesen werden. Das Fehlen von Komponenten aus dem Liegenden der Abschiebung weist darauf hin, dass die Beckensedimente geschüttet wurden, als die hochdruckmetamorphen Einheiten noch nicht an der Erdoberfläche anstanden und der Erosion ausgesetzt waren.

Faziesanalysen zeigen, dass die Beckenfüllungen in unterschiedlichen Milieus abgelagert wurden. Im nördlichen Arbeitsgebiet liegen terrestrische Schuttfächerablagerungen vor, im südlichen bestehen die Sedimente aus subaerischen und submarinen Bildungen.

Die terrestrischen Bildungen im nördlichen Areal („Topolia-Schuttfächer“, Topolia alluvial fan complex), die eine Mächtigkeit von mehr als 500 m erreichen können, sind hauptsächlich auf die Ablagerung von Schuttströmen (debris-flow) zurückzuführen. Sie zeigen weitgehend schlechte Sortierung, sind klastenreich, matrixgestützt und stammen aus einem Einzugsgebiet, das hauptsächlich aus Kalksteinen und Dolomiten bestand. Die Schichtung ist meist nur undeutlich ausgebildet. Das Liefergebiet des klastischen Materials lag im Süden. Die Klasten wurden nach Norden transportiert, wie die in dieser Richtung abnehmende Korngröße und zunehmende Rundung zeigen. Auch die Mächtigkeit der Ablagerungen und das Einfallen der Schichten nehmen in Richtung des Transportweges ab. Untersuchungen mit dem Rasterelektronenmikroskop und mit der Kathodolumineszenz ergaben, dass die Sedimente nach der Ablagerung kompaktiert und zementiert wurden. Die verschiedenen Zementgenerationen bilden dabei die postsedimentäre Entwicklung der Schuttfächer ab, die zunächst unter den Meeresspiegel abgesenkt und anschließend wieder herausgehoben wurden.

Im Gebiet zwischen Paleochora und Lissos liegt ein Sedimentkeil vor, der aus terrestrischen und marinen Schuttbildungen aufgebaut ist („Lissos-Schuttdelta“, Lissos coastal alluvial fan complex). Die Sedimente können mehr als 250 m mächtig werden. Sie bestehen hauptsächlich aus Brekzien, Konglomeraten und mergeligen Kalken. Untergeordnet treten turbiditische Ablagerungen mit Wühlspuren auf, stellenweise sind Olistolithe eingeschaltet.

Der Kontakt zwischen den unter- bis mittelmiozänen Beckensedimenten und der Pindos-Einheit ist meist von Schuttmassen verdeckt oder tektonisch überprägt. Jedoch ergibt sich aus der Kartierung eindeutig eine sedimentäre Auflagerung. Dagegen konnte ein sedimentärer Kontakt zwischen den Beckensedimenten und der Tripolitza-Einheit nicht belegt werden.

Als Folge anhaltender Dehnung treten die westkretischen Beckenfüllungen heute stellenweise direkt mit der hochdruckmetamorphen Phyllit-Quarzit-Einheit in tektonischen Kontakt. Analog zu den Lagerungsverhältnissen in einem „metamorphic core complex“ wird dies durch Bewegungsvorgänge entlang der flachen Abschiebung erklärt, welche die hochdruckmetamorphen Einheiten im Liegenden von den nicht metamorphen Einheiten im Hangenden trennt.

Im Bereich der Abschiebungsbahn sind die Gesteine stark brekziiert. Stellenweise bilden diese Brekzien eine mehrere zehn Meter mächtige Zone. Eine typische Erscheinung der Brekzien ist ihre Mineralisation mit fein verteiltem und rissfüllendem Goethit.  $\delta^{18}\text{O}$ -Werte des Goethites zeigen eine niedrigtemperierte (31-40°C) Entstehung der Erze an. Durch die Imprägnation mit Eisenhydroxid erhält der brekziierte Bereich eine von weitem sichtbare gelb-orange-rote Farbgebung. Eine solche „ferruginous alteration“ ist typisch für flache Abschiebungsbahnen innerhalb von „metamorphic core complexes“ in der nordamerikanischen Kordillere. Die Eisenerzvorkommen von Ravdoucha und Kakopetros in Westkreta verdanken ihre Entstehung diesem Prozess.

Kalkgerölle mit Großforaminiferen des höheren Miozäns bis tieferen Obereozäns zeigen, dass die Beckenfüllungen jünger sind. Andererseits müssen sie älter sein als die transgressiv auf ihnen lagernden marinen Sedimente des mittleren Torton. Somit kann über den paläontologischen Befund das Alter der Beckenfüllungen auf die Zeitspanne zwischen 35 und 10 Ma eingengt werden.

Eine weitere Einengung des Alters der Beckenfüllungen kann indirekt über die Thermochronologie der Phyllit-Quarzit-Einheit erfolgen. Danach ergibt sich für die Anlage einer „detachment fault“ zwischen hochdruckmetamorphen und nicht metamorphen Einheiten sowie die damit korrelierte Beckenbildung in der Hangendplatte ein Höchstalter von 20 Ma. Der Prozess der Exhumierung und damit die Sedimentation der Konglomerat- und Brekzienkalke, die frei von Komponenten aus der Phyllit-Quarzit-Einheit sind, war vor etwa 15 Ma abgeschlossen.

Sedimente (Prina-Komplex) an der Basis des Neogens im Graben von Ierapetra (Ostkreta) erinnern in ihrer Fazies an die Konglomerat- und Brekzienkalke in Westkreta. Vergleichende Betrachtungen zeigen jedoch, dass die Sedimentation in den beiden Regionen von unterschiedlichen tektonischen Prozessen gesteuert wurde. Die Sedimente in Westkreta wurden während einer Dehnungsphase abgelagert, die Sedimente in Ostkreta hingegen entstanden während einer Einengungsphase.

Die unter- bis mittelmiozänen Beckenfüllungen in Westkreta zeichnen eine Phase kontinuierlicher Dehnung im Forearc der Hellenischen Subduktionszone auf und geben Einblick in die tektonische Entwicklung der Plattengrenze zwischen Afrika und Eurasien in der Zeitspanne zwischen 20 und 15 Ma (Burdigal bis Langh/Serravall) vor heute, die sonst geologisch schlecht belegt ist.

## List of Figures

Figure 1: Overview of the geographical distribution of the synorogenic sediments.....	3
Figure 2: Cartoon showing a schematic cross section of the Hellenic subduction zone and the geographic and tectonic setting of Crete in the central fore arc.....	5
Figure 3: Schematic illustration of the tectonostratigraphy of Crete.....	6
Figure 4: Generalized geological map of western Crete.....	8
Figure 5: Outsized clast in a matrix-rich debris-flow deposit.....	10
Figure 6: Two intercalations of sand- to mudstone beds (lithified dolomite sands) in conglomerates of the Topolia alluvial fan complex, Topolia gorge.....	12
Figure 7: Clast-supported water-flow deposits northwest of Mesavlia.....	13
Figure 8: Schematic block diagram showing the catchment (drainage basin) and the depositional features of the Topolia alluvial fan complex.....	15
Figure 9: Vertical sections of the Topolia alluvial fan complex depicting facies and stratigraphy.....	15
Figure 10: Lithified debris-flow deposit near Lissos.....	17
Figure 11: An olistolith of grey limestone embedded in dark lithified dolomite sands of facies G.....	18
Figure 12: Detailed vertical log through a fine-grained sequence of the submarine part of the Lissos fan delta, at the western flank of cape Elides.....	19
Figure 13: (a) Succession of different facies types of the distal slope/basin plain. (b) Succession of colored marly limestones and limestones.....	20
Figure 14: Schematic diagram showing the mid-Miocene half graben, the catchment and the depositional features of the coastal alluvial fans in the surroundings of Lissos.....	22
Figure 15: Simplified radial cross section of Lissos slope-type fan delta illustrating different depositional settings and facies types.....	22
Figure 16: Schematic cross section illustrating the depositional setting of the Topolia alluvial fan complex. The alluvial fan is situated beneath a fault scarp (model 1).....	23
Figure 17: Schematic cross section illustrating the depositional setting of the Topolia alluvial fan complex. The alluvial fan is situated beneath the range front (model 2).....	24
Figure 18: Paleogeographic model at the time of deposition of the two clastic wedges.....	25
Figure 19: Part of Eh-pH diagrams for the systems Mn-O-H and Fe-O-H.....	27
Figure 20: SEM photomicrographs of marine sediments of the Lissos fan delta complex.....	28
Figure 21: SEM photomicrographs of subaerial sediments of the Lissos fan delta complex.....	29
Figure 22: Stylolites in clast-supported fanglomerates of the Topolia alluvial fan complex in the region north of Milia.....	29
Figure 23: SEM photomicrographs of the Topolia alluvial fan complex.....	30
Figure 24: (A) Cathodoluminescence photomicrograph of calcite cement in a sample from the Topolia alluvial fan complex. (B) Elemental maps of the area which is marked by white arrows in figure A.....	31
Figure 25: Elemental maps and photomicrographs of calcite cements in a fanglomerate sample from the Topolia alluvial fan complex.....	32

---

Figure 26: Cathodoluminescence photomicrograph and elemental maps of calcite cement in a sample from the Topolia alluvial fan complex. ....	33
Figure 27: Photomicrographs of meniscus calcite cement in a fanglomerate sample from the Topolia alluvial fan complex. ....	33
Figure 28: Sketch of the diagenetic evolution showing a cross section of the Topolia alluvial fan complex and a magnified vug. ....	34
Figure 29: Schematic succession of cement generations and pathway of tectonically controlled subsidence and uplift of the Topolia alluvial fan complex with hypothetical evolution of pore water Eh during diagenesis. ....	35
Figure 30: View from east of Katsimatado to the northwest in the Topolia gorge. ....	36
Figure 31: Photomicrograph of a stained thin section of a partially dolomitized limestone clast. ....	37
Figure 32: (a) and (b) Clasts of biomicrites with rudists in the sediments of the Topolia alluvial fan complex. ....	39
Figure 33: Photomicrographs of clasts embedded in the Topolia alluvial fan complex. ....	40
Figure 34: Classification of calcite twins into 4 categories according to their appearance in thin section. ....	44
Figure 35: Photomicrographs of carbonate rocks with type A microstructure in thin section. ....	46
Figure 36: Microstructure of a sample of a marble in ultra thin section. ....	47
Figure 37: Microstructures of calcite marbles. ....	49
Figure 38: Orientation of c-axis of calcite of three rock samples as determined by EBSD. ....	49
Figure 39: Microstructures of marbles from the HP-LT metamorphic Phyllite-Quartzite Unit. ....	50
Figure 40: Tectonic contact of the nonmetamorphic basin fill with the HP-LT metamorphic Phyllite-Quartzite Unit. ....	55
Figure 41: Schematic cross section showing the tectonic contact of the breccio-conglomerates and the Tripolitza/Pindos Unit with the high-pressure metamorphic rocks of the Phyllite-Quartzite Unit. ....	56
Figure 42: Stereographic projection showing the orientations of main low-angle to moderate-angle brittle normal faults in outcrops of the Phyllite-Quartzite Unit in the working area in western Crete. ....	57
Figure 43: (a) Horst structure in the Phyllite-Quartzite Unit of western Crete. (b) Brittle low-angle normal faults in the Phyllite-Quartzite Unit at the roadside south of Sfinari. ....	58
Figure 44: Photomicrograph of a brecciated marble (rauhwacke) of the Phyllite-Quartzite Unit. ....	59
Figure 45: Photomicrograph of a brecciated quartzite marking the detachment in the roof of the Phyllite-Quartzite Unit. ....	59
Figure 46: Fragments of the breccio-conglomerates in upper Miocene terrestrial sediments. ....	61
Figure 47: Borelis melo in thin sections. ....	61
Figure 48: (A) Photograph of the detachment zone which is characterized by ferruginous alteration. (B) Photograph of rauhuckles within the detachment fault of the Phyllite-Quartzite Unit. ....	64
Figure 49: Electron backscattered photomicrograph of laminated goethite ore. ....	65
Figure 50: Reflected light photomicrograph of laminated hardbands of Ba-rich cryptomelane alternating with goethite. ....	66

Figure 51: (A) Reflected light photomicrograph of Ba-rich cryptomelane and goethite. (B, C, D). Electron microprobe maps of the same area showing the relative contents of potassium, iron and manganese. ....	66
Figure 52: Reflected light photomicrograph showing a quartzite breccia with angular clasts. The veins are filled predominantly by goethite. ....	71
Figure 53: Fluid flow pattern within the detachment zone. ....	72
Figure 54: Results of lineament analyses for western Crete. (A) SAT image. (B) Aerial photograph. ...	74
Figure 55: Rose diagrams of (A) SPOT image and (B) aerial photograph. ....	75
Figure 56: General map showing the geographical position of the outcrop of breccio-conglomerates west of Iraklion. ....	78
Figure 57: Rock samples in thin section. (A, B) Photomicrographs of an amphibolite underlying the breccio-conglomerates west of Iraklion. (C) Photomicrograph of a volcanic clast in the graben fill. ....	79
Figure 58: Schematic cross sections showing progressive stretching of the brittle upper crust. ....	82
Figure 59: Successive steps in the paleogeographic evolution of Crete since the Burdigalian. ....	83
Figure 60: Cartoon showing a schematic cross section of the Hellenic subduction zone and the southern Aegean region during lower to middle Miocene times. ....	84

## List of Tables

Table 1: Electron probe microanalyses (wt%) and cation proportions per formula unit of dolomite and calcite from sample M1-22. ....	53
Table 2: Microprobe analyses of selected goethite samples from the Kakopetros iron ore deposit. ....	65
Table 3: Microprobe analyses of Mn-rich laminae and bands in samples from the Kakopetros iron ore deposit. ....	67
Table 4: Chemical composition of the ore and associated breccias and impregnated country rock of the iron ore deposits of Kakopetros and Ravdoucha as determined by X-ray fluorescence analysis. ....	68
Table 5: $\delta^{17}\text{O}$ and $\delta^{18}\text{O}$ values of goethite samples from Kakopetros. ....	69
Table 6: Chemical composition of volcanite clasts as determined by X-ray fluorescence analysis. ....	80

## Appendix

### List of samples cited in Figures and Tables

sample	location	rock type
M1-1	S of Ravdoucha	iron ore
M1-2	W of Ravdoucha	iron ore
M1-22	N of Wigles	dolomite marble
M1-60	graben of Iraklion	volcanite clast within the graben fill
M1-62	graben of Iraklion	volcanite clast within the graben fill
M1-66	graben of Iraklion	amphibolite of the Uppermost Unit
M1-114	W of Wigles	calcite marble
M1-118	W of Wigles	calcite marble
M1-119	W of Wigles	calcite marble
M1-147	N of Milia	calcite marble
M1-169	E of Wigles	calcite marble
M1-184	1 km W of Kontokinigi	calcite marble
M1-185	Wigles	calcite marble
M1-189	Wigles	calcite marble
M2-23	Topolia gorge	clast within the Topolia alluvial fan complex
M2-35	Topolia gorge	calcite marble
M2-38	Sasalos canyon	matrix from a debris-flow deposit of the Topolia alluvial fan complex
M2-40	NNW Mesavlia	breccia within the detachment zone
M2-53	Papura	marine sedimentary rocks of the Lissos coastal alluvial fan complex
M2-124	SW of Kakopetros	breccia within the detachment zone
M2-137	NNW of Mesavlia	clast within the Topolia alluvial fan complex
M2-177	W of Lissos	marine sedimentary rocks of the Lissos coastal alluvial fan complex
M2-198	W of Katsimatado	matrix from a debris-flow deposit of the Topolia alluvial fan complex
M2-214	SW of Kakopetros	quartzite breccia with iron ore
M2-215	SW of Kakopetros	iron ore
M2-216	SW of Kakopetros	quartzite breccia with iron ore
M2-219	E of Roka	matrix from a waterlaid deposit of the Topolia alluvial fan complex
M2-232	NE of Paleochora	Neogene deposits
M2-241	NNW Mesavlia	waterlaid deposit of the Topolia alluvial fan complex
M2-242	Pass W of Kakopetros	dolomite marble
M2-286	Wigles	calcite marble
M2-296	NNW Mesavlia	iron ore
M2-311	W of Wigles	subaerial sediments of the Lissos coastal alluvial fan complex
M2-326	Roka	matrix from a waterlaid deposit of the Topolia alluvial fan complex
M9-17	WSW of Kakopetros	iron ore

Altogether 570 samples were collected for this study.

### Abbreviations

PPL plane-polarized light; XPL cross-polarized light

amp amphibol; cal calcite; dol dolomite; ep epidote; pl plagioclase; qtz quartz



---

## Acknowledgements

During my investigations I have been helped immeasurably by many people who pointed out geological problems, gave me thoughtful comments and prepared or carried out measurements. Among these I am especially grateful to

Prof. Dr. Eberhard Seidel (Institut für Mineralogie und Geochemie, Universität zu Köln) for the suggestion of the interesting topic, for joint field work in Crete and for thoughtful discussions and continuous help while preparing this thesis.

Prof. Dr. Bernhard Stöckhert (Institut für Geologie, Mineralogie und Geophysik, Ruhr-Universität Bochum) for the suggestion of the interesting topic, helpful discussions and comments and continuous support.

Dr. Andreas Pack (Institut für Mineralogie und Geochemie, Universität zu Köln) for performing oxygen isotope measurements at the University of New Mexico, Albuquerque, and for helpful discussions.

Dr. Reiner Kleinschrodt (Institut für Mineralogie und Geochemie, Universität zu Köln) for help and discussions concerning calcite microstructure.

Dr. Markus Klein and Thorbjörn Schönbeck (Institut für Mineralogie und Geochemie, Universität zu Köln) for performing XRF analyses and for their help.

Philip Kegler and Dr. Thomas Pletsch for friendship and help while sharing the room at the IMG.

The staff of the Institut für Mineralogie und Geochemie der Universität zu Köln for continuous help and support.

Prof. Dr. Werner Ricken (Geologisches Institut, Universität zu Köln) for helpful discussions about sedimentary environment and sedimentological features.

Dr. Harald Tragelehn (Geologisches Institut, Universität zu Köln) for fossil determination.

Dr. Peter Bruckschen, Dr. Jutta Weber, Dr. Oliver Swientek, Markus Hirschfeld and Heiko Freitag (Geologisches Institut, Universität zu Köln) for numerous discussions and help.

Dr. R. Neuser for carrying out SEM and CL studies and Dr. M. Wachmann for carrying out EBSD studies at the Ruhr-Universität Bochum.

Evdoxia Mystakidou and Prof. Dr. Georg Kostakis (Technical University of Chania) for their organizational support.

Dr. Andreas Peterek and Jochen Schwarze (Universität Bayreuth) for providing SPOT images, aerial photographs and digital topographic data and for discussions.

Dr. Spiridon Bellas and Prof. Dr. H. Keupp (Freie Universität Berlin) for reprints and help.

Prof. Dr. Lukas Hottinger (Universität Basel) for determination of *Borelis melo*.

Prof. Dr. Martin Burkhard (Université de Neuchâtel) for instructions how to make ultra thin sections.

Prof. Dr. G.H. Davis (University of Arizona, Tucson, AZ) and Prof. Dr. J.B. Brady (Smith College, Northampton, MA) for reprints and unpublished manuscripts.

the DFG (grants SE 282/15 and STO 196/14, PP 1006 - ICDP) and the University of Cologne for financial support.

Lisanne Holzbach and Manfred Schnitzlein for improving the English.

my family for numerous support.

my girl-friend Silke Benner for continuous support and love.

Ich versichere, dass ich die von mir vorgelegte Dissertation selbstständig angefertigt, die benutzten Quellen und Hilfsmittel vollständig angegeben und die Stellen der Arbeit - einschließlich Tabellen, Karten und Abbildungen -, die anderen Werken im Wortlaut oder dem Sinn nach entnommen sind, in jedem Einzelfall als Entlehnung kenntlich gemacht habe; dass diese Dissertation noch keiner anderen Fakultät oder Universität zur Prüfung vorgelegen hat; dass sie – abgesehen von unten angegebenen Teilpublikationen – noch nicht veröffentlicht worden ist sowie, dass ich eine solche Veröffentlichung vor Abschluss des Promotionsverfahrens nicht vornehmen werde. Die Bestimmungen dieser Promotionsordnung sind mir bekannt. Die von mir vorgelegte Dissertation ist von Herrn Prof. Dr. Eberhard Seidel betreut worden.

Köln, den

Markus Seidel

Abstracts:

SEIDEL, M., SEIDEL, E. & STÖCKHERT, B., 2000, Petrographie und Strukturgeologie synorogener Sedimente in Westkreta. ICDP/KTB-Kolloquium, Wissenschaftliches Programm und Abstracts, 207-208, Bochum.

SEIDEL, M., SEIDEL, E. & STÖCKHERT, B., 2001, Tectono-sedimentary evolution of exhumation-related middle Miocene extensional fore-arc basins (Western Crete, Greece). ICDP/KTB-Kolloquium, Wissenschaftliches Programm und Abstracts, 189-190, Bochum.

SEIDEL, M., SEIDEL, E. & STÖCKHERT, B., 2001, Sedimentary facies assemblages in middle Miocene extensional fore-arc basins of western Crete, Greece. 21st IAS Meeting of Sedimentology, Davos.

SEIDEL, M., 2001, Analyses of middle Miocene basins related to an extensional detachment (Western Crete, Greece) – insights into the evolution of the fore-arc of the Hellenic subduction zone. 2001 Margins Meeting, Schriftenreihe der Deutschen Geologischen Gesellschaft, 14, 196-197.

SEIDEL, M., SEIDEL, E. & STÖCKHERT, B., 2002, Sedimentology of middle Miocene supra-detachment basins, western Crete. ICDP/KTB-Kolloquium, Wissenschaftliches Programm und Abstracts, Potsdam.

Paper:

SEIDEL, M., PACK, A., SHARP, Z.D., SEIDEL, E. & STÖCKHERT, B., 2002, The Kakopetros and Ravdoucha iron ore deposits (western Crete, Greece) - insight into along-fault fluid transport and mineralization within a detachment zone. Economic Geology, subm.

# LEBENS LAUF

## Persönliche Daten

Name	Seidel
Vorname	Markus
Geburtsdatum	01. Februar 1972
Geburtsort	Tegernsee
Familienstand	ledig
Staatsangehörigkeit	deutsch
Wohnanschrift	Döbrabergstr. 4, 50765 Köln
E-Mail	markus.seidel@uni-koeln.de

## Schule und Studium

1978 - 1982	Volksschule Valley
1982 - 1991	Gymnasium Miesbach, Allgemeine Hochschulreife
ab 1991	Studium der Geologie an der Technischen Universität München am Lehrstuhl für Allgemeine, Angewandte und Ingenieur-Geologie
11.1993	Vordiplomprüfung
11.1994 – 02.1997	Studentische Hilfskraft am Lehrstuhl für Allgemeine, Angewandte und Ingenieur-Geologie der Technischen Universität München
10./11.1995 + 04./05.1996	Diplomkartierung auf dem Peloponnes/Griechenland
05./06.1997	Hauptdiplomprüfung und Abgabe der Diplomarbeit

## Anstellung

01.09.1997 – 31.08.1999	Wissenschaftlicher Angestellter am Bayerischen Geologischen Landesamt, Abteilung Geologische Landesaufnahme
-------------------------	---

## Promotionsstudium und Anstellung

seit 01.09.1999	Wissenschaftlicher Mitarbeiter am Institut für Mineralogie und Geochemie der Universität zu Köln (DFG-Projekt: Priority Programme 1006 - ICDP/KTB)
-----------------	--

Köln, den